PERFORMANCE AND CAPACITY COMPARISON OF TWO NEW LGWP REFRIGERANTS ALTERNATIVE TO R410A IN RESIDENTIAL AIR CONDITIONING APPLICATIONS

By

AUVI BISWAS

Bachelor of Science in Mechanical Engineering

Bangladesh University of Engineering and Technology

Dhaka, Bangladesh

2009

Submitted to the Faculty of the
Graduate College of the
Oklahoma State University
in partial fulfillment of
the requirements for
the Degree of
MASTER OF SCIENCE
December, 2012

PERFORMANCE AND CAPACITY COMPARISON

OF TWO NEW LGWP REFRIGERANTS

ALTERNATIVE TO R410A IN RESIDENTIAL AIR

CONDITIONING APPLICATIONS

Thesis Approved:

Dr. Lorenzo Cremaschi

Thesis Adviser

Dr. Daniel Fisher

Dr. David G. Lilley

ACKNOWLEDGEMENTS

Firstly I would like to thank my adviser, Dr. Lorenzo Cremaschi for helping me out throughout my work not only through his supervision but also for providing hands on help and troubleshooting whenever asked for. Heartiest thanks to the committee members, Dr. Fisher and Dr. Lilley for spending their time and effort in reviewing, commenting, making suggestions and finally adjudicating the thesis. A lot of thanks go to Atharva Barve, fellow project-mate, for his overall assistance in fabrication, instrumentation and testing. We worked well in collaboration to make this project successful. Next I would like to thank Gary D. Thacker, the ATRC building manager, for spending his extra hours behind this project in making the electric connections and for his unyielding effort to ensure safe working conditions all the time. A lot of gratitude should go to Oklahoma State University and AAON for sponsoring the fantastic facility of the psychrometric chamber. All the previous students' hard work has helped it making well-renowned across the HVAC industry and academia. I would like to mention the name of Kasey Worthington, a former graduate student, specifically because I learnt almost everything about the chamber and Lab View from him. It was a privilege to work with him for some time. I also want to take the opportunity to thank all my co-workers during these two years, who have helped me in one way or another. Last but not the least, I thankfully acknowledge E.I. du Pont de Nemours and Company for supporting this work and for providing the refrigerant samples for the experimental campaign.

TABLE OF CONTENTS

Chapter Page

LIST OF TABLES

Table Page

LIST OF FIGURES

Figure Page

Figure Page

Figure Page

CHAPTER I

INTRODUCTION

Concerns about energy security, the threat of climate change and the need to meet growing energy demand pose major challenges to energy decision makers (IEA, 2004). In 2009, the residential and commercial building sectors used 5.74×10^{12} kW-hr (19.6 quad; quad is a unit of energy equal to 10^{15} BTU or 1.055×10^{18} Joules in SI units) of delivered energy, that is 21 percent of total U.S. energy consumption. The residential sector for heating, ventilating and air-conditioning (HVAC) alone accounted for 57 percent of that energy use, leaving 43 percent for the commercial sector (EIA, 2011). It is of high priority for the HVAC industry to address this critical energy challenge by improving the energy efficiencies of AC systems (Moezzi, 2000; Althof *et al.*, 2001; and EPA, 2011) and through the use of new low global warming potential (LGWP) refrigerants, thus reducing the direct and indirect greenhouse contributions for AC and heat pump systems in the short terms.

What is GWP?

GWP is the measure of the amount of heat being trapped by the greenhouse gases in the atmosphere. Numerically it is the ratio of heat trapped by a certain mass of a particular gas to the heat trapped by the same mass of carbon dioxide. In other words, the GWP value of CO_2 is standardized to be 1(Forster *et al.*, 2007). EIA defines the GWP as followed, "An index used to compare the relative radiative forcing of different gases without directly calculating the changes in atmospheric concentrations. GWPs are calculated as the ratio of the radiative forcing that would result from the emission of one kilogram of a greenhouse gas to that from the emission of one kilogram of carbon dioxide over a fixed period of time, such as 100 years"(EIA, 2011).

The factors that affect the value of GWP are:

1. The absorption of infrared radiation
2. Spectral location of absorbing wavelengths
3. Atmospheric lifetime

The radiative properties of a substance decides how much a unit mass can radiate at a given point of time, but the overall lifetime signifies how long that radiative component retains in the atmosphere (Ramaswamy *et al.*, 2001). GWP in shorter time horizon can be of great interest if the rate of climate change is more important than the overall magnitude (IPCC, l994; Fuglestvedt *et al.*, 2000).

The radiative forcing capacity (RF) is the amount of energy per unit area, per unit time, absorbed by the greenhouse gas. The higher the RF value, the more it is going away from the radiative heat balance on the atmosphere. It can be determined from equation (1-1) (Forster *et al.*, 2007):

$$RF = \sum_{n=1}^{100} \frac{Abs_i * F_i}{(pathlength * density)} \quad (1\text{-}1)$$

GWP is then calculated as the ratio of the integrated RF values of the greenhouse gas in question and CO_2 over a certain time horizon. This is the formula that has been adopted in the Kyoto Protocol (Kyoto Protocol, 1997) as in equation (1-2).

$$GWP_i = \frac{\int_0^{TH} RF_i(t)dt}{\int_0^{TH} RF_r(t)dt} = \frac{\int_0^{TH} C_i(t).[x(t)]dt}{\int_0^{TH} C_r(t).[r(t)]dt} \quad (1\text{-}2)$$

Here, TH is the time horizon, RF_i is the global mean RF of component i, a_i is the RF per unit mass increase in atmospheric abundance of component i (radiative efficiency), $[C_i(t)]$ is the time-dependent abundance of i, and the corresponding quantities for the reference gas (r) in the denominator. The numerator and denominator are called the absolute global warming potential (AGWP) of i and r respectively (Forster *et al.*, 2011). All the GWP values quoted in this work are based on the 100 year lifetime method and taking CO2 as the reference gas.

It should also be noted that besides this direct global warming effect of the greenhouse gases, there are also indirect effects of the degradation products, which could contribute in a lower or higher GWP value. While the direct effect of the degradation products, such as CH_4 (Methane), CO (Carbon Monoxide), NO_x (Nitrogen Oxides) and other organic compounds are negligible (WMO, 2003), they can lead to ozone formation or destruction, changing the lifetime of CH_4, and secondary aerosol formation (Prather *et al.*, 2001; Ramaswamy *et al.*, 2001; Collins *et al.*, 2002, Berntsen *et al.*, 2005, Shine *et al.*, 2005a).

Other Assessing Metrics

Since the introduction of use of GWP as a governing parameter in climatic evaluation, it has been well debated if it is really adequate or not. Although it's a simple and straightforward index, it is questionable because of the basis of equivalence of emissions for different gases (Smith and Wigley, 2000) and also the fact of being rather inappropriate for short-lived aerosols. A revised GWP method, including climate efficacies was proposed by Fuglestvedt *et al.* (2003) which was later implemented by Berntsen *et al.* (2005).

Another relative emission metric has been proposed by Shine *et al.* (2005b), namely "Global Temperature Potential", which is the ratio of global mean temperature increase at a future time horizon for gas x to the reference gas r (generally CO2) following an emission and calculated from equation (1-3) :

$$GTP_x^{TH} = \frac{\Delta T_x^H}{\Delta T_r^H} \qquad (1\text{-}3)$$

Life Cycle Climate Performance (LCCP) is another parameter which not only takes into account the direct emissions due to refrigerant leakage, but also the indirect emissions that come from the primary energy source while the power is being generated. LCCP covers the system performance, ambient temperature, system load and also the CO_2 emission rate in electricity generation. LCCP is the sum of direct and indirect emissions. Pappassava *et al.* (2010) described a model for calculating LCCP, which was later expanded by Abdelaziz *et al.* (2012) as in equation (1-4) and equation (1-5):

$$Em_{direct} = Em_{leakage} + Em_{servicing} + Em_{accidents} + Em_{EOL\ lost} + Em_{leakage\ (prod.\&trans.)} \qquad (1\text{-}4)$$

Where,

$Em_{direct} = Direct\ emissions$

$Em_{leakage} = Emission\ due\ to\ refrigerant\ leakage$

$Em_{servicing} = Emissions\ due\ to\ leakage\ from\ servicing$

$Em_{accidents} = Emissions\ due\ to\ accidents$

$Em_{EOL\ lost} = Emission\ due\ to\ end\ of\ life\ of\ system$

$Em_{leakage\ (prod.\&trans.)} = Emission\ during\ production\ and\ transportation$

$$Em_{indirect} = Em_{manuf,sys} + Em_{manuf,ref} + Em_{E,EOL,sys} + Em_{E,EOL,ref} + Em_{E,op.} + Em_{E,transp.} \quad (1\text{-}5)$$

Where,

$Em_{indirect}$ = Indirect emissions

$Em_{manuf,sys}$ = Emission due to energy used while manufacturing components

$Em_{manuf,ref}$ = Emission due to energy used while manufacturing refrigerant

$Em_{E,EOL,sys}$ = Emission due to energy used because of end of life of components

$Em_{E,EOL,ref}$ = Emisson due to energy used because of end of life of refrigerants

$Em_{E,op.}$ = Emission due to energy consumtion during lifetime

$Em_{E,transp.}$ = Emission due to energy used to transport equipment

Total Equivalent Warming Number (TEWI) is another metric of measuring the effect of global warming caused by the greenhouse gases directly and indirectly. The concept was initiated as a simplified tool to evaluate lifetime total warming impact. TEWI can be calculated by knowing the total amount of refrigerants and blowing agents being leaked, energy consumed over lifetime and the GWP values. As described in Sand *et al.* (1999), TEWI can be estimated from equation(1-6):

$$TEWI = Mass_{refrigerant} \cdot GWP_{refrigerant} + Mass_{blowing\ agent} \cdot GWP_{blowing\ agent} + \alpha \cdot E_{annual} \cdot L_{years} \quad (1\text{-}6)$$

Where, α is the conversion factor used to convert energy use, E and Lifetime, L to corresponding CO_2 emissions.

Kruse (1998) suggested separate evaluations of direct and indirect emissions following the Kyoto protocol. Only then can be the system tightness compared to the use of refrigerants with lower GWP. The cost comes into play as well in order to build a tighter sand energy efficient system.

Although LCCP and TEWI are probably better parameters to look at for the complete view of global warming effects, GWP is a quite well acclaimed metric in the HVAC industry to evaluate the refrigerants in order to make sure they follow the recent changes in climate protocols.

A review of the literature on the continuous efforts of the researchers to study lower GWP refrigerants characteristics and their performance when retrofitted into the existing HVAC equipment is presented in the following section.

CHAPTER II

LITERATURE REVIEW

The refrigeration and air-conditioning industry has experienced several changes since the last two decades in order to meet the terms of the Montreal Protocol (UNEP, 1987). A gradual phase-out of refrigerants that deplete the ozone layer has occurred (Reasor et al, 2010) and CFCs to HCFCs have been retrofitted with more environmentally friendly refrigerants. However, HFCs and new blends used in modern air conditioning and heat pump systems have still global warming potential (GWP) that is of concern. For example R134a is a hydro fluorocarbon refrigerant with ODP of zero but with GWP of about 1,430 (Forster *et al.*, 2007) and the European Union directed the phase out of R134a in automobile air conditioning in the coming decade. In residential sector, R410A has been a widely used refrigerant until recent concerns about its high GWP value. In this review of literature I am mainly going to describe how R410A retrofitted R22 in A/C systems and how researchers have been approaching to find a proper drop-in replacement for R410A, with lower GWP value.

Use of R410A in HVAC systems

R410A was originally introduced in the HVAC industry as a drop-in replacement for HCFC-22 which was being phased out by the Montreal protocol, with an ODP of 0.05 and GWP value of 1810 in the 100 year horizon. Researchers investigated if R410A could efficiently replace R22 in the already existing systems. Refrigerant R410A is a near-azeotropic blend of R32 and R125, with a critical temperature of 72.8°C (163°F) and a critical pressure of 4.86 MPa (705 psi). Its ozone depletion potential is zero but its GWP is 2,088 (Solomon *et al.*, 2007), which is even higher than that of HCFC-22. But until the Kyoto Protocol, it was not of concern and R410A was adopted in air conditioning and heat pump systems for residential applications (Pande *et al.*, 1996). R410A has better transport property and higher working pressure than R22, which means that the refrigerant pressure loss and its impact on the system performance are relatively smaller. Kim *et al.* (2000) found out that R410A has around 24% higher flow rate than R22 in capillary tubes for air-conditioners. Payne and Domanski (2002) investigated that although at 35.0 °C (95.0 °F) outdoor temperature R410A had roughly the same capacity as R22 and a COP 4% lower, at high ambient temperature of 54°C (130.0 °F) the R410A capacity was 9 % lower and COP was less by 15% in comparison to that of R22. Domanski *et al.*, (2005) discussed that for a 7°C (44°F) evaporator exit saturation temperature, R410A has 10.7% higher capacity and around 2% higher COP in comparison to R22. Chen (2008) experimented on four sets of comparable R410A and R22 split-type residential A/C systems and concluded that R410A systems can have 3 to 12% higher performance than that of R22. He also pointed out that R410A systems can perform more and more efficiently at lower ambient temperatures and also mentioned the fact that R410A systems have a lower LCCP index than that of R22. R410A has been considered as a high volumetric cooling capacity refrigerant, which means that it can absorb significant amount of heat from the air for a unit volume of refrigerant in a direct expansion evaporator.

Replacement of R410A in HVAC systems

Several researchers investigated refrigerants that could potentially retrofit R410A in air conditioning systems. For example R32 has been proposed in mini-split systems, which are popular in China and Japan (Pham, 2010). R32 has a GWP of 675 (Forster *et al.*, 2007). R32 having a larger volumetric capacity than R410A, can work with 50% reduced charge than that of R410A for similar system performance (Taira *et al.*, 2011). Pham and Rajendran (2012) investigated on R32 and other HFO blends as potential low GWP candidates. They found out that R32 can have 2.6 to 3.9% higher capacity with a decrease in 0.8 to 1.5% in COP when used as a drop-in replacement for R410A, and this is accompanied with 20 to 70° F increase in discharge temperature. They also suggest that R32 can be serve as the initial candidate to meet the HFC phase out until 2020, but eventually in order to meet the cap of 15% GWP decrease by 2030 its future is uncertain. Barve and Cremaschi (2012) also suggest similar findings for R32 where it has similar COPs and up to 10% higher system capacity when compared to R410A. The flammability characteristics of R32 pose some concerns in case of leakage or in case of failure of the equipment.

Natural refrigerants have also been proposed as alternative refrigerants to R410A for heat pump systems. Natural refrigerants have zero ozone depletion potential and minimum global warming potential since these fluids are available in nature. However, they usually require a system designed ad-hoc for the specific application, which make retrofitting of R410A with natural refrigerants difficult, especially in existing equipment (Yin *et al.*, 1998). CO_2 (R744) has a GWP value of 1, but the refrigeration cycles are transcritical, that means it requires cooling the compressed fluid at supercritical high-side pressure (Kim *et al.*, 2004). Numerical results and experimental validations for CO_2 air conditioning cycles are present in literature (Rasmussen *et al.*, 2003; Rigola *et al.*, 2004). Results for CO_2 transcritical heat pumps for residential application were presented in Richter *et al.* (2003).

Few studies on refrigerants that have zero ozone depletion potential and GWP less than 500 are available in the literature. Minor and Spatz (2008) presented R1234yf as a candidate for replacing R134a in automobile air conditioning systems and reported that it could perform within 10% of the system performance compared to the original refrigerant. R1234yf showed similar refrigeration properties as that of R134A when used in refrigeration applications as well (Leck, 2009). Because of its low working pressure, R1234yf might not be considered as a direct drop-in replacement for R410A.

Following the work of Kontomaris *et al.* (2009), low GWP new blend DR-11 (Kontomaris *et al.*, 2010) and XP10 (Kontomaris *et al.*, 2012) were presented as replacements for R134a in chiller applications with an decrease of 2.5 % and an improvement of up to 8% in COP respectively. Developmental refrigerants L-20 and L-41 were presented as replacements for R407C and R410A respectively in positive displacement chiller applications with similar COPs (Spatz, 2012). The author also described the potential replacement refrigerants N-12 and N-13 in centrifugal chiller applications. An overview of the objectives of low GWP refrigerants and how these new fluids can be implemented into existing equipment can be found in McLinden (2011). Yana Motta *et al.* (2012) reported new low GWP developmental refrigerants N-40 and N-20 that offered great reduction of environmental impact in current and future refrigeration systems.

Some experimental studies for retrofitting R410A in small split systems have been published in the recent years. Horie *et al.* (2010) discussed the refrigerant cycle characteristics of R32 and R1234yf with respect to R410A in heat pump applications. The authors highlighted the benefits and shortcomings of these two refrigerants with respect to R410A. Developmental refrigerants from various refrigerant manufacturers were retrofitted in existing systems lately and preliminary findings seemed to suggest that new development refrigerants were viable options. Yana Motta *et al.* (2010) investigated on a 3-ton 13 SEER split system R410A unit with a heating capacity of 10.1 kW and an HSPF of 8.5. The two new refrigerants, HDR-06 and HDR-11 exhibited up to

7% reduction in capacity and up to 4% improvement in COP in comparison with R410A. Both these refrigerants caused lower thermal and volumetric efficiencies associated with slight increase in discharge temperatures with respect to R410A. Pham and Rajendran (2012) presented experimental results for three new HFO blends, with GWP values around 500, tested in R410A optimized A/C and HP units. These blends reportedly have system capacities within -10% to +1% and EER within -4% to +7% of that of R410A.

Wang *et al.* (2012) presented a summary report on thirty eight promising alternative low GWP refrigerants, accumulating results from industry-wide co-operative research by AHRI. The GWP values of these refrigerants ranged from 0 to 1500. Thermodynamic modeling results and experimental data for all these refrigerants during compressor calorimeter tests, direct drop-in tests and soft-optimization tests were compared to those of baseline refrigerants. AHRI specified that all the tests were carried out following AHRI standard 210/240 and ASHRAE standard 37 for testing unitary air-conditioners and heat pumps. Drop-in tests were conducted with only minor modifications, if needed, and for the soft optimization tests, even evaporator and condensers circuitry might have been changed ensuring that the total heat transfer areas remained the same.

A summary with an overview of all the refrigerants mentioned in the literature review is presented in Table 1.

Table 1: Summary of the refrigerants in literature review

Refrigerant	Authors	Year	Applications
R410A	Kim *et al.*	2000	Capillary tubes
	Payne and Domanski	2002	Split type residential A/C
	Domanski *et al.*	2005	NIST evaporator model
	Chen	2008	Split type residential A/C
R32	Pham	2010	Mini-split system
	Taira *et al.*	2011	Split type residential A/C
	Pham and Rajendran	2012	Unitary A/C and H/P
	Barve and Cremaschi	2012	Split type residential H/P

	Horie *et al.*	2010	Heat Pump
CO_2	Yin *et al.*	1998	Existing A/C system
	Rasmussen *et al.*	2003	Numerical analysis
	Richter *et al.*	2003	Residential H/P
	Kim *et al.*	2004	Split type residential A/C
R1234yf	Minor and Spatz	2008	AutomobileA/C
	Leck	2009	Refrigeration
DR-11	Kontomaris *et al.*	2010	Chiller, replacement of R134a
XP10	Kontomaris *et al.*	2012	Chiller, replacement of R134a
L-20 and L-41	Spatz	2012	Positive displacement chiller
N-12 and N-13	Spatz	2012	Centrifugal chiller
N-40 and N-20	Yana Motta *et al.*	2012	Refrigeration
HDR-06 and HDR-11	Yana Motta *et al.*	2010	Split type residential A/C

New developmental refrigerants and their characteristics

This thesis extends the previous studies from (Leck, 2010) to R410A heat pump split system for ducted HVAC installations and for residential applications. This thesis presents data of the thermal performance and capacity of two new lo GWP refrigerants that are still in the R&D stage and are referred throughout this report as DR-4 and DR-5 (DR- refer to as developmental refrigerant). Some properties of the candidate refrigerants are presented in Table 2.

Table 2: Some properties of refrigerants investigated in this thesis

	R410A	**DR-4**	**DR-5**
Temperature Glide (K)	0.1	5	1
GWP	2088	<300	<500
Toxicity	Non-toxic	Non-toxic	Non-toxic
Flammability	Class 1	Class 2L	Class 2L
Lubricant compatibility	POE	POE	POE

DR-4 and DR-5 had temperature glides of 5°C (9°F) and 1°C (1.8°F) respectively during phase change from saturated liquid to saturated vapor. DR-5 has a GWP value less than 500, while DR-

4 has an even lower value, less than 300. They were not toxic, compatible with POE lubricant, chemically stable, not corrosive, and had flammability characteristics of class 2L refrigerants according to ASHRAE standard 34 (Leck and Yamaguchi, 2010), which means they have mild flammability and lower flame propagation rate. One of the major constituent of these two refrigerants was R1234yf.

While the details will be discussed later in the thesis, Figure 1 shows the *P-h* diagram and the refrigeration cycle analysis of R410A, DR-4 and DR-5. The diagrams were constructed based on the measured data for each refrigerant when charged into a heat pump unit, which ran at AHRI standard 210 A-Test cooling mode conditions. DR-4 had a refrigeration cycle that was similar to that for R410A but shifted toward the lower pressure range. DR-5 cycle was wider than those for R410A and DR-4. The pressure lift across the compressor was lower for both DR-4 and DR-5 compared to R410A. The pressure ratio, defined as the ratio between the discharge pressure and suction pressure, was about 2.43 and 2.60 for DR-4 and DR-5, respectively, whereas the compressor ratio of R410A was about 2.64. The discharge pressure of DR-4 was lower than R410A discharge pressure by about 570 kPa (83 psi) while DR-5 discharge pressure was 90 kPa (13 psi) lower than the corresponding discharge pressure for R410A at similar operating conditions. The superheat and sub-cooling and the pressure drops in the evaporator and condenser are shown in the *P-h* diagram. The degree of suction superheat was about 5.2°C (9.4°F) for R410A and, by adopting the same TXV, 1.9°C (3.4°F) for DR-4, and 3.5°C (6.3°F) for DR-5. The degree of sub-cooling at the TXV inlet location was about 5.5°C (10°F) for R410A, 3.2°C (5.7°F) for DR-4, and 6.3°C (11.3°F) for DR-5. The refrigerant flow rates were 101 g/s (810 lb_m/hr) for the unit with R410A, 81 g/s (646 lb_m/hr) for DR-4, and 82 g/s (656 lb_m/hr) for DR-5.

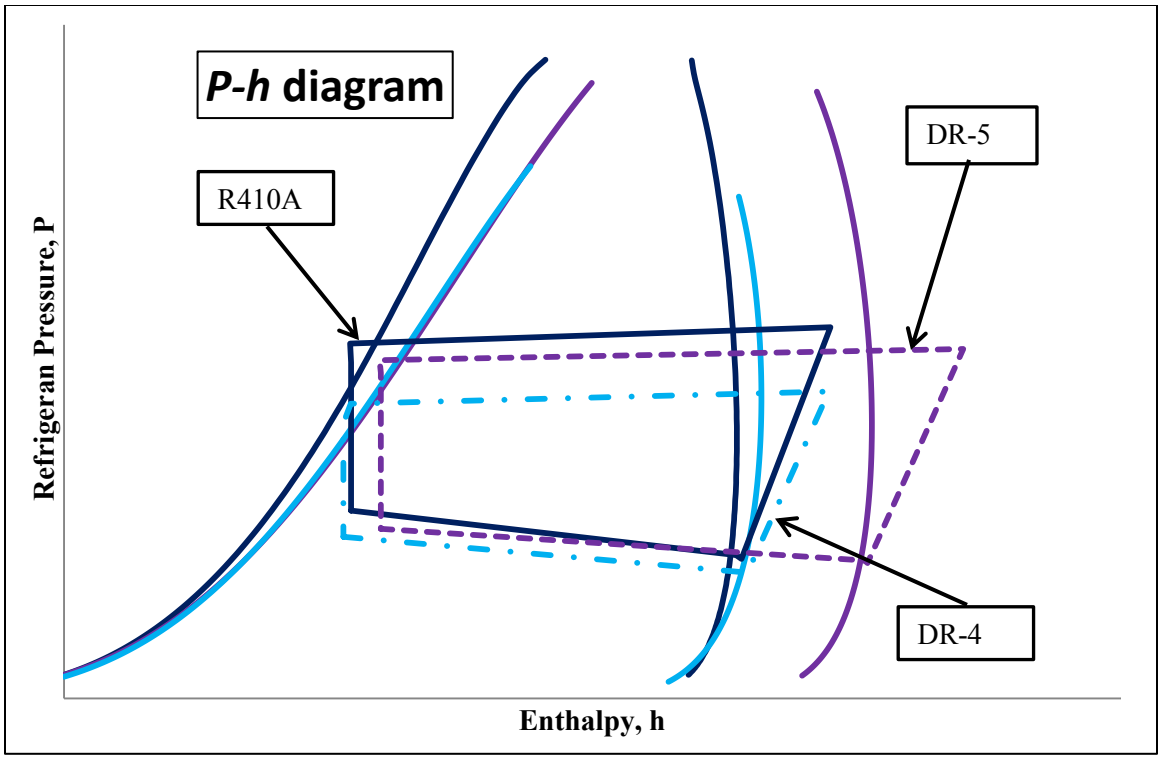

Figure 1: Pressure-enthalpy diagram and refrigeration cycles for R410A, DR-4 and DR-5 at AHRI A test condition (data measured in the present thesis)

Figure 2 shows the *T-s* diagram and the refrigeration cycle analysis of the three refrigerants based on the measured data at AHRI standard 210 A-Test cooling mode operation. In accordance with the *P-h* diagram, the DR-5 cycle was wider than that of R410A and DR-4. The figure depicts that the working temperatures for all the refrigerants are quite similar. Decrease of temperature in the evaporator and condenser coils are shown in the *T-s* diagram. One interesting observation from the cycle in the T-s diagram of Figure 2 is the discharge temperature at the compressor outlet. DR-4 had almost similar discharge temperature compared to R410A while DR-5 had 9.8°F (5.4°C) higher discharge temperature.

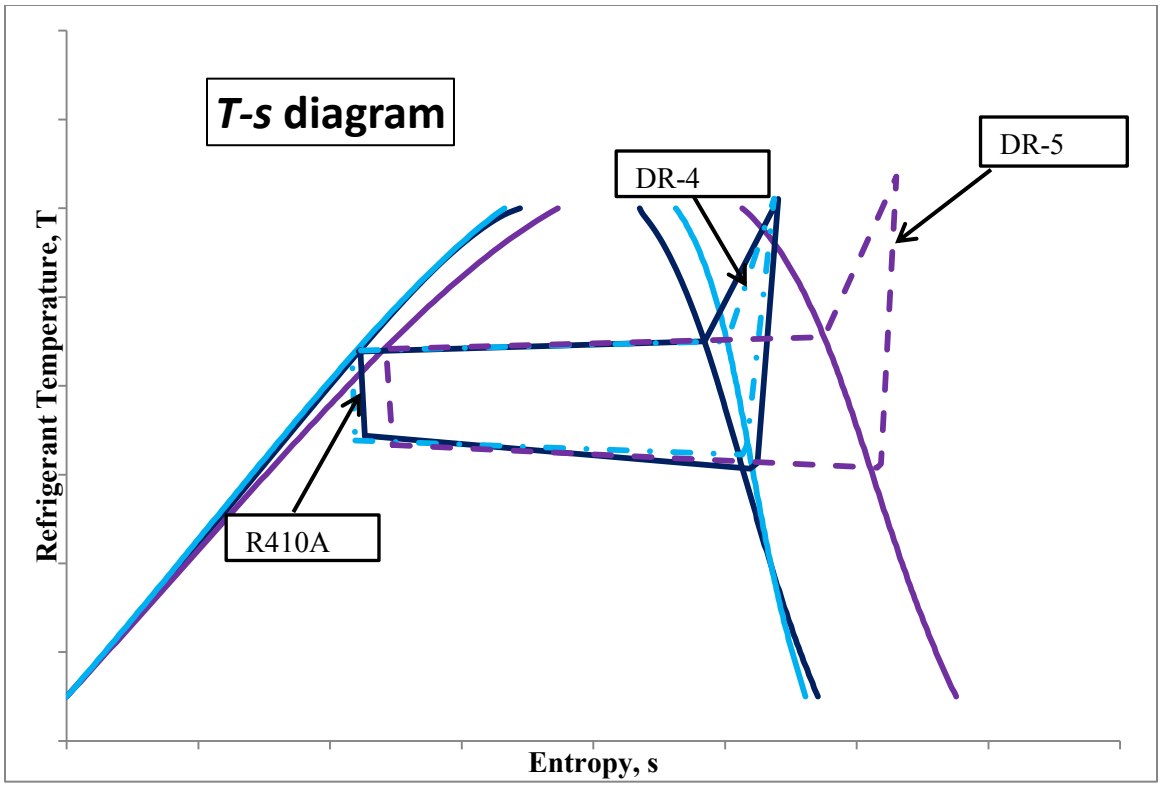

Figure 2: Temperature-entropy diagram and refrigeration cycles for R410A, DR-4 and DR-5 at AHRI A test condition (data measured in the present thesis)

Proposed refrigerants in literature

Leck (2010) presented modeling results and experimental data on DR-4 and DR-5, along with the other low GWP candidates. The AC cooling cycle modeling results were calculated based on evaporator temperature of 7°C, Condenser temperature 47°C, Liquid sub-cooling of 12K, suction gas superheat of 3K and compressor volumetric efficiency of 70%. The modeling was based on ideal cycle assumption with no pressure drops or heat losses and only with preliminary values of the transport properties. Initial findings denoted that DR-5 had similar discharge pressure and a discharge temperature 6°C higher than that of R410A. On the other hand DR-4 had a discharge pressure almost 500 kPa lower and a discharge temperature 4°C lower than R410A. DR-5 was designed to have the similar capacity and COP 1% higher with 75% reduction in GWP, while

DR-4 would have a COP 1.3% higher associated with up to 20% drop in system capacity in comparison with R410A. Similar analysis was done with these refrigerants for a heating cycle in heat pump, with evaporator temperature 0°C and condenser temperature 45° and both DR-5 and DR-4 performance were predicted to be similar as the ones for the cooling cycle. DR-4 had a drop of heating capacity by 20% with 1% higher heating COP and DR-5 had similar heating capacity and 1% lower heating COP. The author suggested that moderate decreases in capacity accompanied with a slight increase in COP could make these refrigerants attractive for use in heating and air conditioning applications.

Leck (2010) extended the work by measuring the system performance in air conditioning experimentally. The test unit was a commercial split system unit with rated capacities of 2.8 KW for cooling and 3.2 kW for heating, and the tests were operated in an environmental chamber. R410A was first run to establish the baseline and then DR-4 and DR-5 were evaluated in drop-in testing without any modifications to the system. The Cooling COP and heating COP was higher by 4% and 1% respectively for DR-5, whereas DR-4 had a drop of 3 to 10% in system performance when compared to that of R410A. Annual Performance Factor (APF) was calculated as the sum of weighted cooling season load plus heating season heat load for Tokyo climate conditions, and it was observed that DR-5 had 3% higher and DR-4 had 3% lower APF values with respect to R410A. The LCCP values of DR-5 and DR-4 were found to be 24% and 21% less respectively than that of R410A. The author suggested that DR-5 could be a potential drop-in replacement for R410A, but DR-4, in spite of having a GWP almost 86% less than R410A, would need system modifications such as increasing the suction line size and heat transfer area to have better system capacities.

DR-5 was later investigated as a potential replacement for R410A in A/C and heat pump applications and thermodynamic cycle modeling was done by AHRI under 5 different testing conditions, varying the evaporator and condenser temperatures, compressor suction superheat and

condenser sub-cooling (Wang, 2012). The report suggests that DR-5 could have relative capacity up to 4% higher and relative COP of 1 to 4% higher in comparison to the baseline capacity of R410A.

From the literature review, it can clearly be observed that there is continuous ongoing effort to meet the environmental protocols for refrigerants with the goal to achieve desirable performance from the existing systems while they are retrofitted with the alternative refrigerants. But besides that, elimination of any loss of refrigerant to the atmosphere should be minimized by design, use, service practices and end of life decommissioning of the equipments. One has to remember that it is still essential to use refrigerants that can give forth higher system performance and hence lower LCCP. The use of high performance refrigerant itself reduces the adverse environmental effect, because that means less energy is required to run the air conditioning and heat pump unit. Less energy translates directly in less fuel consumed upstream that is at the electric power plant. The effort should not just be going after the lower GWP refrigerants based on the GWP cap of useable refrigerants, but rather maintaining a protocol based on a weighted GWP and LCCP based method that could weight direct and indirect contributions of a refrigerant to the greenhouse effects.

CHAPTER III

OBJECTIVE

The main purpose of this particular work is to investigate the possibility of the two new LGWP refrigerants, namely DR-4 and DR-5, to retrofit R410A in residential air conditioning applications. Given the necessity of implementing new refrigerants that satisfy the latest environmental protocols and possibly in the existing systems without major modifications, this work provides some information of two new LGWP refrigerants and studies the performance of these two particular refrigerants if they are used in a conventional R410A split system residential unit.

The specific objectives of this thesis are as follows:

- To test R410A and DR-4, DR-5 (DR- developmental refrigerants) with direct drop-in and soft optimization of TXV
- To optimize the charge and to compare the system capacity and energy performance for each refrigerant at design and off-design conditions
- To estimate the evaporator and condenser coil performance and pressure drop across the evaporator coil

- To assess the compressor performance by investigating the discharge temperatures, thermal and volumetric efficiencies

The approach was to collect data and conduct an evaluation of the energy performance and capacity of the two LGWP refrigerants when they retrofit R410A in a commercially available heat pump system. The experimental study was conducted on a 5 ton nominal capacity heat pump ducted split system at design and off-design conditions of extreme high temperatures. The experiments were conducted in a large scale psychrometric chamber at Oklahoma State University and refrigerant cycle temperatures and pressures were directly measured. The thermal and transport characteristics of the refrigerants are discussed for straight drop-in tests, in which none of the original components of the unit were modified, and for soft-optimization tests, in which the original R410A thermal expansion valve was modified for further optimization of the refrigeration cycles.

CHAPTER IV

EXPERIMENTAL SETUP

This section describes the experimental facility, the test apparatus, instrumentation of all the necessary sensors, acquiring data into the DAQ system and Lab View interfacing and controls built for monitoring the test setup.

The experimental campaign was carried out in a large psychrometric chamber at Oklahoma State University, which has two adjacent rooms simulating the outdoor and indoor ambient conditions. The outdoor and indoor units of the split system heat pump assembly were placed into the psychrometric chamber and connected with copper piping for refrigeration flow. Necessary pressure, temperature and flow sensors were installed on both the refrigeration and air side for analyzing the cycle and measuring the system capacity and performance. The sensors were connected to the already existing data acquisition system of the chamber and read into Lab View for monitoring and further processing of data.

Psychrometric Chamber

The psychrometric chamber at OSU was originally designed for testing HVAC equipments and research. The control variables such as temperature, humidity and air flow rate can be controlled and maintained precisely inside the psychrometric chamber. A psychrometric chamber is different from an environmental test chamber because it is able to maintain conditions with the addition of a live thermal load. It acts as an infinite heat source or sink by balancing the load that an unit rejects or absorbs in order to maintain a desired test condition.

The psychrometric chamber at OSU consists of two similar adjacent rooms, where the outdoor chamber simulates the outdoor weather having a design temperature range of -40 to +130°F and the indoor chamber replicates typical indoor environment with temperature ranging from 55 to 100°F. The chamber was intentionally oversized to minimize the interference of the testing equipment with the walls and the ceiling of the chamber. Uniform air flow distribution is ensured through a raised perforated floor design. More details on the construction and design specifics of the chamber can be found in (Cremaschi and Lee, 2008) and (Lifferth, 2009). Table 3 shows the summary of the chamber specifications.

Table 3: Chamber Specifications

	Outdoor Chamber	**Indoor Chamber**
Dimensions	22x22x17 ft^3 (6.7x6.7x5.2 m^3)	19x22x17 ft^3 (5.8x6.7x5.2 m^3)
Temperature range	-40 to +130°F (-40 to 55°C)	55 to 100°F (13 to 38°C)
Relative humidity	10 to 95%	20 to 90%
Maximum capacity	15 tons (53 kW)	15 tons (53 kW)
Maximum air flow rate	8000 cfm	8000 cfm

The basic operational principal of the psychrometric chamber is to overcool the air than the desired set point by blowing air using variable speed blowers. Air flows across cold cooling coils

and then across electric heaters, controlled by PID (Proportional, Integral, Derivative) scheme. At OSU psychrometric chamber, humidity is maintained by a PID controlled electric steam generator. The steam is injected into the air stream to set the required humidity. In order to make sure that the dry-bulb and wet-bulb measurements are accurate and satisfy ASHRAE and AHRI standards, airside temperatures are mechanically averaged using sampling tree and measured in the wet-bulb probe. The air flow measurements are made following ANSI/ASHRAE Standard 41.2 (1987). There are nozzle banks in both the outdoor and indoor chamber, where air flow rate and air pressure can be varied by changing the blower speed and changing the free flow area. Following ANSI/ASHRAE Standard 37 (2009), the OSU psychrometric chamber is setup for inside or outside air enthalpy methods of measuring system capacity of HVAC equipments. More details on the built-in instrumentations and control strategies of the psychrometric chamber can be found in Worthington *et al.* (2009) thesis.

Heat Pump Unit

The heat pump used for the present experimental campaign was a commercial and off the shelf R410A split system, with a rated capacity of 5 ton, Seasonal Energy Efficiency Ratio (SEER) of 13 and Heating Seasonal Performance Factor (HSPF) of 8.5. The unit was assembled as a typical ducted HVAC residential unit. As shown in Figure 3, there were two units of the heat pump assembly, namely the outdoor unit placed in the outdoor chamber and the indoor unit placed into the indoor chamber. Both the units were placed 3ft away from the walls following the standards to make sure that there was good distribution of air around them. The outdoor unit consisted of a compressor, a coil and a fan, whereas the indoor unit consisted of a blower-fan couple. The unit was powered with a 3-phase, 208 VAC and 60Hz connection using a variable voltage

transformer. The nominal current of the unit was 7.5 Amps and the maximum current was 15.0 Amps.

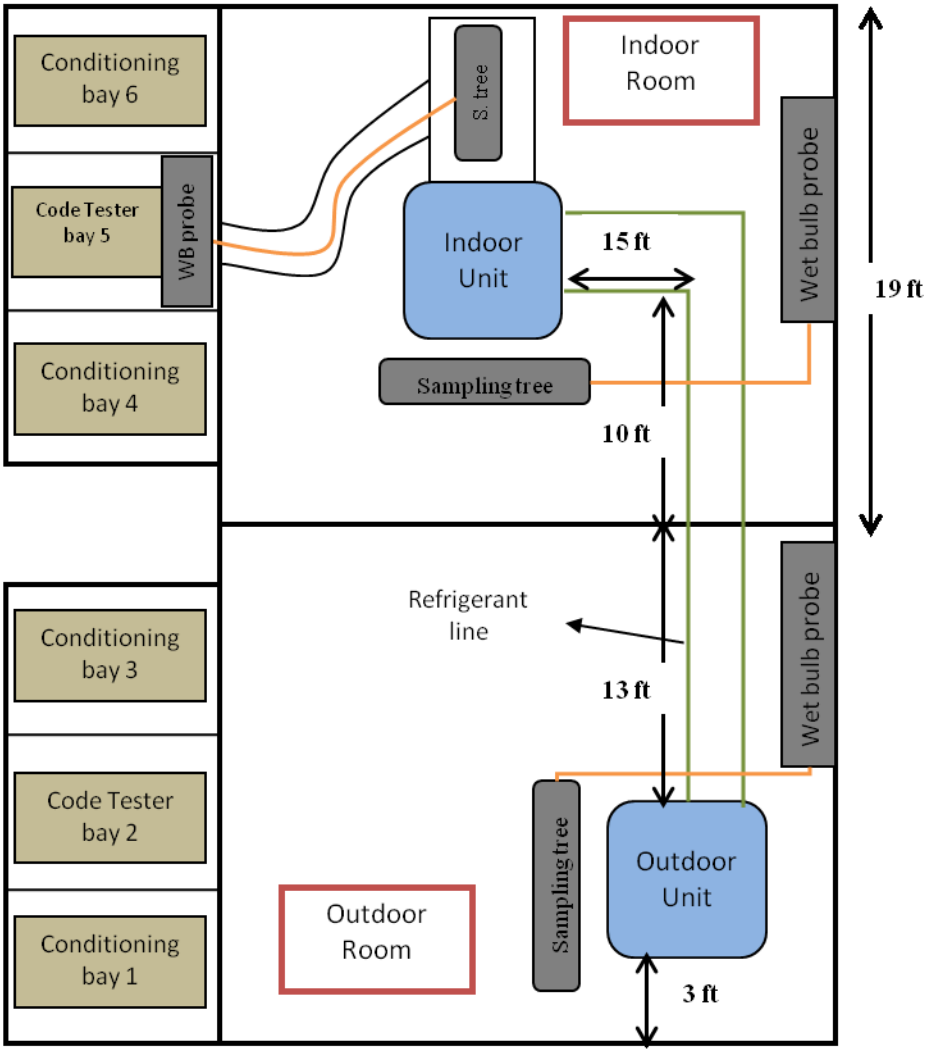

Figure 3: Layout of the Heat Pump system inside OSU psychrometric chamber

The outdoor unit had a fixed speed hermetic scroll compressor, with capacity of 4HP, nominal voltage of 208-230V at 60 Hz and suction and discharge connections of 7/8" and 1/2" respectively. The compressor nominal speed was around 3600 rpm and it had a swept volume of 47.4cm^3/rev and displacement volume of 9.9m^3/h. It was pre-charged with 53oz. of POE

lubricant, which had a viscosity of 30 cSt at 104°F. Additional 22oz. of lubricant was charged into the compressor to compensate for the oil being retained in the additional length of suction line. There was a built-in fixed speed fan in the outdoor unit and a refrigerant suction line receiver, with capacity of 19.2oz, a four way valve that enabled the heat pump to operate both in cooling and heating mode, and a TXV that operated as an expansion device while in heating mode. The outdoor unit would go into a lockout condition if it sensed 263°F at discharge line for 30s continuously. There were also high and low pressure switches to ensure safe operation of the unit.

The indoor unit had a built-in blower with a capacity of 3/4hp and rated voltage of 230VAC. It had a pre-programmed motor which could be set to rotate at 5 different speeds. Motor wires could be connected to motor speed tap receptacles to give the blower various speeds. In order to keep consistency, all through the experimental campaign, the motor was set to give a constant rpm at 208 VAC that would produce around 1800-1900 cfm at 0.2 inWC external static pressure. The speed taps were connected to the ports 3 and 5, as shown in Figure 4. The indoor unit also came with a TXV that performed as the expansion device during cooling operation.

Figure 4: Speed tap connections for the blower motor (model: X13^{TM} FM18)

The outdoor and indoor units were connected through copper piping across the two rooms. The liquid line was a 3/8" OD pipe, while the vapor line came out from the outdoor unit as 7/8" pipe but continued all the way as a 1" pipe. Both the liquid and vapor lines were almost 40ft in length. All the refrigerant line was well insulated with ultra-flexible foam rubber pipe insulation that was 3/8" thick. A P-trap was made at the drain of the pan of the indoor blower and coil assembly to collect the water condensate from the indoor unit. The heat pump specifications are summarized in Table 4.

Table 4: Heat Pump Specifications

	Description	**Model No.**	**Brand**
Rated capacity	5 ton	-	JCI/York
SEER	13	-	-
HSPF	8.5	-	-
Compatible refrigerant	R410A	-	-
Power source	3 phase, 208V, 60Hz	-	-
Compressor type	Hermetic scroll compressor	HRH049U1LP6	Danfoss
Compressor swept vol.	47.4cm^3/rev	-	-
Lubricant	POE oil, viscosity 30 cSt	-	-
Outdoor fan	Fixed speed	F48AA68A50	A.O. Smith
Indoor Blower	Fixed speed	5SME39NXL014A	Genteq
Liquid line	3/8" OD Copper	-	-
Vapor line	7/8" and 1" OD Copper	-	-
TXVs	R410A optimized	S1-1TVM4K1	JCI/York
Suction line receiver	19.2 oz.	QFQ-Y2089-S003-00	Dunan
Insulation	3/8" thick ultra-flexible foam rubber pipe insulation	-	-

The outdoor coil was a serpentine type with six circuitries, while the indoor coil was A-shape with 8 circuitries, as shown in Figure 5. There were distributors at the outlet of the TXVs that ensured proper distribution of refrigerant through the coils. The coil geometries are summarized in Table 5.

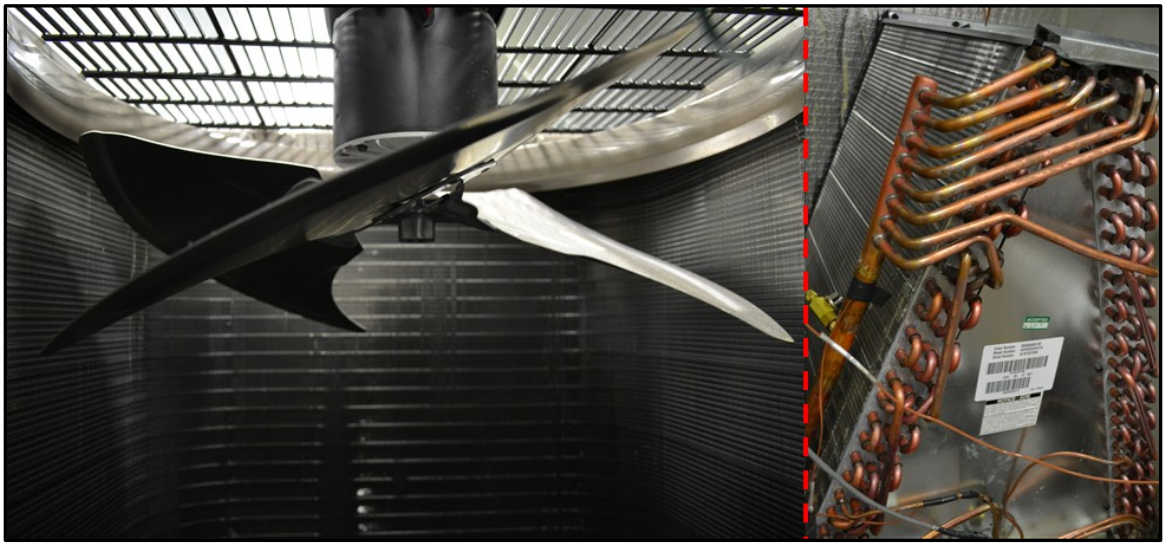

Figure 5: Outdoor coil (left) and Indoor coil (right)

Table 5: Coil Geometry

	Indoor Coil	**Outdoor Coil**
Type/Configuration	A-shape	Serpentine
No. of circuiting	8	6
Pipe nominal size	9.5 mm (3/8 inch)	12.2 mm (½ inch)
Fin density	5 fins per cm (13 fins per inch)	9 fins per cm (23 fins per inch)
Dimensions	45cm x 70cm x 2 (17.5" x 27.5" x 2)	84cm x (81cm x 2+66cm) (33" x (32" x 2+26")
***** The measurements in this table were made at Oklahoma State University on off-the-shelf coils. They represent a small number of physical measurements and they were not given by the manufacturer		

Once the refrigerant lines were established, the next step was to configure the air side for flow, pressure and temperature measurements. Figure 6 shows the air side construction of the heat pump setup.

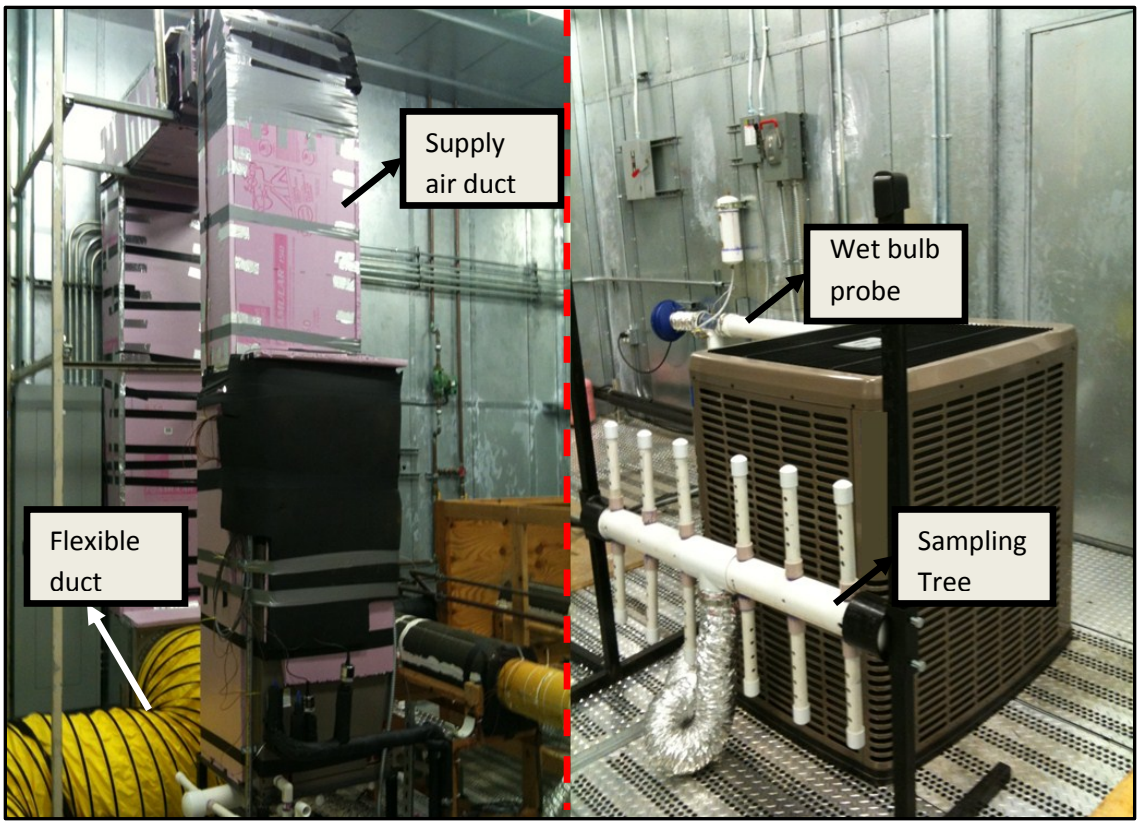

Figure 6: Indoor Unit (left side) and Outdoor unit (right side)

ASHRAE standard 41.2 describes that air has to be sampled at a minimum distance of 4ft (1.2 m) from the outlet of the blower in order to measure the pressure and temperatures at the indoor unit outlet. As shown in Figure 6, a 4ft (1.2 m) tall duct was built from the unit outlet to sample the supply air. For better accessibility and suitability of the flexible duct connections, the ductwork dropped down to a well insulated 2ft x 2ft x 2ft (0.6m x 0.6m x 0.6m) box. 12" X 24"X 48" (0.3ft x 0.6 m x 1.2m) rectangular aluminum ducts were used for erecting the ductwork and 1" thick foam insulation panels were used for constructing the box. The ductwork was well insulated with

board foam insulation of 1" (0.025m) thickness. A 24 inch (0.6m) diameter flexible yellow duct was connected the box to the code tester as shown in Figure 6. More details on the air side duct construction can be found in (Barve, 2012).

Instrumentation

Both the refrigerant side instrumentation and the air side instrumentation will be discussed in this sub-section, where the sensor installations will be described and explained in details.

Refrigerant side instrumentation

Figure 7 shows the instrumentation along the refrigerant line in cooling mode. The target was to put pressure and temperature sensors in pairs in such a way that together they represent the corresponding state point defining two independent refrigerant properties. These data are useful for monitoring the system and can also be used later on to calculate the enthalpies and entropies to determine the refrigerant capacity, system heat balance and energy balance.

In the diagram, absolute pressure transducers are denoted with P_i, inline thermocouples with T_i, surface thermocouples with $T_{s,i}$ and mass flow meter with MFM. The discharge inline thermocouple and pressure transducer, designated by P_1 and T_1 were installed right after the reversing valve, because it was not possible to install them inside the unit casing due to space constraints. The 4 way reversing valve was well insulated and the pipeline in between were well insulated to minimize heat losses between the discharge port and the location of the sensors. P_2 and T_2 were located at condenser outlet and after about 40ft of pipeline P_3 and T_3 were installed at the TXV inlet.

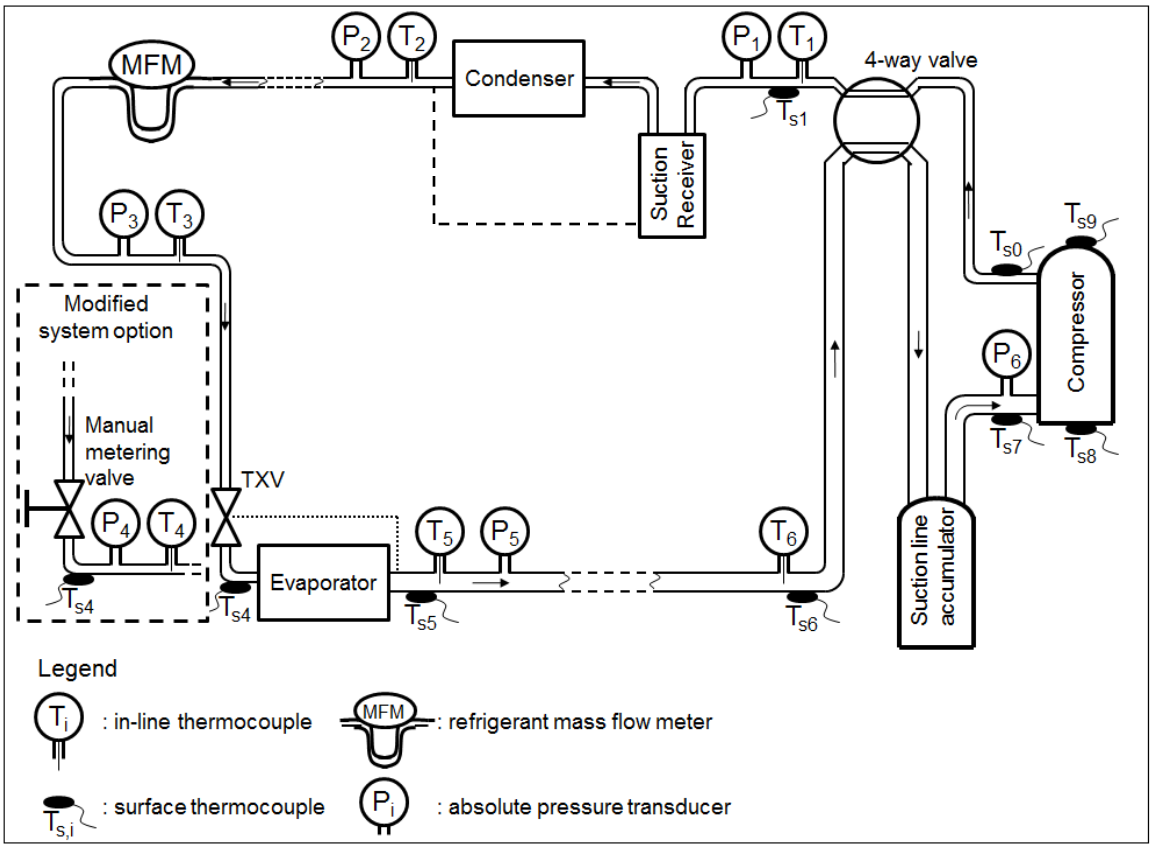

Figure 7: Refrigerant side instrumentation of the experimental setup

With the original unit it was not possible to put sensors after the TXV because the distributor was connected directly after the TXV. When the TXV was later replaced with a manual expansion valve, as shown in Figure 8, during the soft optimization of TXV, P_4 and T_4 were installed right after the TXV to measure the pressure drop across the coil. The details of the soft optimization will be discussed later in the test procedure sub-section. After the evaporator, P_5 and T_5 were installed to measure the properties at evaporator outlet. Although the pressure transducer at compressor suction was placed right before the suction port, the inline thermocouple to the suction temperature was located before the 4-way valve and at about 3ft of pipeline distance from the compressor suction port.

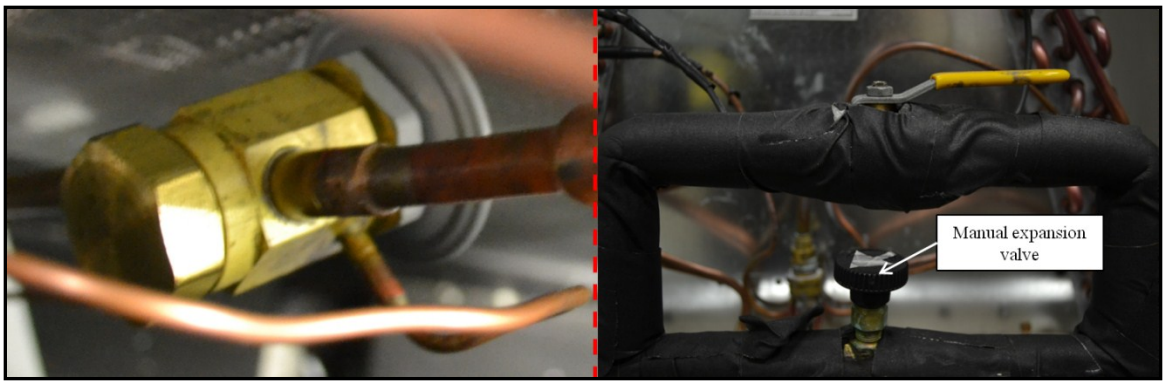

Figure 8: TXV (left side) and Manual metering valve (right side)

The suction pressure is directly measured by using the outdoor unit access valve, shown as P_6 in Figure 7. The port for P_6 is at only few inches from the compressor suction port. There was not enough space to install a pressure transducer right after the compressor discharge port. Instead I measured the compressor discharge pressure after the 4-way valve by using the pressure transducer P_1 in Figure 7. The sensors P_1 and T_1 were located at about 2 feet of pipeline from the compressor discharge port and after the 4-way valve. Surface thermocouples were installed right at the compressor discharge and suction ports. These thermocouples and the corresponding in-line thermocouples were used to compensate for the temperature drop across the pipe line and estimate the discharge and suction temperatures. There were also surface thermocouples installed on the top and bottom shell of the compressor to monitor the compressor crankcase temperature.

For measuring the refrigerant flow rate, a Coriolis type one directional flow meter was installed in the liquid line after the condenser. The flow meter was installed on the liquid line, because its accuracy is better when the liquid fluid is circulated on the flow meter. The flow meter was from Micromotion, model: CMF025 Elite, serial no: 14090445, with a nominal range of 100 to 4750lb_m/hr and an accuracy of ±0.1%. Because the outdoor room goes to very high and very low temperatures, the flow meter was placed on the liquid line in the indoor room to ensure safety of

the electronics. The flow meter being one directional had to be associated with a set of 4 ball valves since the direction of the refrigerant flow changes for cooling and heating operation. As shown in Figure 9, for cooling operation the refrigerant flow was from right to left and only ball valves 1 and 2 were open. For heating operation only ball valves 3 and 4 were open so that the flow always passes through the flow meter in the same direction.

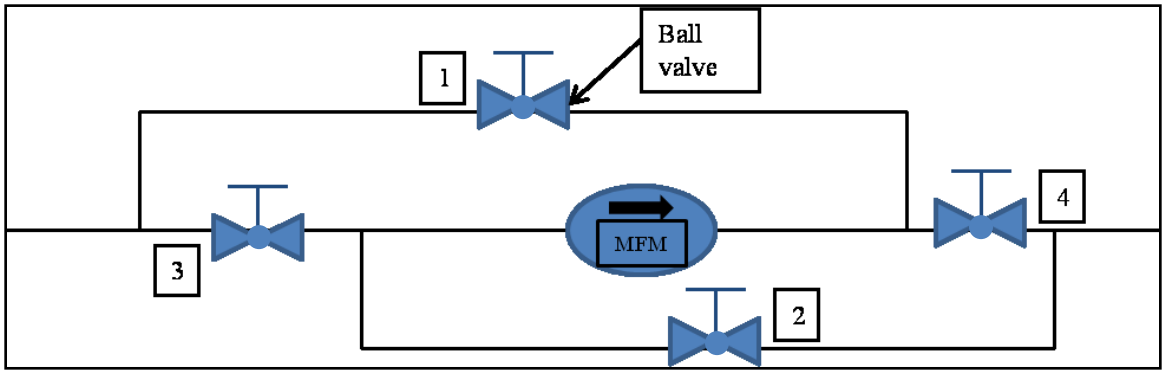

Figure 9: Directional flow corrector for mass flow meter

Air side instrumentation

Although the refrigerant side measurements were important to understand the cycle and functioning of the unit, the primary measurements being used for capacity and performance calculation were determined from the air side instrumentation. For maintaining the standard dry bulb and wet bulb temperatures in the outdoor chamber, a sampling tree was placed in front of the outdoor unit as shown in Figure 3. A sampling tree is an instrument that mechanically averages the air around it and then takes the air through a 4" silver flexible duct to the wet bulb probe, which is a psychrometric device used to measure the dry bulb and wet bulb temperatures of the air using very precise temperature sensor RTD and following ASHRAE standard 116. A typical sampling tree and a wet bulb probe are shown in Figure 10. Details about the construction and working principle of the wet bulb probe can be found in Worthington *et al.* (2011). In addition to

the RTDs, as a secondary checkpoint RH sensors are used in the wet bulb probes as well. The RH values measured with the RTDs and the one measured from the RH sensor had to be within 3% as the checkpoint of a good calibration before commencing the test.

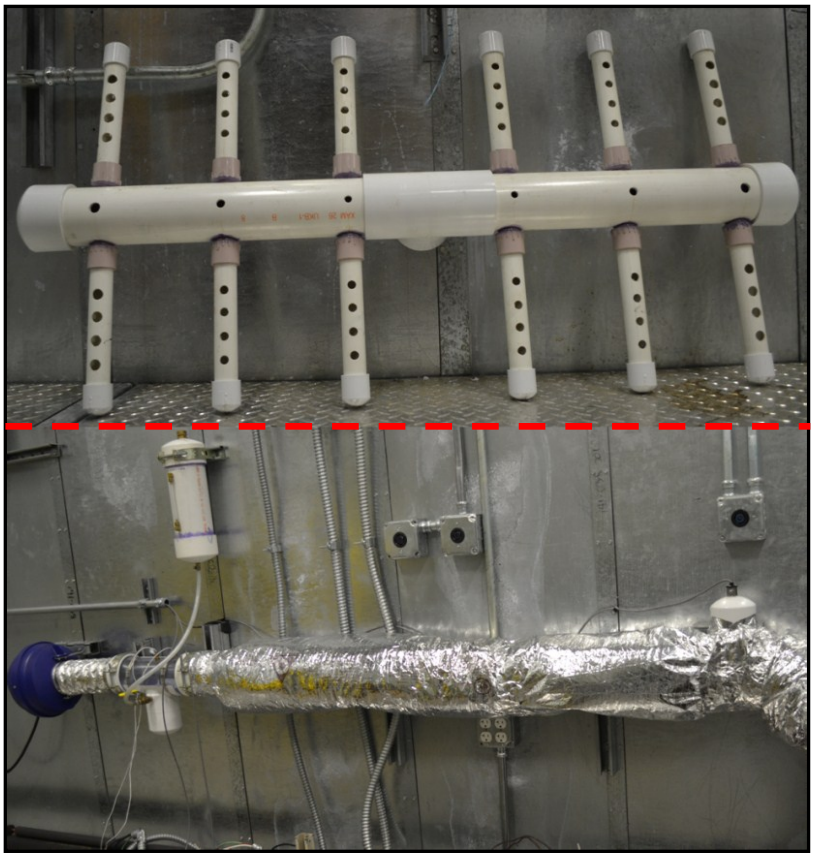

Figure 10: Sampling tree (top) and Wet bulb probe (below)

Similar approach was followed for measuring the psychrometric properties of the indoor ambient and unit return air. The sampling probe was placed beneath the indoor unit at the coil inlet of air and it was connected to a wet bulb probe similar to the one shown in Figure 10.

For measuring the supply air properties the sampling probe was placed right near the bend of the ductwork shown in Figure 6 and was connected to a wet bulb probe located inside the indoor code tester as shown in Figure 3. Because there was about 15 ft (4.6m) distance from the sampling tree to the wet bulb probe some discrepancy in the measured and the supply

temperatures was observed. To account for this a mesh of 5 thermocouples was installed before the sampling tree at only 4ft (1.2m) from the blower discharge section to measure the average supply temperature inside the rectangular duct. The calculation approach of the supply air properties is later discussed in the data reduction section. Additionally, to see the temperature distribution after the indoor coil, a mesh of 7 thermocouples was installed right after the coil.

In order to measure the air side pressure drop across the supply and return of the indoor unit, one pressure tap was open to the ambient and another pressure tap was open to the supply air inside the duct at a height of 4ft from the unit outlet. These two taps were connected to a differential pressure transducer. To make sure that the pressure at the supply air is well averaged, a set of 4 pressure taps along the periphery of the rectangular duct was installed, as shown in Figure 11.

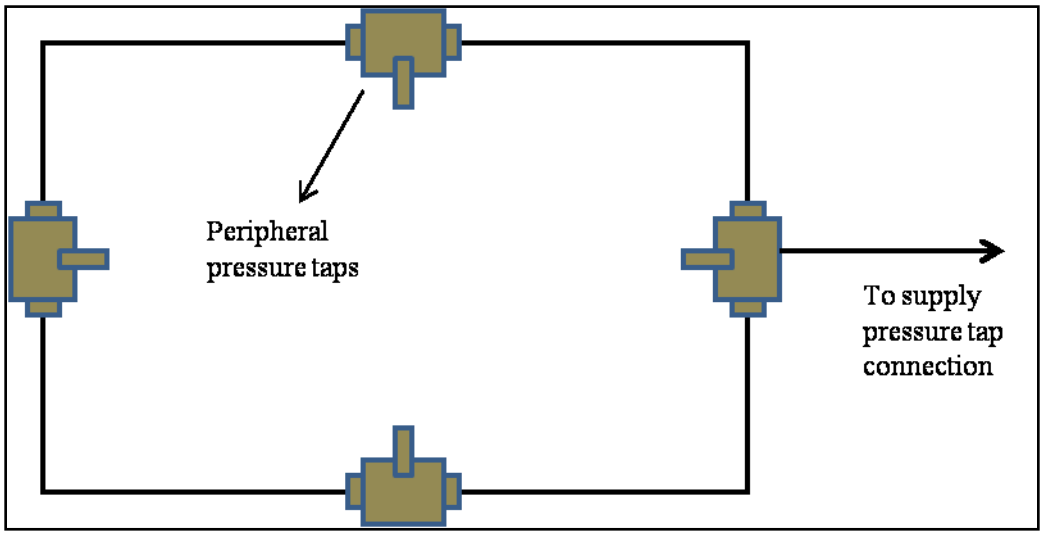

Figure 11: Pressure taps in the supply duct

The volume flow rate of air was measured using an in-house nozzle bank located at the code tester of the indoor chamber. The supply air would be blown through the aluminum duct and then via the box, entered the flexible duct and was carried to the code tester. The nozzle bank is inside the code tester just below an in-house blower and on top of a set of dampers. The nozzle bank

consists of 9 nozzles, as shown in Figure 12: 6 of them have diameter of 5.5", 2 of them 4" and one has diameter of 3". Pressure taps across the nozzle bank measured the pressure drop. Knowing the desired flow rate and the desired pressure drop, only a number of nozzles were kept open and the others were closed with plastic film and duct tape. The nozzle configuration for this experimental campaign is shown later in Figure 21. The flow rate was calculated using a Lab View code by taking the nozzle free flow area and pressure drop across nozzle as inputs. The code tester blower speed was adjusted to maintain a desired external static pressure between supply and return to 0.2 inWC. In addition the pressure drop across the nozzle bank was set in the range of 2 to 3 inWC.

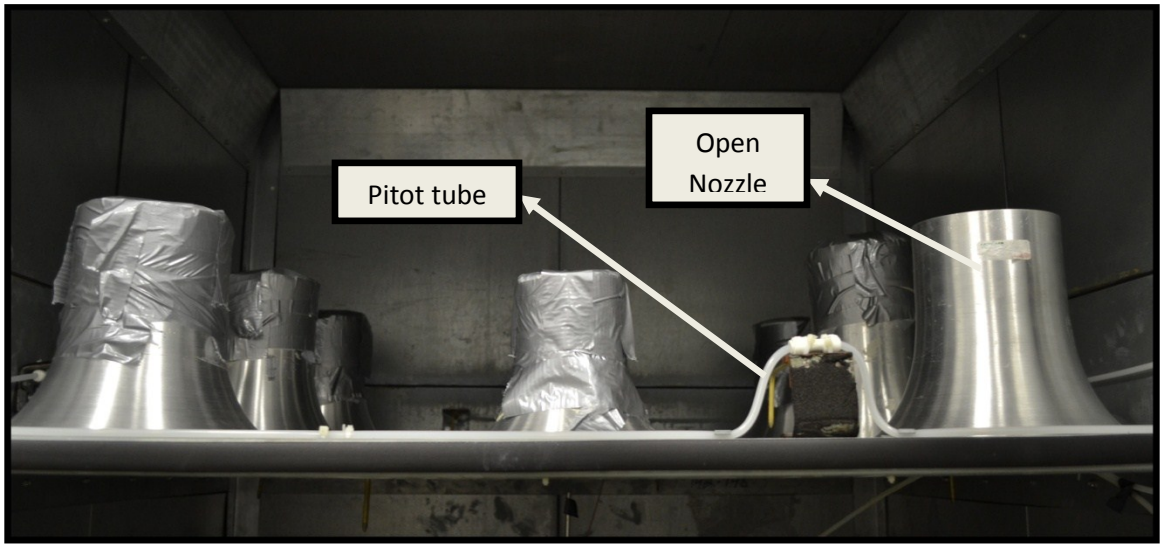

Figure 12: Flow nozzle bank

The combined power of the outdoor unit fan, the compressor and the indoor unit blower was measured with a watt transducer, as shown in Figure 13. It is a 3000V and 50A transducer and had a 4-20 mA current output representative of the electric power in watts. The unit power is required to determine the performance of the unit during its runtime.

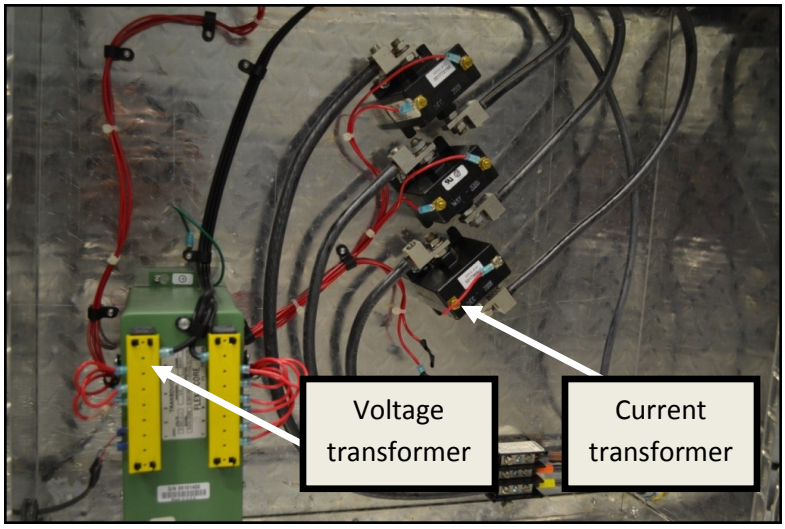

Figure 13: Watt transducer

The unit was connected to a control board provided by the manufacturer, which on the other side was connected to the DAQ system and Lab View controls of the chamber, as shown in Figure 14. Thus the blower, the compressor and the reversing valve could be actuated individually from Lab View. The defrost controls were also on-board.

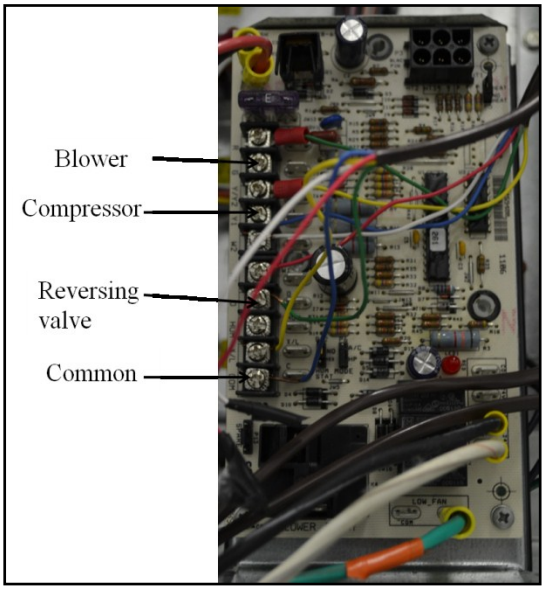

Figure 14: Unit control circuit board

Data Acquisition

The built-in data acquisition system of the chamber was used for acquiring all the data from the sensors to the chamber computer for further processing. While the details of the data acquisition system can be found in Worthington *et al.* (2012), I am going to describe briefly here in this sub-section.

As shown in Figure 15, all the sensors other than the thermocouples were powered using relays and the relays could be turned on from Lab View main program. Once the sensor is powered, it senses the corresponding quantity as a resistance and sends a current or voltage output through the wiring first to the DAQ box and then to the National Instruments PXI via the terminal block and module. The signal is then sent to the main Lab view code called 'Target'. The signal is processed, converted to the variable value and then sent for further processing and monitoring to the secondary Lab View code named 'Host'.

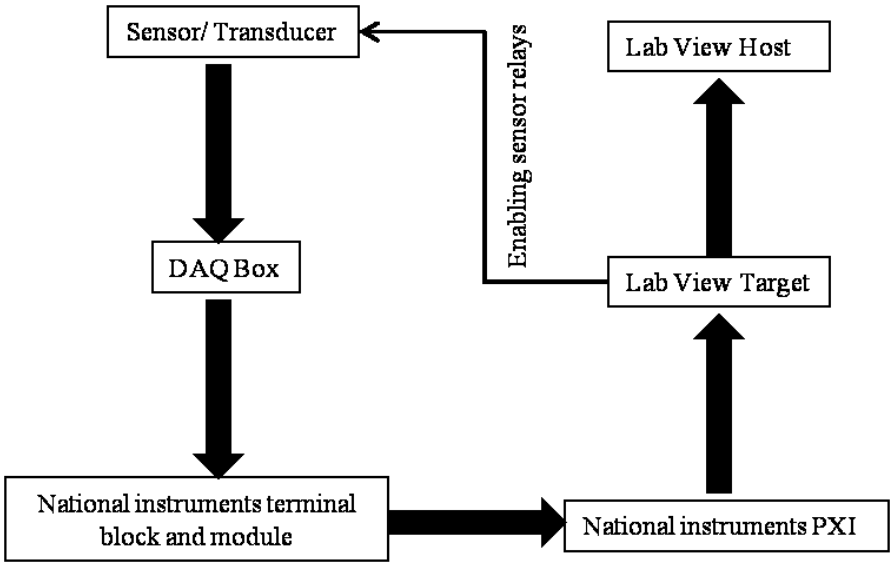

Figure 15: Data acquisition system

The DAQ box, as shown in Figure 16, works as a quick connection junction for the chamber DAQ and the sensors. There are terminal strips for connecting the thermocouples and speaker connectors for connecting RTDs and other in/out signals.

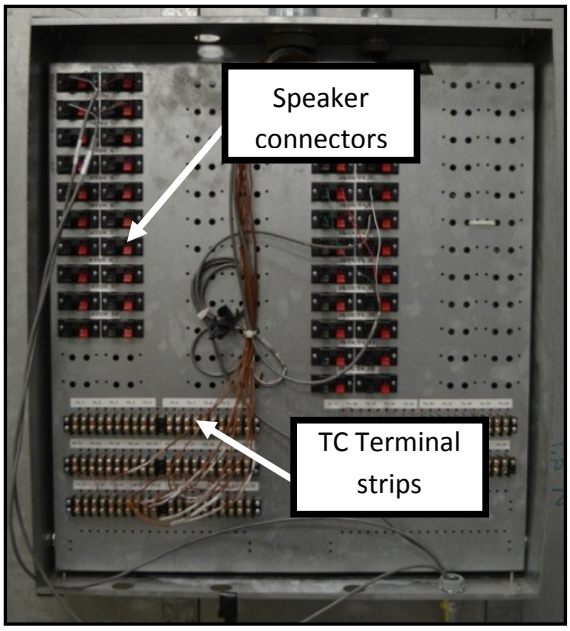

Figure 16: DAQ box

From the back of the DAQ box, the wires go to the corresponding National instrument terminal block and module, as shown in Figure 17. There are different dedicated modules for thermocouples, RTDs, relays and other input signals. All the modules are put into the slots of NI SCXI-1001 cards. There are two of them in the chamber DAQ system. The cards are connected via data cables to NI PXI-1042Q, which acts like a CPU. The Lab View code is loaded in to the PXI. So eventually when all the channels in the modules are configured by automation explorer, which is more like an OS to a normal computer, the sensors are ready to be read in Lab View for further processing. Besides the two SCXIs, there are also 2 SCB-68 cards connected to the DAQ system, which can send analog or digital output signals. These two are mainly used for controlling variable frequency driven devices. All the channels in the DAQ system are referred to by index numbers in the order they are read by the PXI.

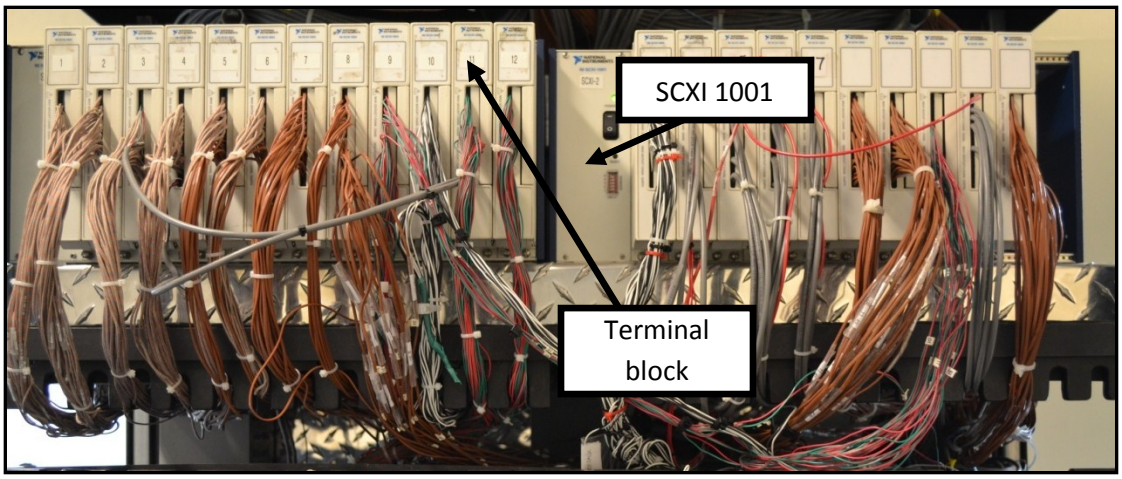

Figure 17: National instruments SCXI and modules

The DAQ system of all the in-house instrumentation of the chamber has been discussed in Worthington *et al.* (2012). The instrumentations adhered to this particular work are tabulated in Table 12 of the Appendix B. The function of the refrigerant side thermocouples and pressure transducers are described referring to Figure 7.

Lab View

The Lab View real time software for the chamber had two main VI (Virtual instruments). The first one was the 'target', that ran in the remote PXI while the second one was the 'host', that ran in a common CPU. The function of the target was to read in all the sensors dedicated to the chamber, convert them to engineering units, control and monitor the chamber conditioning and ensure safe operation of the chamber equipments. All the data were processed in the target and then sent to the host computer for further processing, mostly for creating graphical user interfaces and plotting graphs dedicated to individual projects. Both the target and host were designed with user friendly graphical interfaces that make monitoring the system intuitive. The details of the graphical interface and its associated hard coding and the wiring diagrams have been described in

(Worthington, 2011). Some of the screenshots of the target interface have been attached to Appendix C. In this sub-section only the portions of Lab View related to this particular work is going to be discussed.

Figure 18 shows the outdoor and indoor room conditioning interfaces on the target. For both the rooms the user had to specify the desired dry bulb and wet bulb temperatures as per the standards and turn the heater and humidifier on to let the PID to take control of conditioning the room and attain steady state and stable temperatures. The user could fine tune the proportional, integral and derivative gains of the PID controls. The PID gains used throughout this campaign are listed in Table 6.

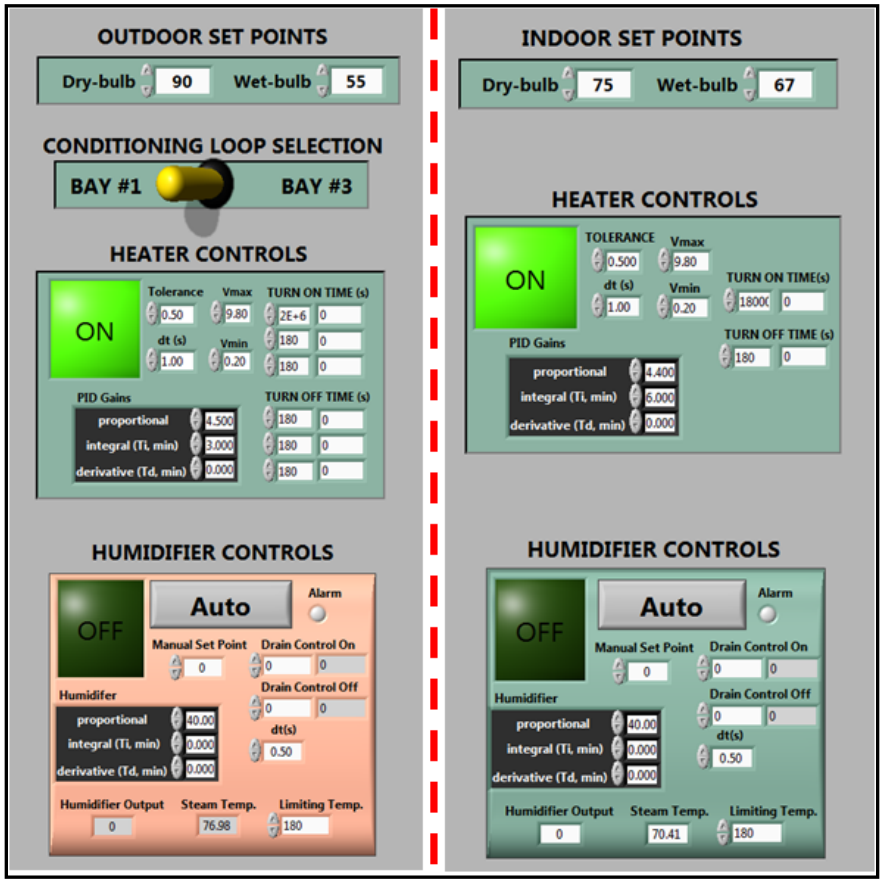

Figure 18: Outdoor and indoor room conditioning on Lab View

Table 6: PID gains

	Proportional	Integral	Derivative
Outdoor heater	4.5	3.0	0.0
Indoor heater	4.4	6.0	0.0
Humidifier	40.0	0.0	0.0

As discussed earlier, the unit was controlled through control wires connected to a circuit board. The control wires were activated by relays administrated from target Lab view target interface in the 'HVAC unit' tab, as shown in Figure 19. Here not only the relays for the blower, the compressor and the four way valve can be activated, but also the unit power, and high and low side pressures could be monitored to investigate if the unit has really started running or not. For cooling mode operation, the blower (G), the reversing valve (O) and the compressor (Y1) were activated. For heating mode, only the blower (G) and the compressor (Y1) were activated.

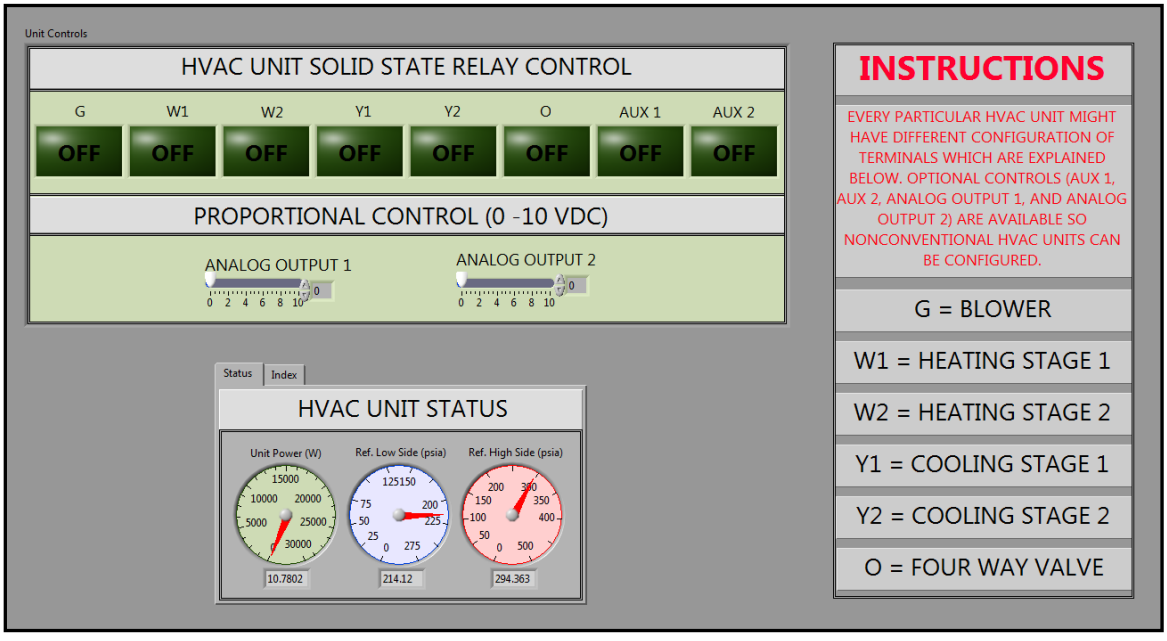

Figure 19: Unit solid state relay control on Lab View

Figure 20 shows the code tester interface, where the user can adjust the in-house blower speed and the damper positions in order to get the desired flow rate and pressure drop across the unit. The psychrometric condition of the code tester and the nozzle temperatures are monitored here as well. Another function of the target VI is to establish the shut-off limits for the unit operation. There were cut-off limits set for high discharge pressure, low suction pressure and high unit power. If any of those limits were reached during the test, then the LabView controls I developed in this thesis automatically shut down the unit. This was a safety procedure of the LabView controls.

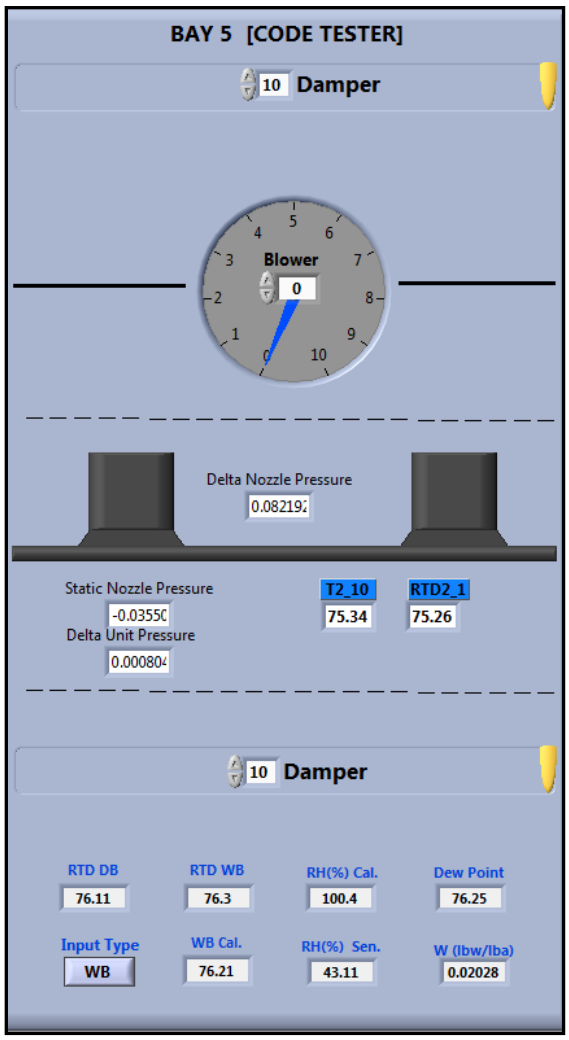

Figure 20: Code tester interface

Once all the sensors are read in the target, they are sent over to the host computer and the secondary Lab View code is used to graphically represent the data associated with a particular project. Figure 21 shows the flow nozzle selection interface for a desired flow rate and the nozzle configuration for the present work. The user would put a desired value of flow rate and Lab View would recommend a nozzle configuration based on the code following ASHRAE standards 216. The user still has to configure the nozzle bank manually as suggested in the instrumentation sub-section.

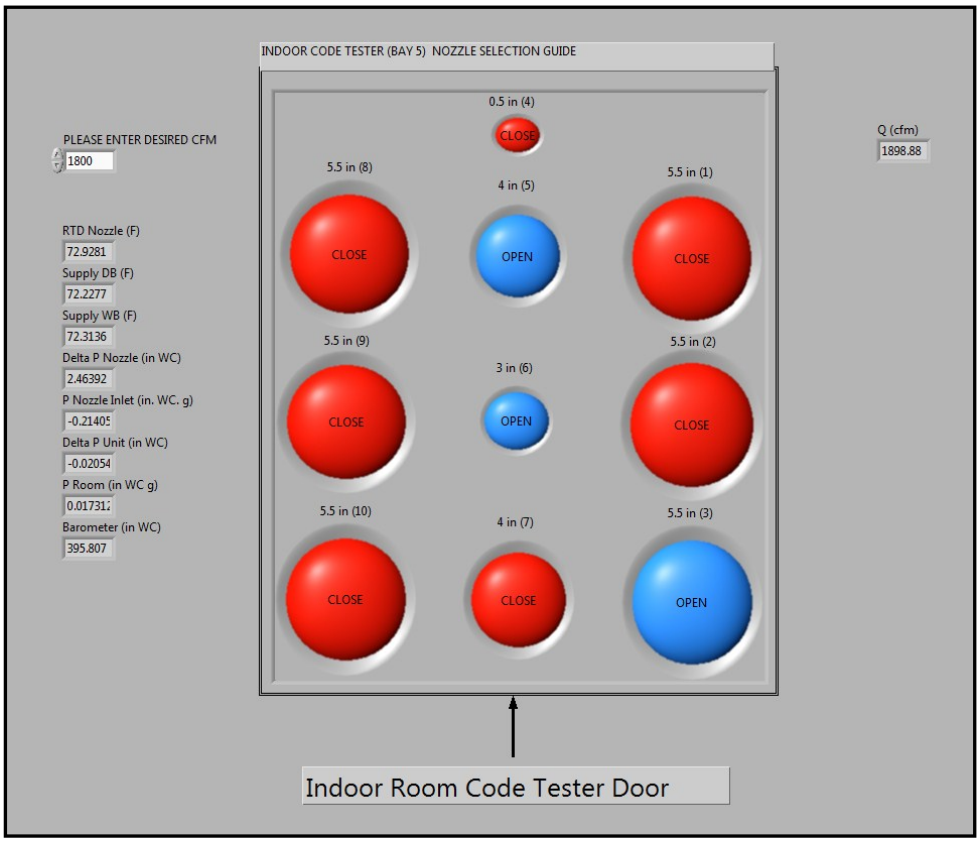

Figure 21: Host interface for the nozzle bank

Figure 22 and Figure 23 represent two different tabs for monitoring the heat pump setup in cooling and heating modes respectively. They show all the components and instrumentation on the refrigerant side. All the data are displayed every 2 seconds.

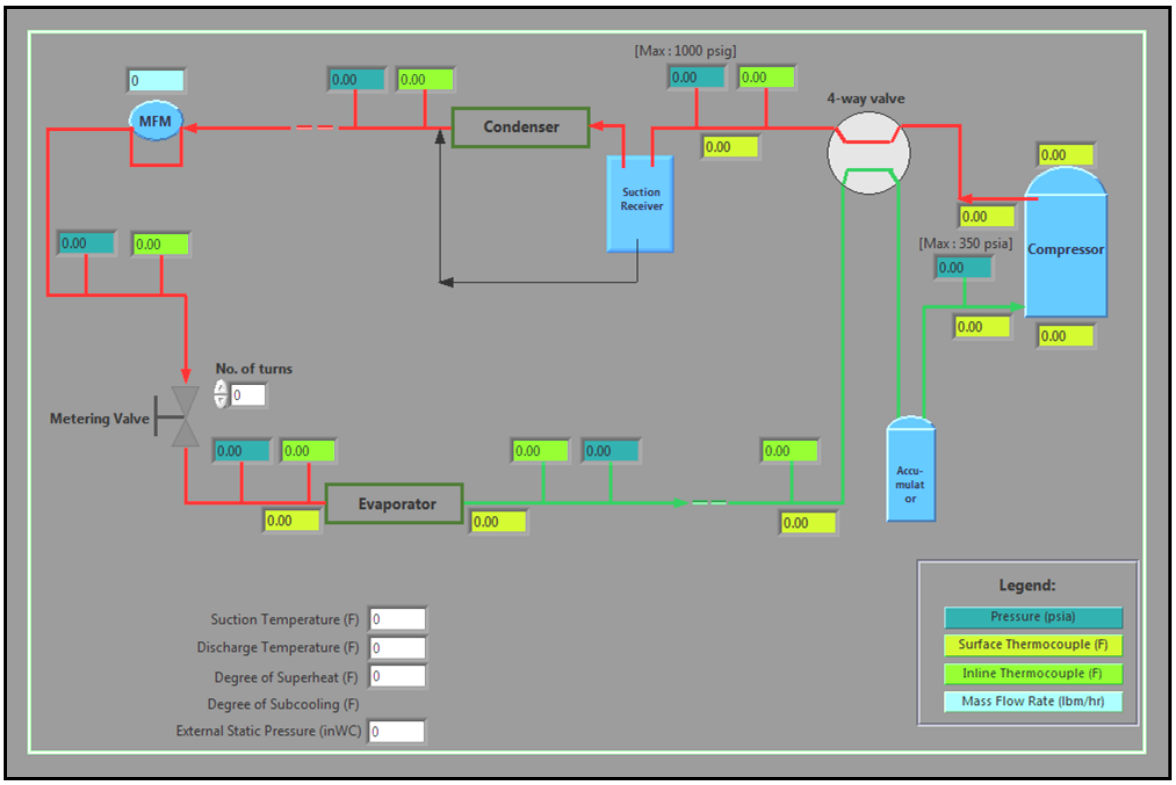

Figure 22: Heat pump setup in the host (cooling mode)

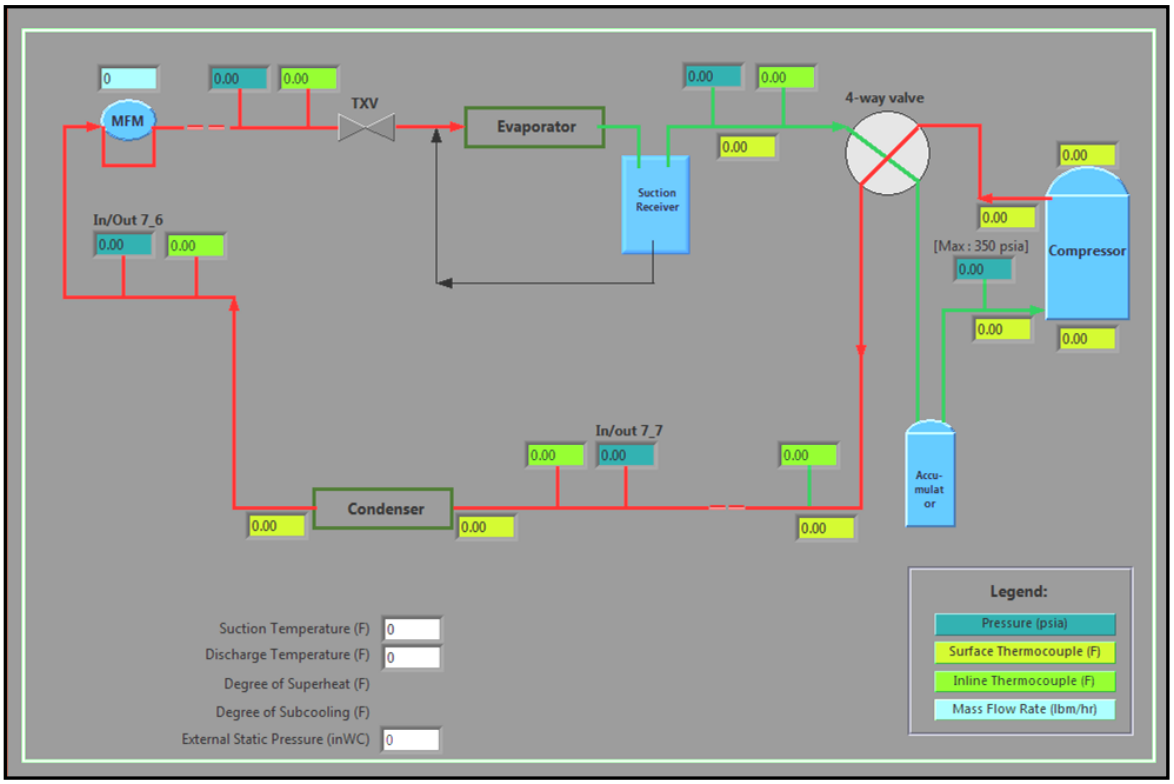

Figure 23: Heat pump setup in the host (heating mode)

In addition to the loop diagrams, for closer monitoring of the system steadiness and stability, there are plots of pressures, temperatures and flow rate being displayed. The instantaneous unit power, system capacity and COP are calculated and plotted as well, as shown in Figure 24.

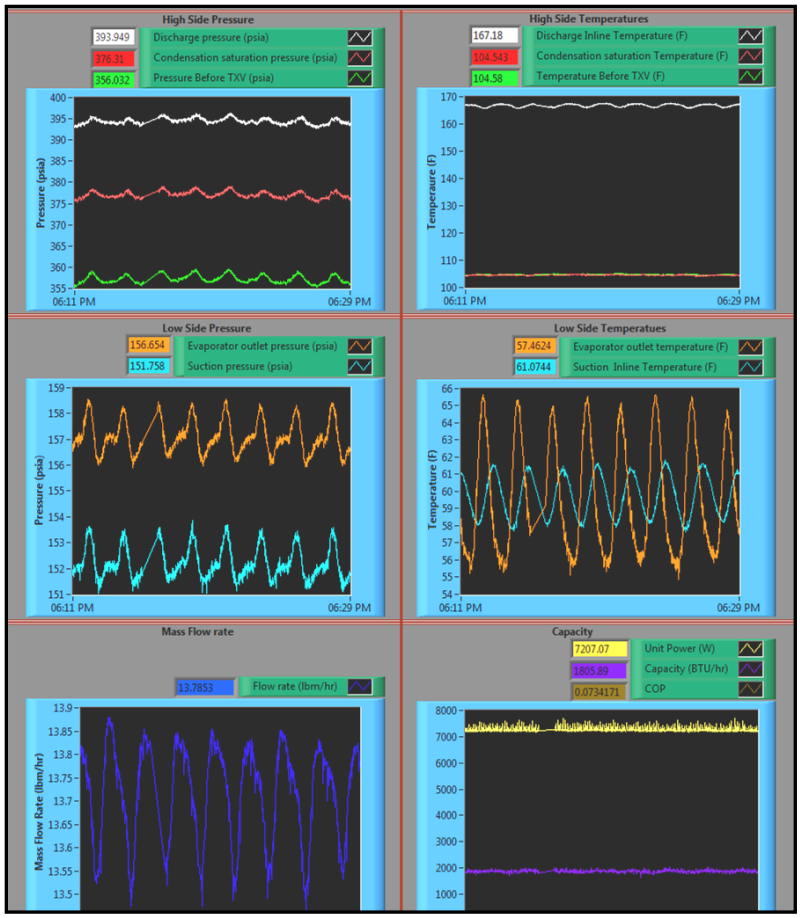

Figure 24: Plots for monitoring the refrigerant side in the host

Figure 25 shows the interface where the thermocouples for the supply temperature and the temperature distribution across the indoor coil are displayed. The plot of the supply thermocouples is mostly useful when there is frost-defrost cycling during heating conditions. It is very easy to identify the initiation of defrost cycles by monitoring the plot. The mesh temperatures are useful to monitor as well because they tell the user if the evaporator is flooded or not.

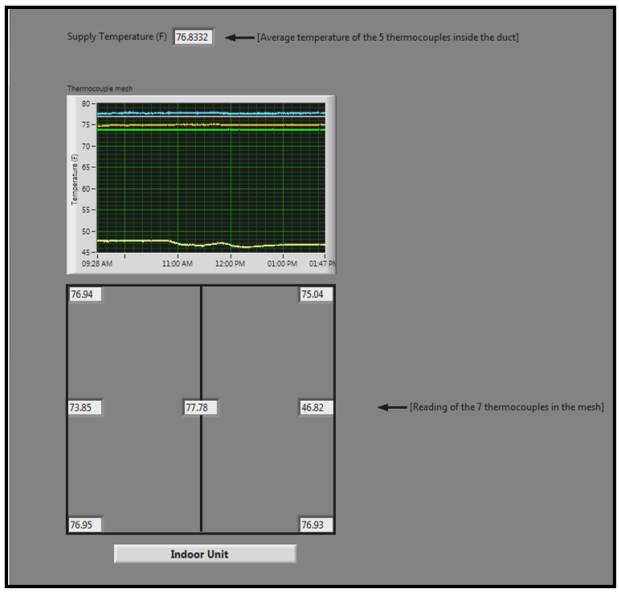

Figure 25: Monitoring the airside in the host

A sample wiring diagram window in the host VI is shown in Figure 26. The wiring is done in a clean and formatted way so that the users later on can easily follow the logic of the program. The index number of the sensor is used to refer to the channel that it is being read in. Necessary calculations, logical and numerical operations are performed in the wiring diagram as well.

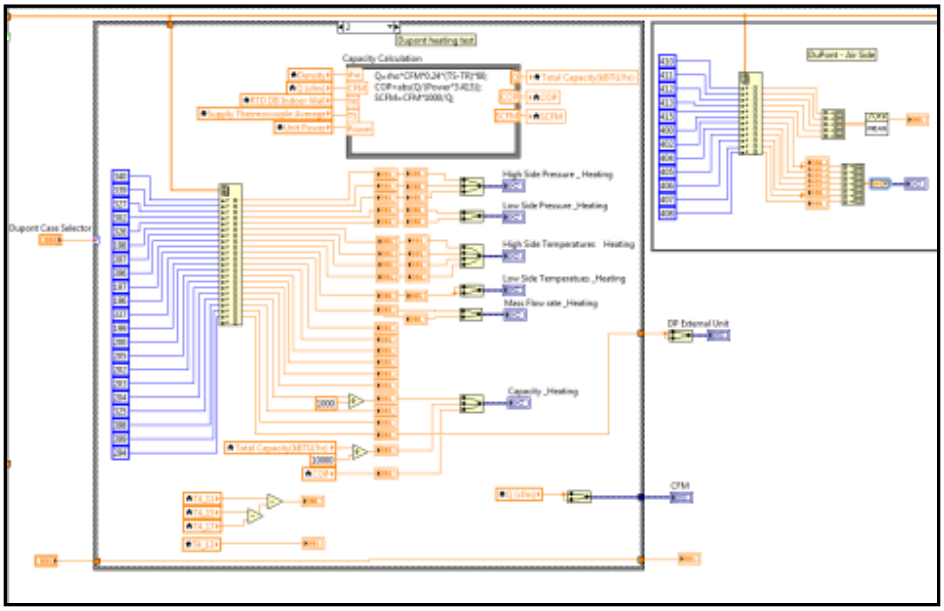

Figure 26: Wiring diagram window in the host

After the system reached steady state and required conditions, data are recorded using a recording module in the Lab View host, as shown in Figure 27. User can specify the recording rate and the duration. The general procedure is to record the data for an hour at each test condition with a rate of 2 seconds for each sample. The recorded data is saved as a text document, which can be opened in an excel spreadsheet for data reduction and analysis.

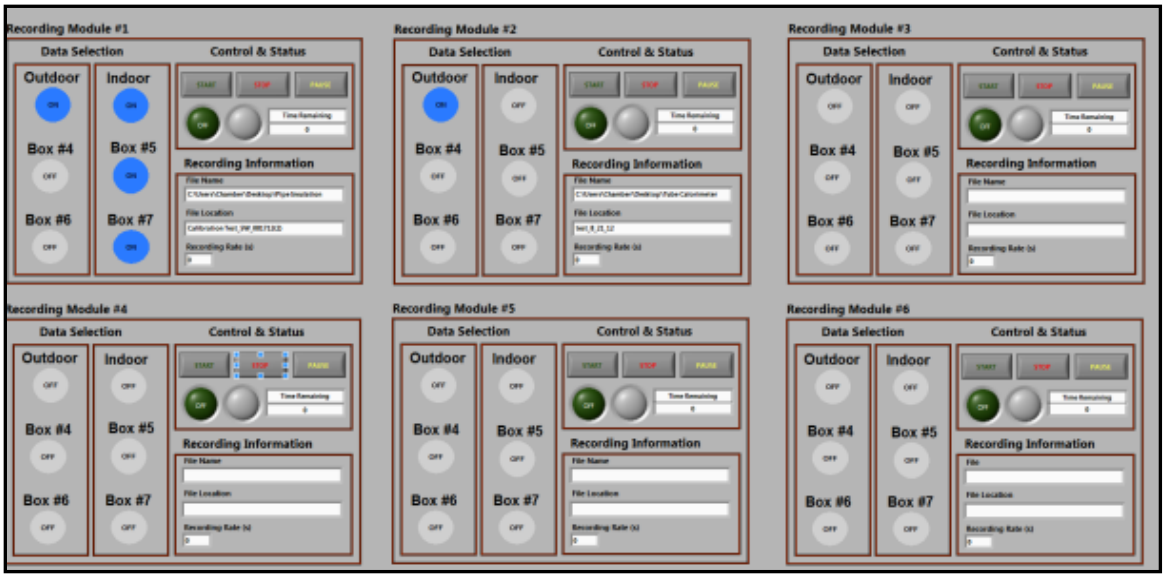

Figure 27: Recording module

CHAPTER V

DATA REDUCTION

This section is mainly dedicated to the process of reducing the data from the sensor readings to meaningful quantities. The process starts from recording the data in an excel spreadsheet as discussed before, then scanning through the data for necessary parameters and finally using basic thermodynamic relations, such as mass and energy balances to come out with quantities such as the system capacity and COP.

As any instrumentation has some uncertainty involved with it, there is bound to be a propagation of error throughout the calculation. Although the effort is to keep the systematic error to the minimum, for example by calibrating the thermocouples and RTDs to increase their accuracy level, there are still precision errors involved with all the instrumentation. It is important to point out the level of uncertainty and also study the parametric effect of different inputs in the measurement of critical quantities. An uncertainty analysis is carried out and described in this section.

.

Data reduction

The primary calculations of the system capacity and performance are based on the air side measurements and the indoor side air enthalpy method. Engineering Equation Solver (EES) is used to determine the properties of moist air. The refrigerant side calculations are mainly used as secondary method to check the accuracy of the instrumentation before commencing a test.

Air side calculations

First of all, the volumetric flow rate ($\dot{V}$) of air is calculated from the nozzle bank data using ANSI/ASHRAE Standard 41.2. The density of air (ρ_{air}) and Specific heat (C_p) values are determined as functions of the nozzle dry bulb tempertaure and the supply humidity ratio (ω_{supply}). Then the mass flow rate of air ($\dot{m}$) is calcualted using equation (5-**1**)

$$\dot{m} = \dot{V} * \rho_{air} \tag{5-1}$$

The supply humidity ratio is a function of the dry (DB_{supply}) and wet bulb (WB_{supply}) temperatures measured in the code tester wet bulb probe, and supply pressure (P_{supply}). Once this value is known, it is used along with the average temperature of the 5 thermocouples placed inside the duct ($T_{supply, avg}$) to calculate the supply enthalpy (h_{supply}). The water liquid enthalpy (h_f) and vapor enthalpy (h_g) are measured at $T_{supply, avg}$ as well.

The air return properties, such as the return enthalpy (h_{return}) and return humidity ratio (ω_{return}) are directly measured with the dry (DB_{return}) and wet bulb (WB_{return}) temperatures measured in the room wet bulb probe.

The total airside system cooling capacity ($Q_{total,\ air}$) is then calculated using equation (5-2):

$$Q_{total,\ air} = \dot{m} * (h_{return} - h_{supply}) \tag{5-2}$$

Sensible ($Q_{sensible}$) and latent (Q_{latent}) capacities are calculated respectively using equations (5-3) and (5-4).

$$Q_{sensible} = \dot{m} * C_p(T_{return} - T_{supply,avg}) \tag{5-3}$$

$$Q_{latent} = \dot{m} * (h_{g-}h_f) * (\omega_{return} - \omega_{supply}) \tag{5-4}$$

Where T_{return} is the dry bulb temperature of the return air (in °F or °C). $T_{supply,\ avg}$ is the average of the temperatures from 5 thermocouples in the supply duct. For heating, the total capacity is equal to the sensible capacity, as there is no moisture removed during the process. The value of $T_{supply,\ avg}$ is bigger than T_{return} though.

The latent heat is also measured using a mass balance method by collecting and weighing the condensate from the indoor unit. A latent heat balance is carried out using equation (5-5) to make sure that the air side measurements are accurate enough. A value 0f 10-15% is considerably good enough.

$$HB_{latent} = \frac{Q_{latent} - Q_{mass}}{Q_{latent}} * 100\% \tag{5-5}$$

Where, Q_{mass} is the latent heat of vaporization estimated by collecting the mass of water, calculated using

$$Q_{mass} = \frac{1}{t} * m_w * h_{fg} \tag{5-6}$$

Where, m_w is the mass of water collected in time period of the test, t and h_{fg} is the latent heat of vaporization.

Once the system capacity was measured, it was divided by the total unit power to measure the co-efficient of performance (COP), both in terms of Btu/hr as in equation (5-7).

$$COP = \frac{Q_{total,air}}{W_{unit} * 3.413} \tag{5-7}$$

Where, W_{unit} is the measured unit power, that is compressor power plus outdoor fan power plus indoor blower power.

Energy Efficieny Ratio (EER) is another quantity to denote the system performance with the unit power in watts and system capacity in Btu/hr, as in equation (5-8).

$$EER = \frac{Q_{total,air}}{W_{unit}} \tag{5-8}$$

A standard volume flow rate (SCFM) was also calculated in terms of per Btu/hr of refrigeration produced, as in equation (5-9).

$$SCFM = \frac{\dot{V}}{Q_{total,air}} \tag{5-9}$$

For the frost-defrost H2 test condition, the averaged integrated capacity, power and EER values are calculated using the set of equations listed below. First of all, the differences between the supply and return temperatures are integrated over time as γ as in equation (5-10). The average integrated capacity is calculated as a function of volume flow rate, C_p, humidity ratio at the nozzle, specific volume at the nozzle and the duration of a full frost-defrost cycle, as suggested in equations (5-11) and (5-12). Then the averaged EER value is calculated by dividing it with the averaged integrated power (E_h) as in equations (5-13) and (5-14).

$$\gamma = \sum [(T_{supply,avg} - T_{return}) * 2/3600] \tag{5-10}$$

$$C_p = 0.24 + 0.444 * W_n \tag{5-11}$$

$$Q_h = \frac{60 * \dot{V} * C_p * \gamma}{t_{cycle} * V_n * (1 + W_n)} \quad (5\text{-}12)$$

$$E_h = \frac{\sum[W_{unit} * 2/3600]}{t_{cycle}} \quad (5\text{-}13)$$

$$Averaged\ EER = \frac{Q_h}{E_h} \quad (5\text{-}14)$$

Where, Q_h is the average integrated capacity. C_p, W_n and V_n are respectively the specific heat, humidity ratio and specific volume of air at nozzle dry-bulb temperature. t_{cycle} is the time from the end of one defrost cycle to the end of the next one. E_h is the average integrated power.

Refrigerant side calculations

All the refrigerant side enthalpies, entropies and saturation properties were calculated either with EES or manually using the tables provided by the refrigerant manufacturer. As described previously in the instrumentation sub-section, there were some modifications required in the temperature measurement of the inline thermocouples. With reference to Figure 7, the modified temperatures are as shown below:

$$T_{Suction} = T_6 - (T_{s6} - T_{s7}) \quad (5\text{-}15)$$

$$T_{Discharge} = T_1 + (T_{s0} - T_{s1}) \quad (5\text{-}16)$$

These corrections allow to estimate the actual refrigerant temperature at suction and discharge from the nearest wall surface temperature by interpolation.

Refrigerant side capacity is essentially calculated from the mass flow rate of refrigerant ($\dot{m}_{ref}$) and the enthalpy difference across the indoor coil, regardless of cooling or heating operation, as is equation (5-17).

$$Q_{total,\ ref} = \dot{m}_{ref} * (\Delta h) \quad (5\text{-}17)$$

The enthalpy difference, Δh for cooling and heating are respectively as below:

$$\Delta h = h_{indoor\ coil,out} - h_{indoor\ coil,in} \quad (5\text{-}18)$$

$$\Delta h = h_{indoor\ coil,in} - h_{indoor\ coil,out} \quad (5\text{-}19)$$

Where, $h_{indoor\ coil,\ in}$ and $h_{indoor\ coil,\ out}$ are the refrigerant enthalpies at the inlet and outlet of the indoor coil.

As the inlet fluid at the evaporator inlet is in two phase, it is not possible to measure the enthalpy just from the pressure or temperature. So it is measured with the assumption that the expansion process is isenthalpic, or the enthalpy at the indoor coil inlet is equal to the TXV inlet enthalpy. The coil inlet quality can also be measured with this assumption. The properties at the evaporator outlet, compressor suction and compressor discharge are measured from the superheated vapor table whereas the properties at condenser outlet and TXV inlet are calculated assuming sub-cooled liquid. It is ensured from the saturation properties whether there is really superheat and sub-cooling though. These quantities are measured from the difference in the saturation temperature and the actual temperature.

The compressor work and the outdoor coil capacity are calculated as well with the refrigerant flow rate and enthalpy change across those components. A refrigeration loop energy balance is carried out, showed in equation (5-20) to check if there were any heat losses due to improper insulation and if the instrumentation worked properly and was properly calibrated. In ideal cases this value should be 0, but as some heat losses through the insulation were expected or due to the precision of the instrumentation, an energy balance of 2 to 3% is considered quite good.

$$Energy\ balance = \frac{(Q_{condenser} - (W_{compressor} + Q_{evapaorator}))}{Q_{condenser}} * 100\% \quad (5\text{-}20)$$

As shown in Figure 28, the energy balance residual for all the tests done during this campaign are well within ±3%.

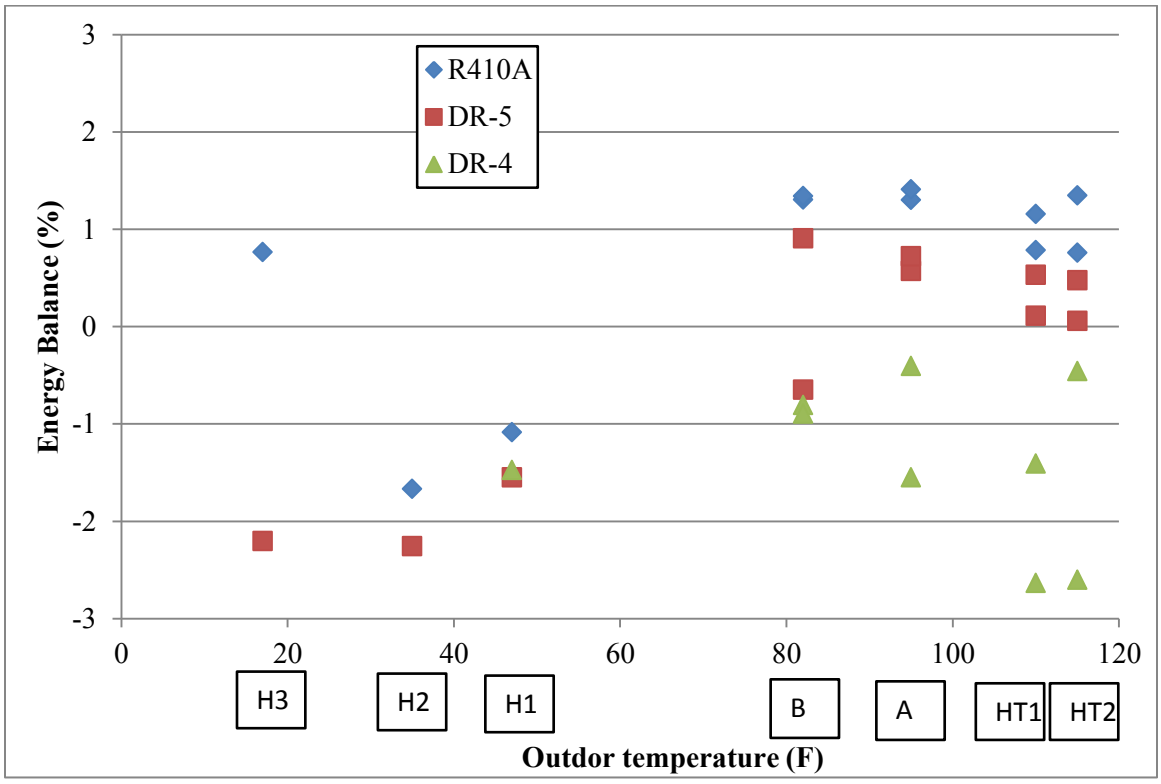

Figure 28: Energy Balance on tests

For the TXV soft-optimization tests, the pressure drop across the evaporator is as in equation (5-21).

$$\Delta P_{evaporator} = P_{evap,in} - P_{evap,out} \quad (5\text{-}21)$$

Where, $P_{evap,\,in}$ and $P_{evap,\,out}$ are the pressures at the inlet and outlet of the evaporator.

The degree of superheat at evaporator outlet and the degree of sub-cooling at condenser outlet are calculated as governed respectively by equations (5-22) and (5-23).

$$SH_{evap,out} = T_{evap,out} - T_{sat@P=P_{evap,out}} \quad (5\text{-}22)$$

$$SC_{cond,out} = T_{cond,out} - T_{sat@P=P_{cond,out}} \quad (5\text{-}23)$$

Where, $T_{sat@P=Pevap,\ out}$ and $T_{sat@P=Pcond,\ out}$ are the saturation temperatures at evaporator and condenser outlet pressures. $SH_{evap,\ out}$ and $SC_{cond,\ out}$ are the degree of superheat at evaporator outlet and the degree of sub-cooling at condenser outlet respectively.

Compressor volumetric efficiency (η_v) is calculated by using equation (5-24) and then normalized ($\eta_{v,\ N}$) with respect to that of R410A as in equation (5-25).

$$\eta_v = \frac{Actual\ measured\ mass\ flow\ rate}{Ideal\ mass\ flow\ rate} = \frac{Actual\ measured\ mass\ flow\ rate}{(suction\ density)\ \cdot\ \dot{V}_{comp}} \quad (5\text{-}24)$$

$$\eta_{v,N} = \frac{\eta_{v,ref}}{\eta_{v,R410A}} \quad (5\text{-}25)$$

Where $\dot{V}_{comp}$ is the compressor volumetric capacity and it was estimated from the manufacture data. The suction density was calculated from the data of pressures and temperatures measured at the suction port.

Thermal efficiency of the compressor (η_T) was defined as shown in equation (5-26), and then normalized ($\eta_{T,\ N}$) with respect to R410A data by using equation (5-27).

$$\eta_T = \frac{Isentropic\ work\ of\ compressor}{Actual\ work\ done\ by\ compressor} = \frac{h_{comp,dis.,isentropic} - h_{comp,suc.}}{h_{comp,dis,actual} - h_{comp,suc.}} \quad (5\text{-}26)$$

$$\eta_{T,N} = \frac{\eta_{T,ref}}{\eta_{T,R410A}} \quad (5\text{-}27)$$

Where $h_{comp,\ dis.,\ actual}$ and $h_{comp,\ dis.,\ isentropic}$ are the actual and isentropic enthalpies at compressor discharge and $h_{comp,\ suc}$ is the compressor suction enthalpy. The isentropic work was calculated from the measurements of suction temperature and pressure and discharge pressure and the actual work was calculated based on the compressor suction and discharge temperatures and pressures. It should be noted that the discharge pressure and temperature sensors were located on the

refrigerant discharge line after the 4-way. The distance between these sensors and the compressor discharge port was about 0.6 m (2 ft) of pipeline. The 4-way valve and the refrigerant pipelines were well insulated to prevent heat losses to the ambient. However, some heat exchange was expected to occur between the hot vapor in the discharge line and the cold vapor in the suction line when the refrigerant crossed the 4-way valve.

Compressor pressure ratio (P_r) is calculated as a ratio of the discharge pressure over the suction pressure as in equation (5-29)

$$P_r = \frac{Compressor\ discharge\ pressure}{Compressor\ suction\ pressure} = \frac{P_{discharge}}{P_{suction}} \quad (5\text{-}28)$$

Where $P_{discharge}$ and $P_{suction}$ are the compressor discharge and suction pressures respectively.

Heat balance

To demonstrate that the instrumentation worked properly, was installed and connected correctly and calibrated properly a heat balance between the air side and the refrigerant side capacities was carried out for each test. All heat balance tests are reported in Figure 30 and they had a reasonable heat balance within 5%. To determine the heat balance, the first law of thermodynamics was applied on the control volume of the indoor unit. Air side capacity was considered as the base value for the heat balance. A schematic of the heat balance at the indoor unit for both cooling and heating modes is shown in Figure 29.

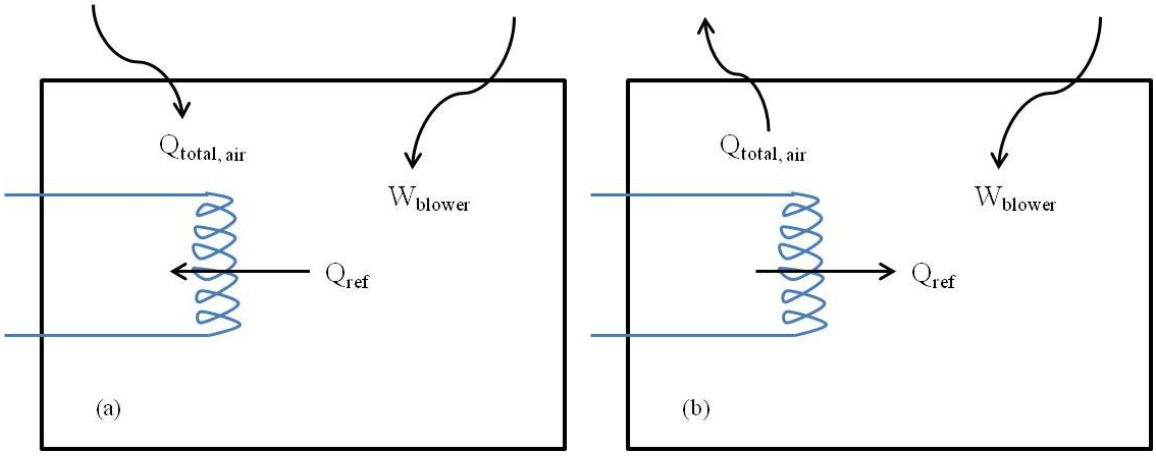

Figure 29: Schematic of the heat balance at the indoor unit for (a) cooling mode and (b) heating mode

The blower work (W_{blower}) was determined by running the blower separately and was measured to be about 1194 Btu/hr (350W). For cooling and heating mode, equation (5-29) and equation (5-30) govern the corresponding heat balances at the indoor unit.

$$HB_{cooling} = \frac{(Q_{total,air} + W_{blower} - Q_{ref})}{Q_{total,air}} * 100\% \quad (5\text{-}29)$$

$$HB_{heating} = \frac{(Q_{total,air} - W_{blower} - Q_{ref})}{Q_{total,air}} * 100\% \quad (5\text{-}30)$$

Where, $Q_{total,\,air}$ is given in equation (5-2) and Q_{ref} is given in equation (5-17).

Figure 30 shows the heat balance on all the tests done during the experimental campaign of this thesis. 80-85% of the tests are well within ±5% of heat balance. The outlying points on the plot are for tests with DR-4, where it was hard to maintain sufficient degree of sub-cooling at the condenser outlet. So the refrigerant entering the flow meter might have had some vapor entrained in the liquid and the mass flow rate of refrigerant might have been less accurate in such conditions. As a result the calculated refrigerant side capacity might not be accurate and higher heat balance was observed.

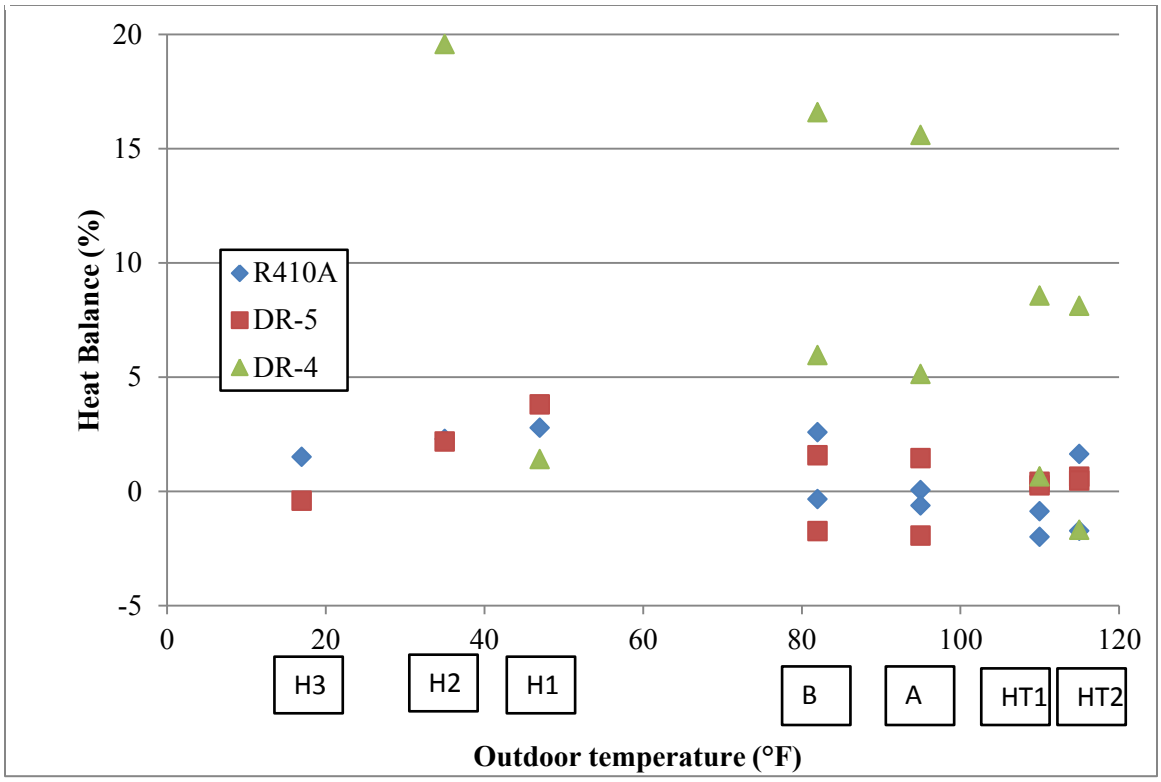

Figure 30: Heat balance on all tests conducted in the present work

Uncertainty Analysis

There is uncertainty involved with all instrumentations used in the test apparatus. Manufactures provide the accuracy of some instrumentation as a percentage of its full scale reading, whereas the thermocouples and the RTDs were calibrated in-house and in-situ using a thermal bath and a precision thermometer for better accuracy and to account for the effect of having long wires from the sensor to the chamber DAQ system. Table 7 shows the instrumentations used in the test apparatus and their accuracy level.

Table 7: Nominal values and accuracies of instrumentations

Measurement	Manufacturer	Model	Nominal Value	Accuracy level	
				Manufacturer	OSU Chamber
Unit supply DB RTD	Omega	PT-100	12.8°C to 22.5°C (55.04°F to 72.5°F)	±0.1°C (±0.2°F)	±0.05°C (±0.1°F)
Unit supply WB RTD	Omega	PT-100	12.8°C to 18.8°C (55.04°F to 65.84°F)	±0.1°C (±0.2°F)	±0.05°C (±0.1°F)
Unit return DB RTD	Omega	PT-100	19.8°C to 27.65°C (67.64°F to 81.77°F)	±0.1°C (±0.2°F)	±0.05°C (±0.1°F)
Unit return WB RTD	Omega	PT-100	11.95°C to 20.6°C (53.51°F to 69.08°F)	±0.1°C (±0.2°F)	±0.05°C (±0.1°F)
Nozzle DB RTD	Omega	PT-100	12.8°C to 22.5°C (55.04°F to 72.5°F)	±0.1°C (±0.2°F)	±0.05°C (±0.1°F)
Supply thermocouples	Omega	T-type	12.5°C to 45.1°C (54.5°F to 113.18°F)	±0.3°C (±0.5°F)	±0.05°C (±0.1°F)
Diff. PT across nozzle	Setra	Model 264	0-3 in WC	±0.25% F.S.	n/a
Diff. PT across unit	Setra	Model 264	0-3 in WC	±0.25% F.S.	n/a
Barometer	Vaisala	PTB110	0.002 to 1100 in WC	±0.12 in WC	n/a
Refrigerant gauge PT	Setra	Model 206	0-500 psig	±0.13% F.S.	n/a
Refrigerant MFM	Micromotion	CMF025 Elite	100-4500 lb_m/hr	±0.1% F.S. n/a	-
Unit power	Flex core	AGW	0 to 45,000 watts	±0.2% Rdg	-
Refrigerant charge	Topline	AWS-330BP	0 to 65 lb_m	±0.5 lb_m	-

An EES model was developed for estimating the uncertainty of the experimental setup in measuring the volume flow rate of air, system capacity and system performance. The model is presented in Appendix A: EES code for uncertainty analysis. The EES uncertainty model uses Taylor's series expansion approach by taking into account the error propagation in the measurements. The EES model also does the calculation on the percentage of uncertainty caused by a particular measurement.

Using the model, the calculated uncertainty was 3.4% on system capacity and 3.6% on COP. Table 8 summarizes the sensitivity of measurements on the calculated values for a sample B-test condition for DR-5.

Table 8: Sensitivity analysis of measurements towards error propagation

Measured quantity	% of uncertainty on air volume flow rate	% of uncertainty on airside capacity	% of uncertainty on airside COP
Barometric pressure	0.88%	0%	0%
ΔP_{nozzle}	98.75	1.2%	0.41%
ΔP_{unit}	0%	0%	0%
$P_{before\ nozzle}$	0%	0%	0%
P_{room}	0%	0%	0%
Unit power	0%	0%	65.76%
$T_{supply,\ avg}$	0%	4.86%	1.64%
DB_{nozzle}	0.35%	0%	0%
DB_{return}	0%	0%	0%
DB_{supply}	0%	5.12%	1.75%
WB_{return}	0%	53.81%	18.42%
WB_{supply}	0.01%	35.06%	12.00%

From the analysis, it is certain that the pressure drop across nozzle has maximum effect on the error propagation in CFM calculation. Thus to minimize the error, the nozzle configuration was selected such that at least 2.4 inWC were measured across the nozzle during each test. Since the full scale at the differential pressure transducer was 3inWC, the uncertainty in the volume flow rate was low.

For system capacity the most critical measurements are the WB temperatures on both the supply and the return side. Supply DB and supply mesh thermocouple temperatures have noticeable effects on the uncertainty propagation as well. These parameters have considerable effect on the uncertainty of COP calculation as well, but the most influential one is the measurement of unit power. So in order to get more accurate values of capacity and COP, the RTDs and

thermocouples have to be calibrated very precisely and also the watt transducer needs to be well suited for the range of power being measured.

Test Procedure

This sub-section describes the test procedures followed during this experimental campaign. The experiments were conducted in the psychometric chamber at Oklahoma State University (OSU) and the refrigerant cycle pressures and temperatures were measured at design and off-design conditions with outdoor temperature ranging from -8.3°C (17°F) to 46°C (115°F) and in both heating and cooling modes at full load conditions. Additional tests were conducted at extreme high temperature conditions of 43°C and 46°C (110°F and 115°F) to measure the refrigerant condensation pressure and compressor discharge temperature when the unit is exposed to hot climates. These ambient conditions are extreme but often occur during the summer months in the South and Midwest regions of the United States, as well as in the Middle East areas and Southeast Asia.

The tests were divided into two series. The first one with no modifications to the system, termed as the Drop-in tests, and the second one by changing the TXV with a manual adjustable expansion valve, referred to as the TXV soft-optimization tests.

Drop-in tests

The experimental campaign in this work focused on highlighting the direct drop-in replacement performance of DR-4 and DR-5. A series of experiments were carried out with the TXVs that were originally installed in the unit for R410A. These tests are referred to as drop-in tests.

Charge optimization was conducted for each refrigerant since the refrigerant charge is a key factor for the energy performance of an air conditioning system. Overcharging a system can impair the compressor run during off-design conditions and part load operations. On the other hand studies showed that, a system undercharge by 12 to 19 percent can cause an average reduction of about 13 percent in cooling capacity and about 8 percent in energy efficiency (Kim and Braun, 2010). The charge optimization was conducted at the AHRI 210 A cooling test conditions. Following the same procedures as described in (Barve and Cremaschi, 2012), once the control tolerances were satisfied and steady state conditions were achieved, data were recorded for 1 hour with a sample rate of 2 seconds. The average COPs and cooling capacities were calculated from the data and the refrigerant charge that provided the maximum COP was selected as to the optimum charge for the system. During the charge optimization process the degree of vapor superheat at the compressor suction was constrained to the above of at least 2.2°C (4°F). Then, with the optimum refrigerant charge, the system was run for a broad range of temperatures from -8.3°C (17°F) to 46°C (115°F) and in both heating and cooling modes at full load conditions.

The cycle thermodynamic points and flow rates were measured with outdoor temperature ranging from 27.8ºC (82ºF), referred as B-test in the AHRI standards (AHRI, 2010), to 46.1ºC (115ºF). Extreme outdoor temperature of 43.3ºC (110ºF) is referred to as HT1-test and 46.1ºC (115ºF) is referred to as HT2-test throughout this thesis (HT- refer to High Temperature). In heating mode of the unit, tests were conducted at three different outdoor conditions: H1-test of 8.3ºC DB/ 6.1ºC WB (47ºF /43ºF), H2-test of 1.7ºC DB/ 0.6ºC WB (35ºF /33ºF) and H3-test of -8.3ºC DB/-9.4ºC WB (17ºF/ 15ºF), with the indoor temperature at 21.1ºC DB (70ºF) for all the tests. H2 was a frost-defrost test, and the periodic cycle performances were recorded after at least 6 frost-defrost cycles of the unit. Average integrated capacity and EER were calculated from the transient data of the unit operating under frost and defrost conditions. The design testing

conditions are as that of described for cooling and heating mode for unitary split system having a single speed compressor and a fixed-speed indoor fan. All the testing conditions are summarized in Table 9.

Table 9: Testing Conditions

	Heat Pump Mode	Test Description	Air entering indoor unit temperature				Air entering outdoor unit temperature			
			Dry-bulb		Wet-bulb		Dry-bulb		Wet-bulb	
			°F	°C	°F	°C	°F	°C	°F	°C
Design Conditions	Cooling	A-test	80.0	26.7	67.0	19.4	95.0	35.0	-	-
	Cooling	B-test	80.0	26.7	67.0	19.4	82.0	27.8	-	-
	Heating	H1-test	70.0	21.1	60.0^{max}	15.6	47.0	8.33	43.0	6.11
	Heating	H2-test	70.0	21.1	60.0^{max}	15.6	35.0	1.67	33.0	0.56
	Heating	H3-test	70.0	21.1	60.0^{max}	15.6	17.0	-8.33	15.0	-9.44
Off-design Conditions	Cooling	HT1-test	80.0	26.7	67.0	19.4	110.0	43.3	-	-
	Cooling	HT2-test	80.0	26.7	67.0	19.4	115.0	46.1	-	-

All the cooling and heating tests were first done with R410A in the system. Once done with all the tests, R410A was recovered from the system slowly and then the system was vacuumed. Following this, DR-4 and DR-5 were charged in to the system one after another and the testing procedure described above was repeated for both of them. To observe the effect of any oil carried over during the process of recovering the refrigerants from the system on the measured performance, tests were repeated with optimum charge of R410A. As the two series of tests with R410A before and after DR-4 and DR-5 had capacity and COP within the experimental uncertainty of the test facility, the results presented in this thesis could be considered independent of the order of testing. The final values reported in this thesis were averaged for R410A from the two sets of data.

TXV soft-optimization

Additional tests were conducted to investigate the potential performance of the system with the new refrigerants when minor adjustments to the thermal expansion valve were implemented. These tests are referred in this thesis as tests with soft optimization of the TXV. The optimization is considered "soft" because it required minor adjustments of the expansion valve as compared to major changes of the system components. The TXV on the indoor coil was replaced by a manual expansion valve that served to actively control the degree of superheat at the compressor suction and to set the high side and low side saturation pressures for the new refrigerants when the unit was in cooling mode. Several tests were required to optimize the refrigerant charge with the modified expansion valve. For each charge the opening of the expansion valve was varied in a parametric fashion in search of the maximum COP at similar capacities or of the maximum capacity at similar COPs. The system performance with modified expansion valve were measured for cooling mode only and with outdoor temperature ranging from 27.8ºC (82ºF) to 46.1ºC (115ºF).

CHAPTER VI

RESULTS AND DISCUSSIONS

To validate all the measured and calculated quantities during the experimental campaign, the performance of the unit with R410A were compared against the rating performance data provided by the manufacturer. Parameters such as the supply and return temperatures, standard air flow rate, indoor capacity and EER values were compared. A summary of the comparison between the OSU data and the manufacturer data for AHRI cooling and heating tests is shown in Table 10.

Table 10: Comparison between OSU and manufacturer data for R410A

Test	**Air flow rate, $\dot{V}$**	**Capacity, Q**	**COP**	**Discharge pressure, P_d**	**Suction Pressure, P_s**	**Supply temperature**
	$\frac{\dot{V}_{OSU} - \dot{V}_{man.}}{\dot{V}_{man.}} * 100\%$	$\frac{Q_{OSU} - Q_{man.}}{Q_{man.}} * 100\%$	$\frac{COP_{OSU} - COP_{man.}}{COP_{man.}} * 100\%$	$\frac{P_{d,OSU} - P_{d,man.}}{P_{d,man.}} * 100\%$	$\frac{P_{s,OSU} - P_{s,man.}}{P_{s,man.}} * 100\%$	$T_{OSU} - T_{man.}$
	% difference					(°F)
A	-7.4	2.4	1.8	5.8	14.6	-0.9
B	-7.6	6.5	8.2	6.8	14.8	-1.4
H1	-11.2	5.8	-9.0	24.3	19.6	6.2
H2	-	7.9	-6.8	-	-	-
H3	-9.9	8.8	-18.7	57.9	27.3	4.4
*subscript: OSU= Oklahoma State University; man. = manufacturer						

The volume flow rates of air for the tests conducted at OSU were within 11% of that conducted at the manufacturer facility. This difference was mainly because of the density calculation which is highly sensitive to the measurement of wet bulb temperature. The system capacities calculated from the tests at OSU were a little higher and within 9% of the values from the manufacturer. This could be due to the fact that the system at OSU was slightly overcharged in searching for maximum COP. The increased change in the system capacity was also reflected in lower OSU supply temperatures for the cooling tests and higher OSU supply temperatures for the heating tests in comparison to the data from the manufacturer. The COP values were slightly higher in comparison with the data provided by the manufacturer for cooling tests and up to 19% lower for the heating tests. This can be explained by the observation that the heating tests conducted at OSU had higher compressor suction and discharge pressures. That means the compressor had to work more and resulted in lower COP. Overall the OSU data was in good agreement with the manufacturer data and thus the testing facility was validated.

The purpose of this section of the thesis is to present all the results found throughout the experimental campaign. The discussion of the experimental findings is organized in the following sub-sections: Charge optimization results during Drop-in tests, Performance and capacity comparison during Drop-in tests, Charge optimization results during TXV optimization tests, Performance and capacity comparison during TXV optimization tests, Evaporator and condenser coil performance and Compressor performance.

Charge optimization results during Drop-in tests

For the charge optimization of each refrigerant during drop-in tests, initially a certain amount of refrigerant was charged into the system and the system was run at AHRI A-test condition. Then the charge was increased by a small amount each time and the corresponding capacities and

COPs were calculated. Charge optimization was continued until the COP started to drop. The other parameter of concern was the superheat at compressor suction to ensure the safe operation of the compressor.

Figure 31(a) and (b) show the normalized COP and the superheat at the compressor suction during charge optimization for R410A. The error bar in Figure 31(a) represents the uncertainty in COP. Once the maximum COP was found, the corresponding charge, 19.8 kg was established as the optimum charge and that COP of R410A was set as the baseline for comparing the other refrigerants. The R410A optimized TXV was able to maintain a suction superheat around 10°F even at very high refrigerant charges, as shown in Figure 31(b).

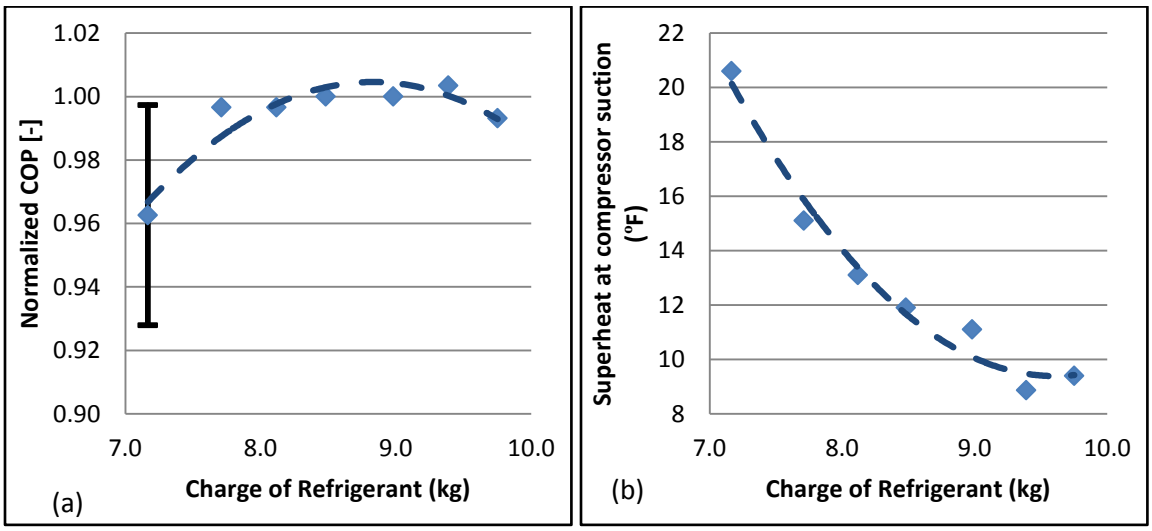

Figure 31: (a) COP and (b) Superheat in drop-in charge optimization for R410A

For DR-4 charge optimization, the refrigerant charge was varied from 7 to 7.45 kg only, and there was no superheat at all if further refrigerant was charged, as shown in Figure 32(b). So the superheat was a more influential criterion in the charge optimization of DR-4. 7.2 kg of refrigerant was selected as the optimum charge on the basis of a favorable superheat and a good enough COP. Figure 32(a) shows the normalized COPs for DR-4 with respect to the COP of R410A with optimum charge.

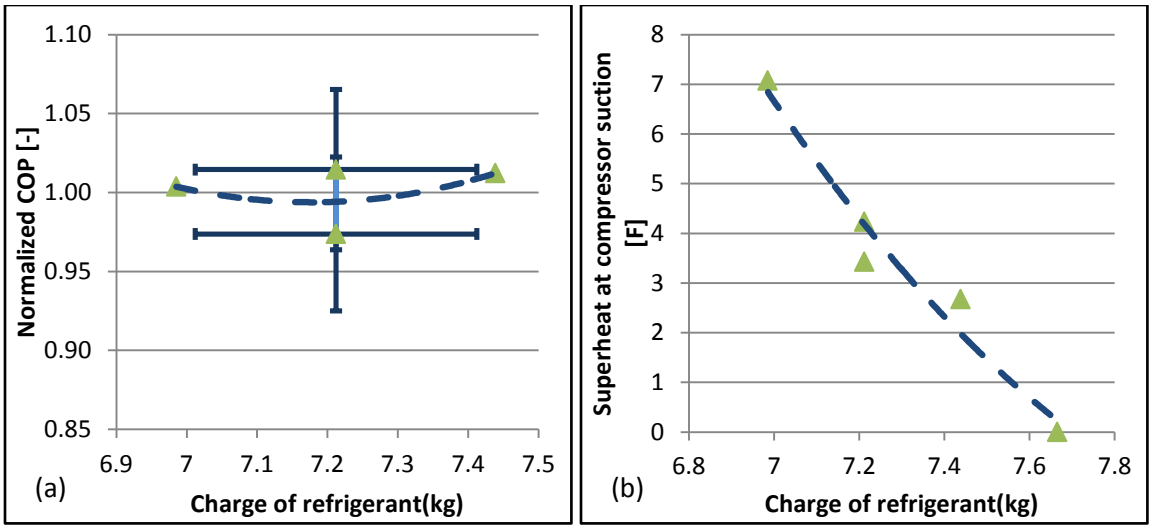

Figure 32: (a) COP and (b) Superheat in drop-in charge optimization for DR-4

As shown in Figure 33(a) and (b), the charge of DR-5 was varied from 6.8 to 9.1 kg in the search of the maximum COP with a favorable degree of superheat at compressor suction. The plot in Figure 33(a) shows that maximum COP with respect to the baseline of R410A was for a charge of 8.4 kg., and thus chosen as the optimum charge for the drop-in tests. As indicated in Figure 33(b), for DR-5 the TXV could maintain the superheat even at higher charges, suggesting that charge management for DR-5 could potentially be a lot easier than that of DR-4. The fact that the superheat actually increased at higher refrigerant charges for DR-5 can be explained by analyzing the mechanism of the externally equalized TXV. The three forces controlling the operation of the TXV were the pressure caused by expansion of the liquid inside the bulb (P_{bulb}), the evaporator outlet pressure (P_{evap}) and the pressure equivalent of the spring force (P_{spring}). The first one is an opening force and the last two are closing forces. The bulb pressure is proportional to the outlet surface temperature at the evaporator.

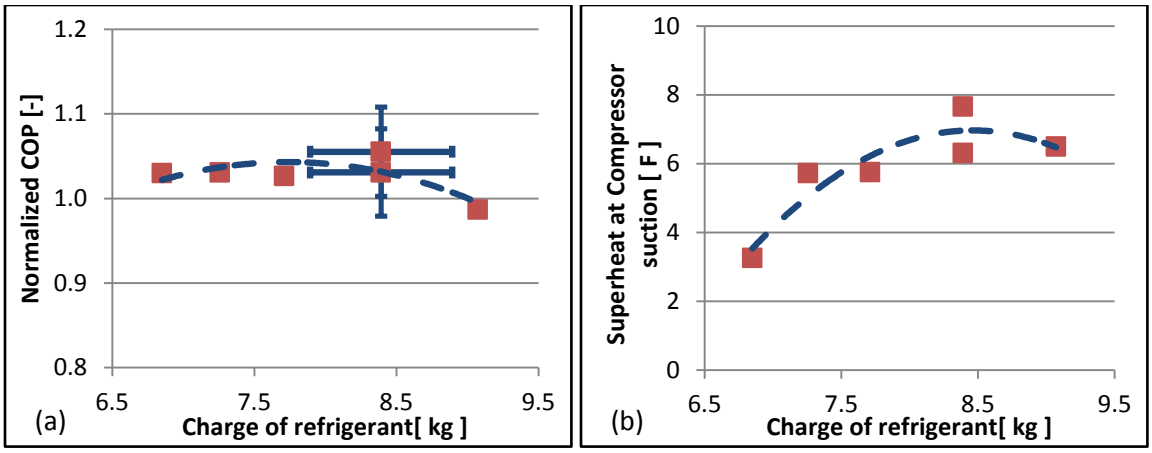

Figure 33: (a) COP and (b) Superheat in drop-in charge optimization for DR-5

As shown in Figure 34, Figure 35 and Figure 36, the evaporator outlet pressure and refrigerant flow rate increased and evaporator outlet surface temperature decreased with increasing charge for both R410A and DR-4. But none of these quantities had any significant and consistent change for DR-5. That means even though more charge was being added, it wasn't really going into the system and having any effect on the refrigerant flow and thus the superheat seemingly increased at higher charges for DR-5.

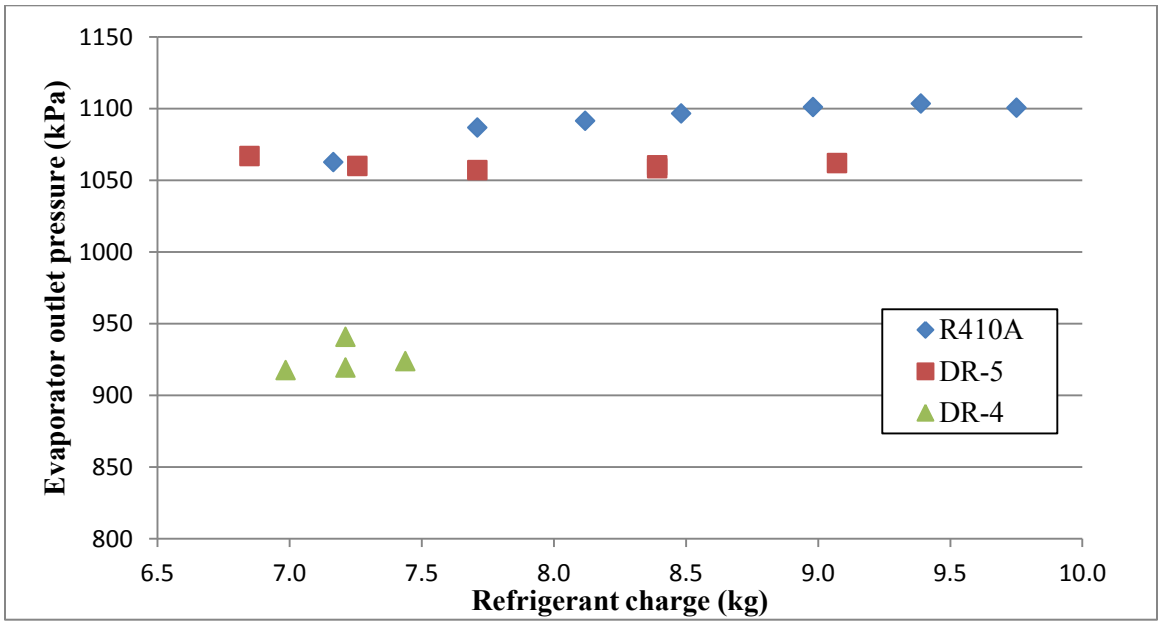

Figure 34: Evaporator outlet pressures for drop-in charge optimization

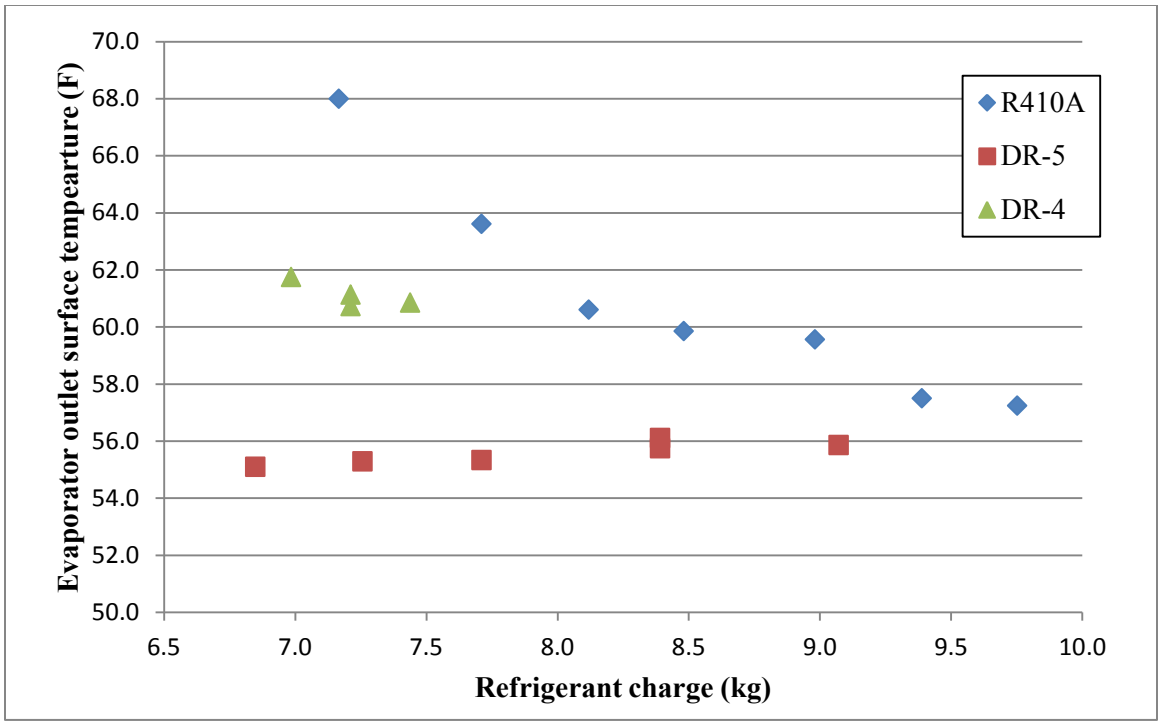

Figure 35: Evaporator outlet surface temperatures for drop-in charge optimization

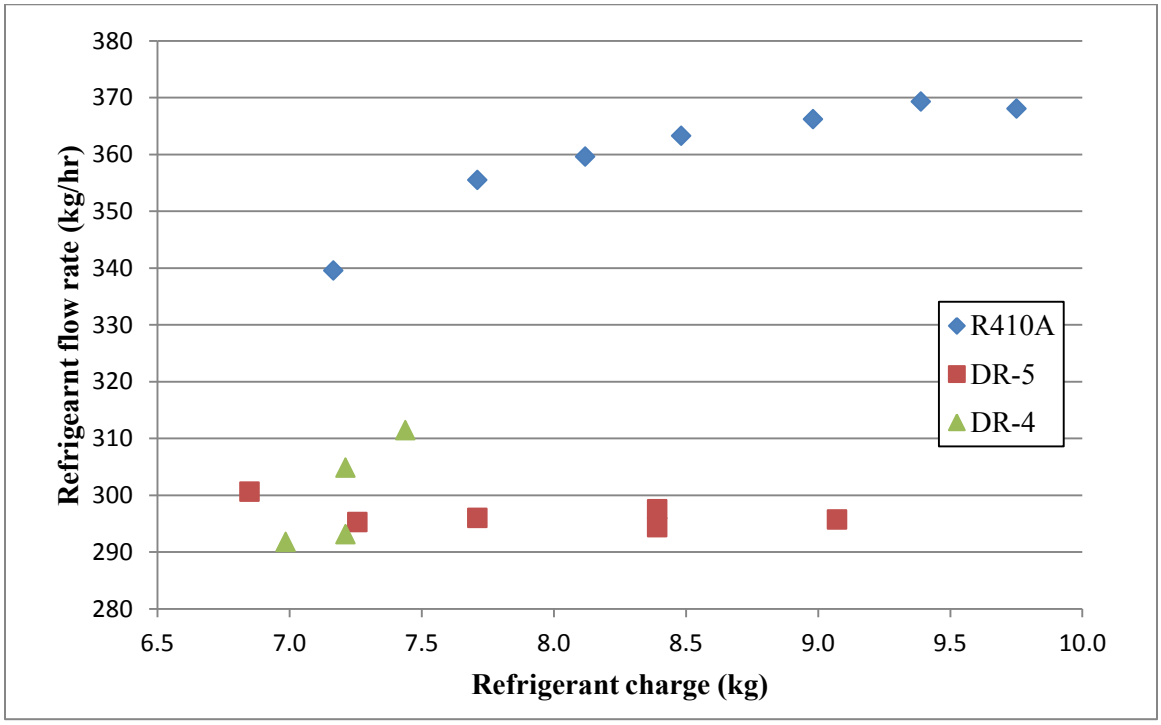

Figure 36: Refrigerant flow rates for drop-in charge optimization

The hypothesis to explain this phenomenon is that while doing the drop-in charge optimization with DR-5, the liquid pipeline after condenser acting as a receiver was never completely full, as shown in Figure 37. So while putting additional refrigerant charge, it was filling up the receiver first and then being circulated into the system. This hypothesis is supported by Figure 38 which shows that the condenser pressure consistently increased for increasing charge of DR-5 similar to R410A and DR-4. This indicates that the additional charge was pumped by the compressor and it went into the condenser but never really affected the overall flow rate or the superheat of the system. Going higher in charge wouldn't make any sense because the COP was already dropping, as indicated in Figure 33(b), but optimizing the system with lower charges could be interesting.

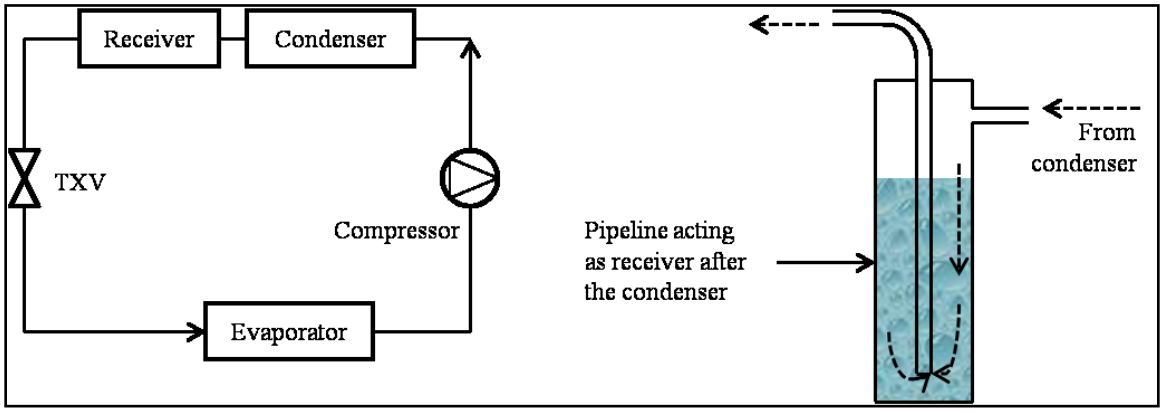

Figure 37: Condenser receiver

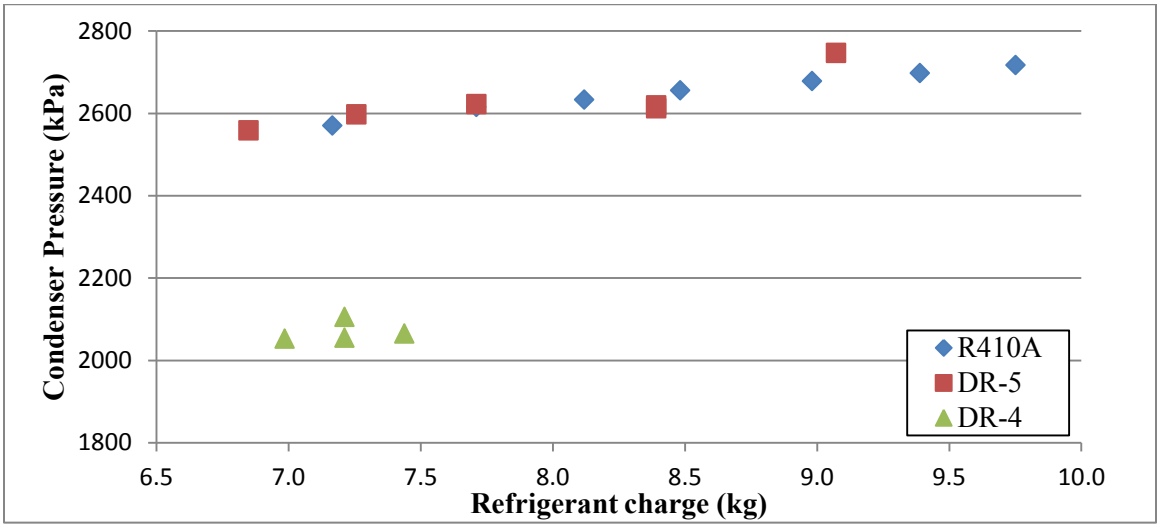

Figure 38: Condenser pressures for drop-in charge optimization

Performance and capacity comparison during Drop-in tests

During the straight drop-in tests, the capacities and COPs for DR-4 and DR-5 at varying range of outdoor temperatures and for both cooling and heating mode operations are shown in Figure 39 and Figure 40, normalized with respect to that for R410A at similar conditions. An increase of 3 to 4% in cooling capacity during cooling mode and a decrease of 5 to 10% in heating capacity during heating mode were observed for DR-5 with respect to R410A. The COP of the unit with DR-5 was from 1 to 7% higher in cooling mode and from 1 to 22% higher in heating mode. Thus, DR-5 performed well when used for retrofitting R410A in the heat pump split system for ducted residential applications used in the present work. The COP of the unit with DR-4 was from 4 to 6% higher in cooling mode and from 11 to 16% higher in heating mode. Both DR-4 and DR-5 performed well in comparison to R410A at extreme high temperature (HT1 and HT2 tests) and extreme low (H3-test) outdoor temperature conditions.

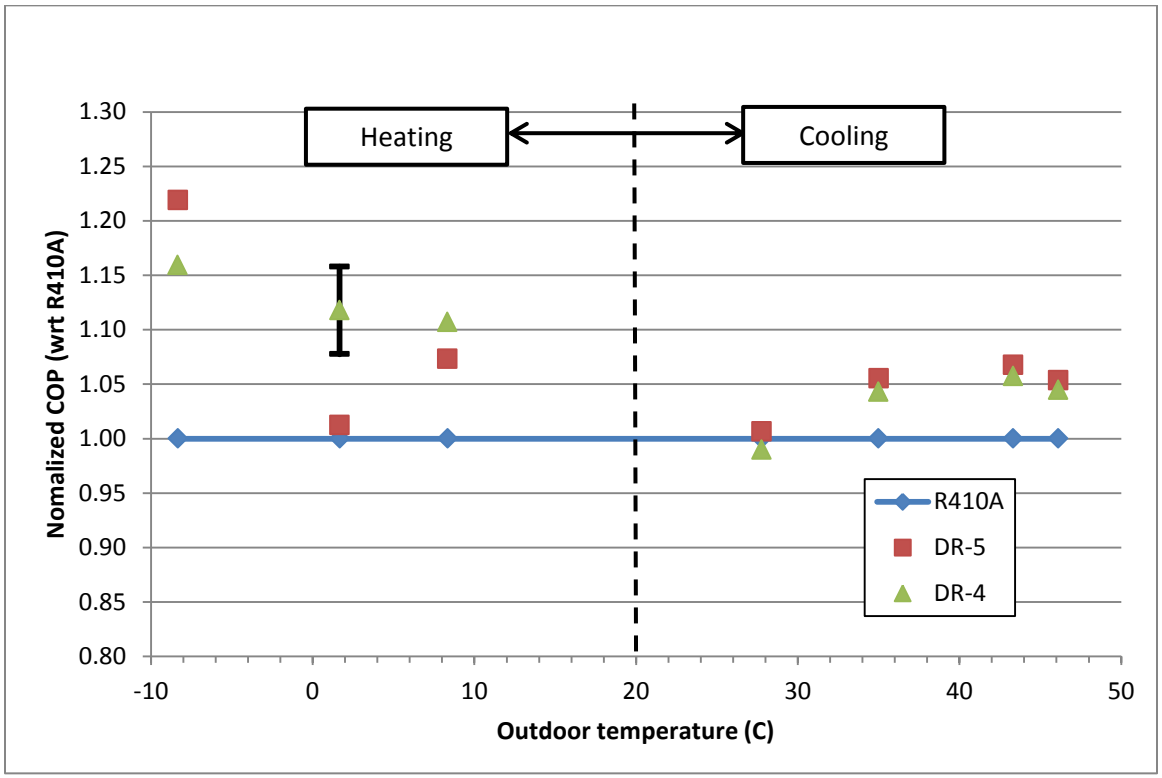

Figure 39: System performance in drop-in testing

As shown in Figure 40, in heat pump mode, while the COPs were higher than R410A the capacity of the system with DR-5 was lower by 5 to 10%. The cooling capacities were up to 4% higher in comparison to R410A. For DR-4, which has the lowest GWP among R410A and DR-5, the straight drop in tests showed that the cooling capacity decreased by about 15 to 18% in cooling mode and by as much as 30% in heating mode with respect to R410A. But the system capacity could be increased by adjusting the TXV, as it will be discussed later in regard to Figure 51.

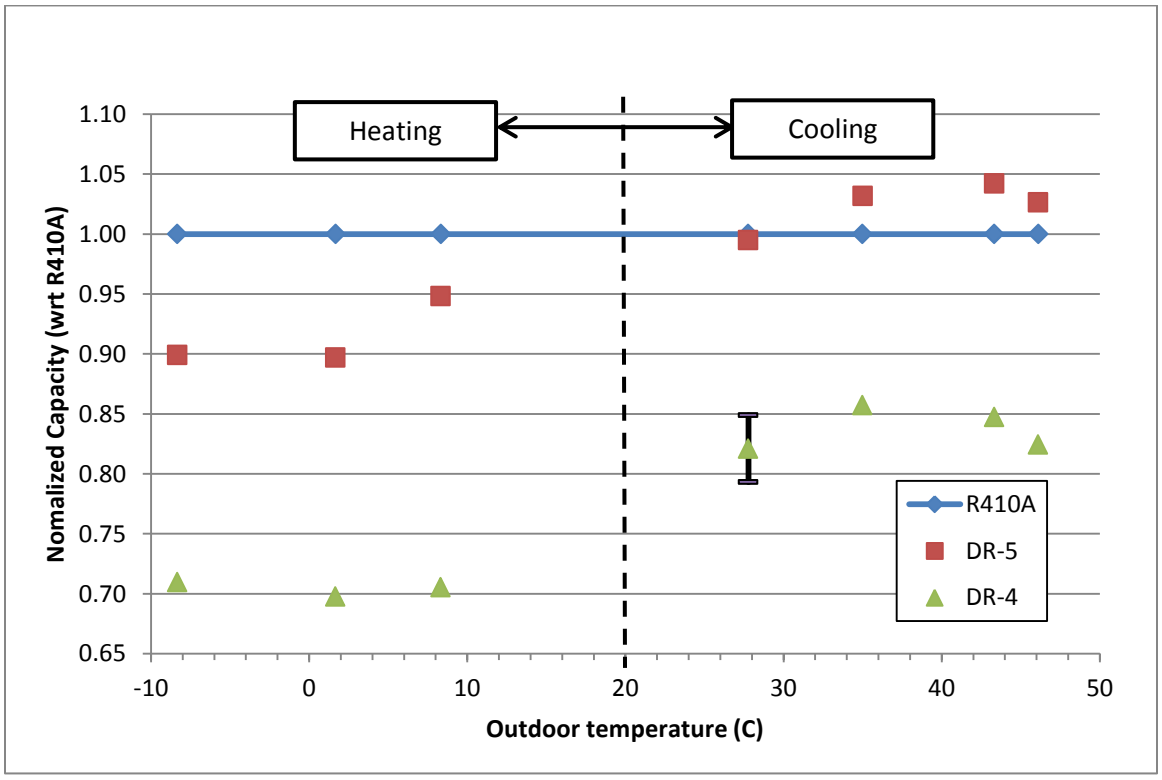

Figure 40: System capacity in drop-in testing

Charge optimization results during TXV optimization tests

The basic procedure to conduct the charge optimization with the modified expansion valve was to start with the optimum charge recorded during the drop-in tests and then open or close the expansion valve to get different degrees of superheat, increase and decrease the charge and adjust

the expansion valve again until maximum COP was measured. This sub-section explains the charge optimization results during the soft-optimization of TXV.

Figure 41 shows the results of COPs from the tests during the charge optimization of R410A with the adjustable manual expansion valve. The values are normalized with respect to the maximum COP and plotted against the normalized pressure ratio. As indicated in the plot, a charge of 9 kg was the optimum charge during drop-in tests. But during TXV-optimization, it was found that for a certain position of the TXV, R410A could produce the maximum COP with a charge of 8.85 kg. This point is highlighted in the plot with an arrow as the optimum charge during TXV-optimization. The two dotted lines denote the establishment of the baseline for comparing the other refrigerants. The data from point (1, 1) in Figure 41 will later be used as the references for evaluating the COPs, capacities and pressure ratios of DR-4 and DR-5 during TXV soft-optimization tests.

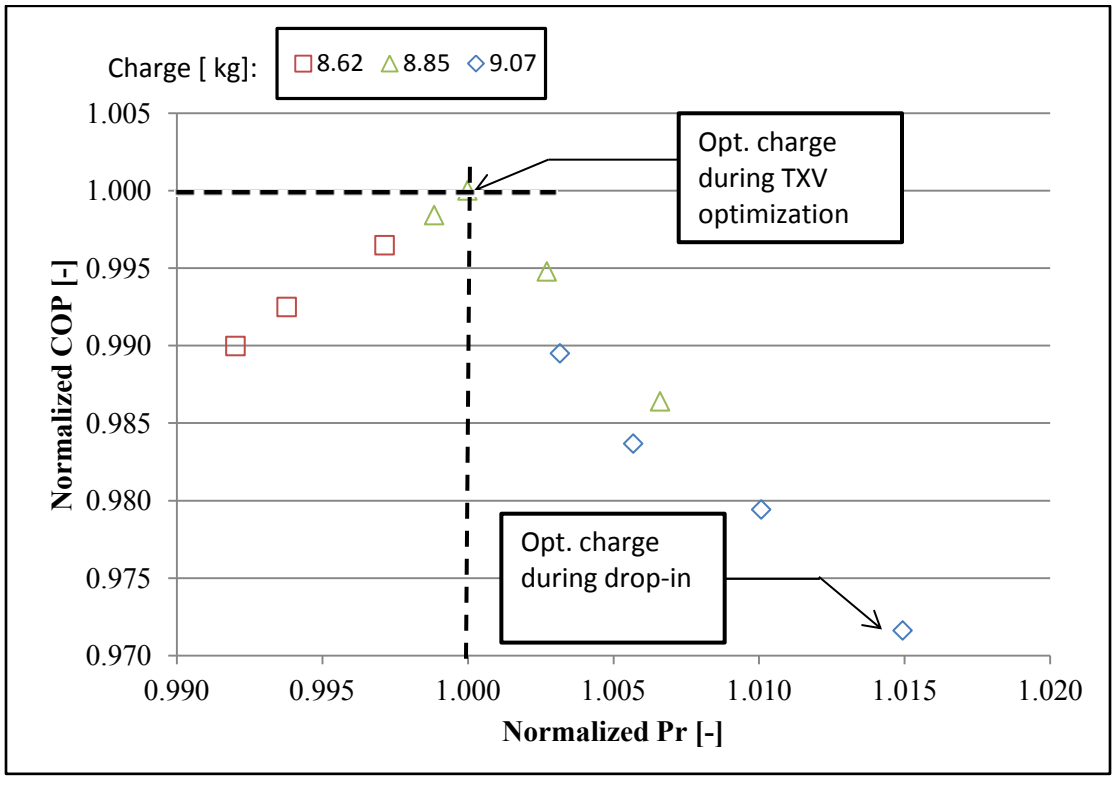

Figure 41: COP vs. Pressure ratio for R410A TXV optimization at AHRI A cooling conditions

Figure 42 shows the capacities during TXV optimization for R410A. Although the maximum COP value was primarily regarded as the standard parameter to look at in order to search for the optimized charge, the system capacity had to be within an acceptable range as well to support it. As indicated in the plot, at point (1, 1) the maximum system capacity was obtained with the optimum charge in the system.

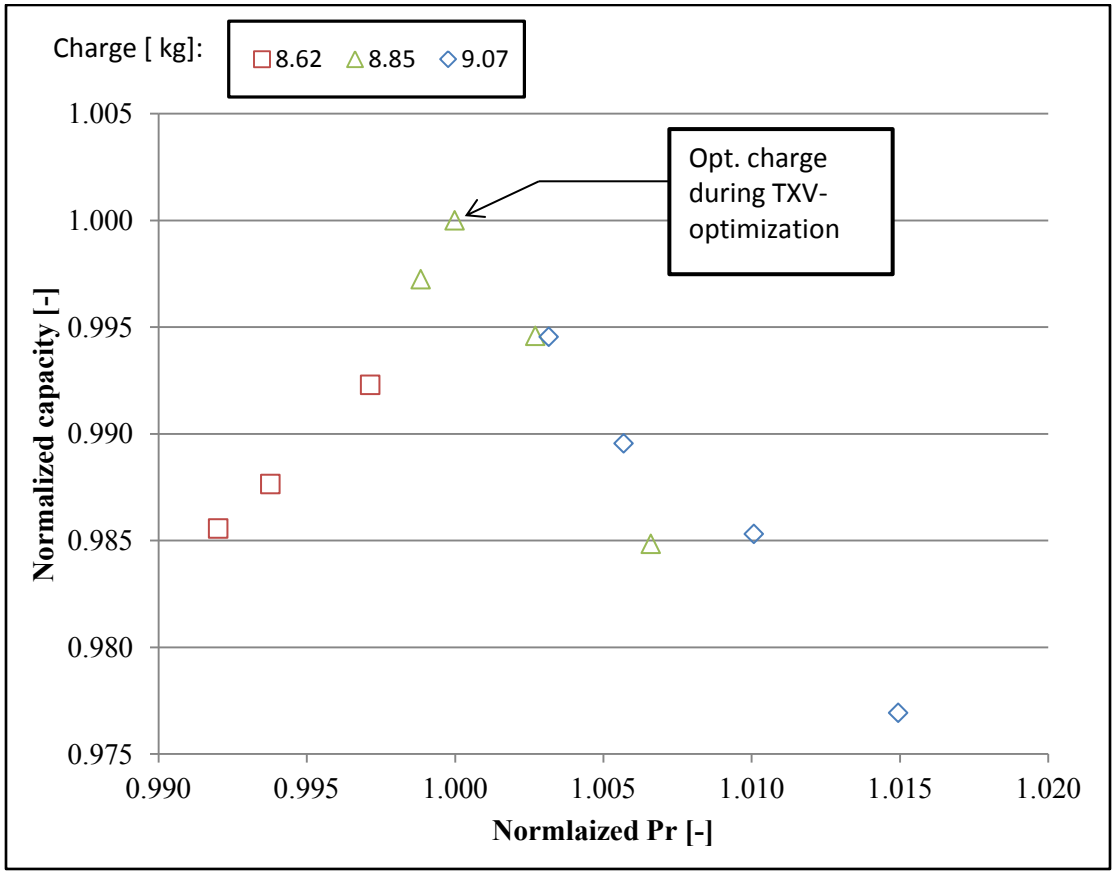

Figure 42: Capacity vs. Pressure ratio for R410A TXV optimization at AHRI A cooling conditions

The superheat at compressor suction is plotted against the pressure ratio for R410A during the TXV optimization in Figure 43. As the original R410A optimized TXV was replaced with the manual expansion valve, a lower superheat could be achieved in comparison to the drop-in tests. As shown in the plot, at optimum charge the superheat was 7.8ºF (4.3°C).

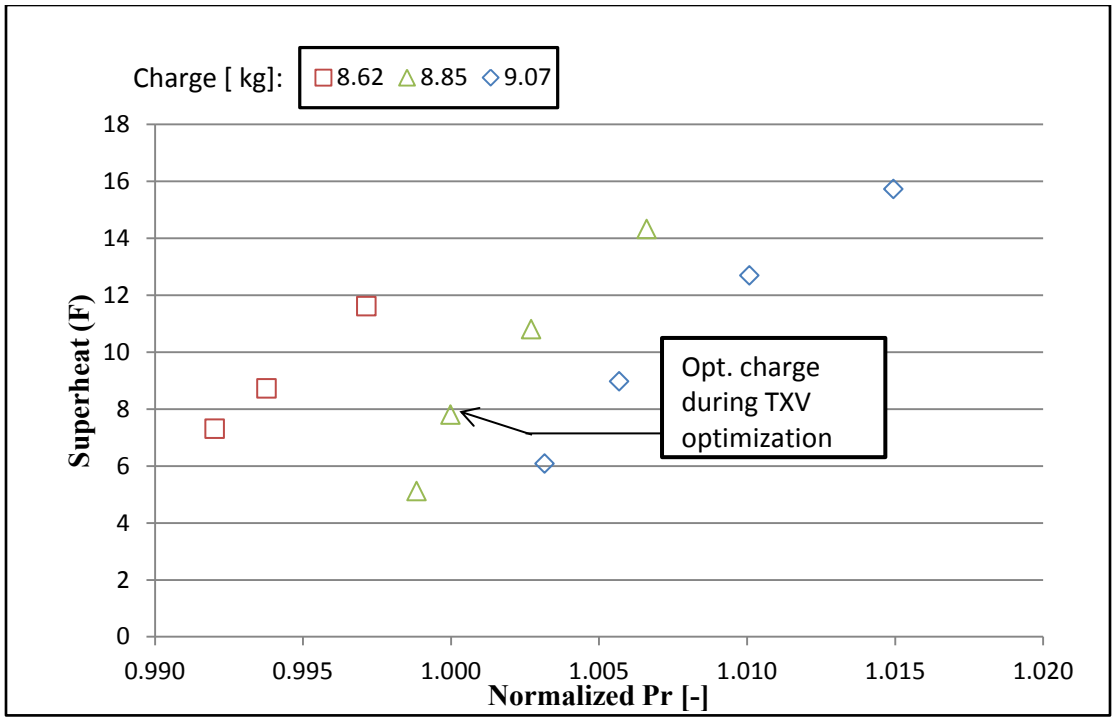

Figure 43: Superheat vs. Pressure ratio for R410A TXV optimization at AHRI A cooling conditions

Figure 44 shows the results of COP from the tests during the charge optimization of DR-4 with the manual adjustable expansion valve installed at the indoor coil of the unit. The data are presented in normalized form, in which the COP for R410A at similar AHRI A cooling conditions was chosen as reference. The COP data are plotted versus the compressor pressure ratios, P_r, which was normalized with respect to the compressor pressure ratio for R410A. For example, for 7.0 kg (15.5 lb_m) of DR-4 charged into the unit, a point was measured and it is highlighted with an arrow in Figure 44. For this point the normalized pressure ratio was 0.935 and the normalized COP was about 1.04. This means that the pressure ratio for DR-4 was 0.935 lower than that for R410A while the COPs of the two refrigerants were similar when the unit ran at A-test cooling conditions. For 7.0 kg (15.5 lb_m) of DR-4 charged into the system there was an optimum opening of the expansion device that provided the maximum COP. Increasing the refrigerant charge of DR-4 into the system yielded to similar COPs at various pressure ratio when

the expansion valve was properly adjusted for each charge. For refrigerant charges of 7.7 kg and 8.2 kg the COPs and capacities were similar to the one measured at 7.0 kg but the compressor ratios were higher. These three charges also provided similar degree of superheat and the charge of 7.0 kg was selected as optimum charge based on the fact that for this charge the refrigerant pressure ratio was the closer to that of the drop-in test and the unit was easier to control. If we look at the degree of superheat shown in Figure 46, different openings of the expansion valve with 7.0kg provided higher degree of superheat. With 7.7 kg it was difficult to increase the superheat and all three data points at this charge of 7.7 kg have superheat between 2 and 4°F. At 8.0 kg only one point is given in Figure 46, which represents the only opening of the expansion valve that provided enough superheat. With this charge any further small adjustments of the expansion valve were not possible because the degree of superheat of refrigerant DR-4 dropped suddenly below 2°F. This could compromise the compressor safety. Thus, 7.0 kg was chosen as optimum charge for DR-4 because it provided the highest COP, highest capacity, and the safest envelope operating conditions for the compressor.

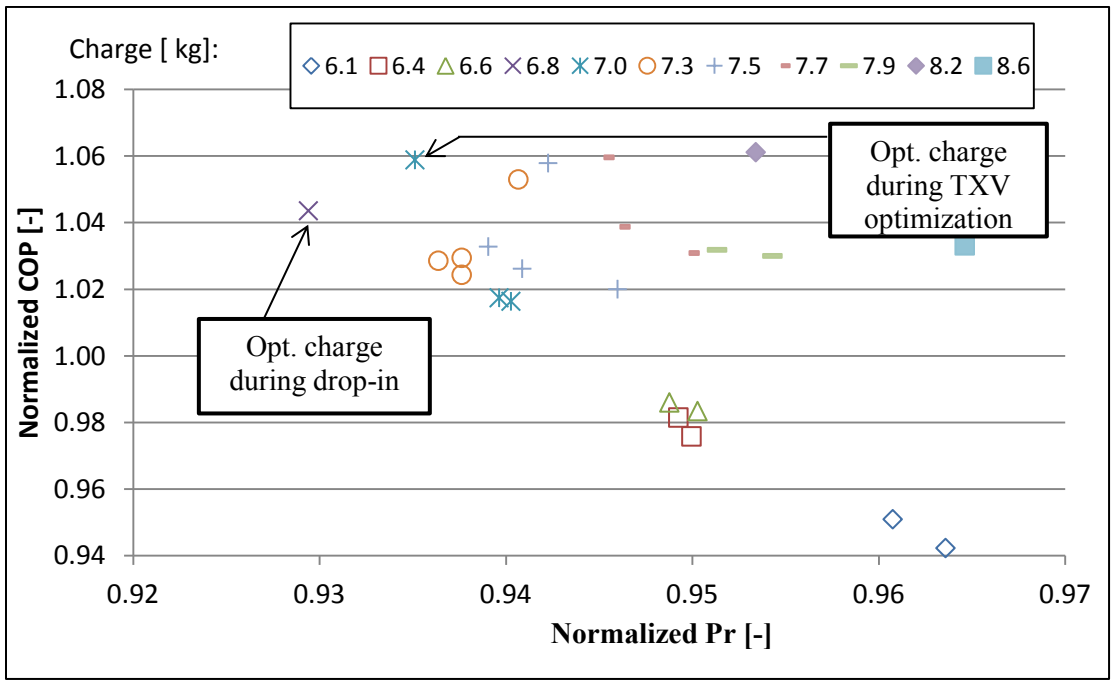

Figure 44: COP vs. Pressure ratio for DR-4 TXV optimization at AHRI A cooling conditions

Figure 45 shows the capacity data during TXV optimization for DR-4. As indicated with the arrow in the plot, the normalized capacity for DR-4 with the optimum charge was 0.91, which was not necessarily the maximum. But this charge was still chosen to be the optimum on the basis of the maximum COP being achieved, with reference to Figure 44. The maximum capacity was achieved at a higher normalized pressure ratio of 0.955.

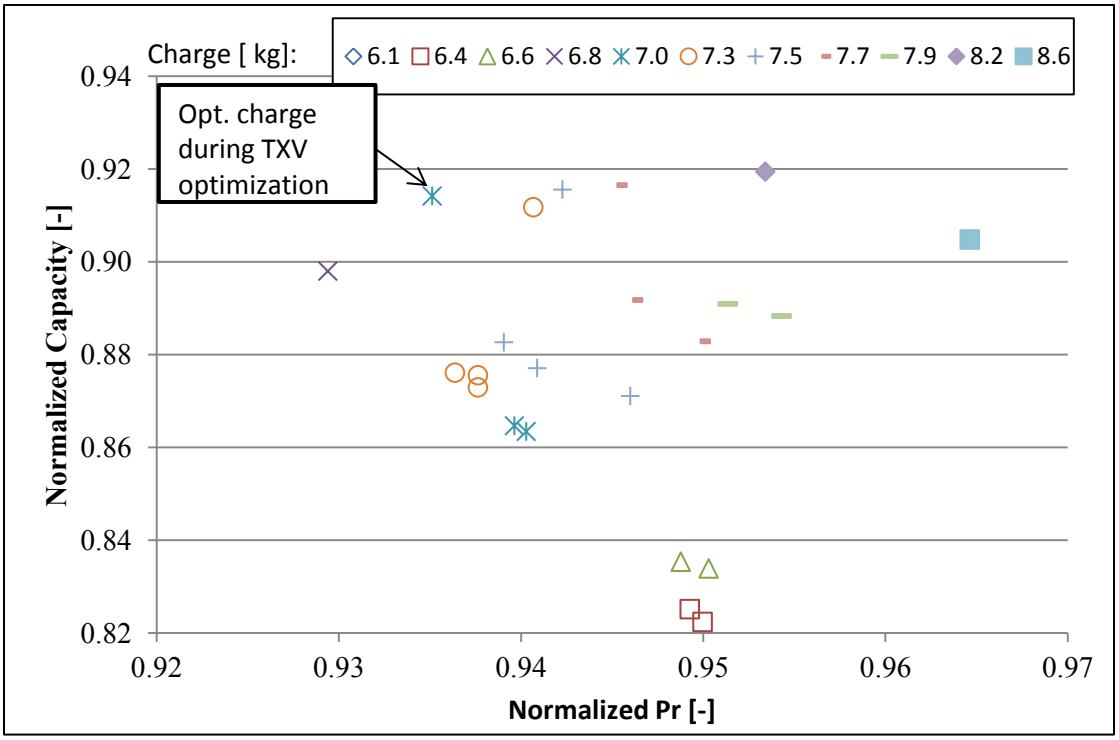

Figure 45: Capacity vs. Pressure ratio for DR-4 TXV optimization at AHRI A cooling conditions

The corresponding measurements of the degree of superheat at the compressor suction during the tests for DR-4 charge optimization in the unit with the adjustable manual expansion valve are plotted in Figure 46. A superheat of about 2.2ºC (4ºF) was the minimum superheat for all refrigerants acceptable for compressor safe operation. It should be noticed that the charge of DR-4 in the unit during straight drop-in tests was 6.8 kg (15 lb_m). This was the optimum charge of DR-4 when the original TXV of the unit was installed and it was the initial amount of DR-4 charged in the unit during the tests for the optimization of the expansion valve.

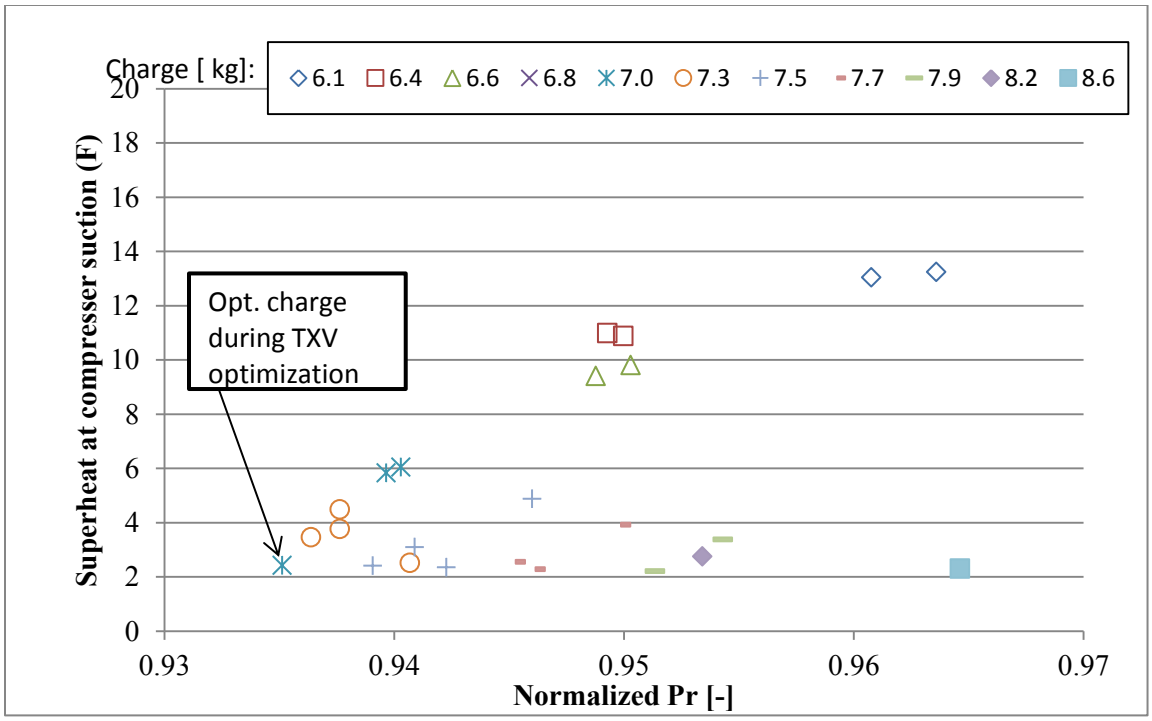

Figure 46: Superheat vs. Pressure ratio for DR-4 TXV optimization at AHRI A cooling conditions

Figure 47 shows the results of the charge optimization for DR-5, with the normalized COP data plotted against the normalized pressure ratio and with the values of R410A chosen as reference. The maximum COP is indicated in the figure with an arrow and it had a normalized pressure ratio of 0.983 and a normalized COP of 1.03 for 7.9 kg (17.5 lb_m) of DR-5 charged into the unit. Once the refrigerant charge was varied and the expansion valve was promptly adjusted, it was observed that this charge yielded to the highest COP, and thus it was chosen as the optimum charge of DR-5 in the unit with the new expansion valve. It should be noticed that the charge of DR-5 in the unit during straight drop-in tests was 8.4 kg (18.5 lb_m). This was the optimum charge of DR-5 when the original TXV of the unit was present. It should be noted that same markers at a given refrigerant charge in Figure 46 represent different openings of the expansion valve.

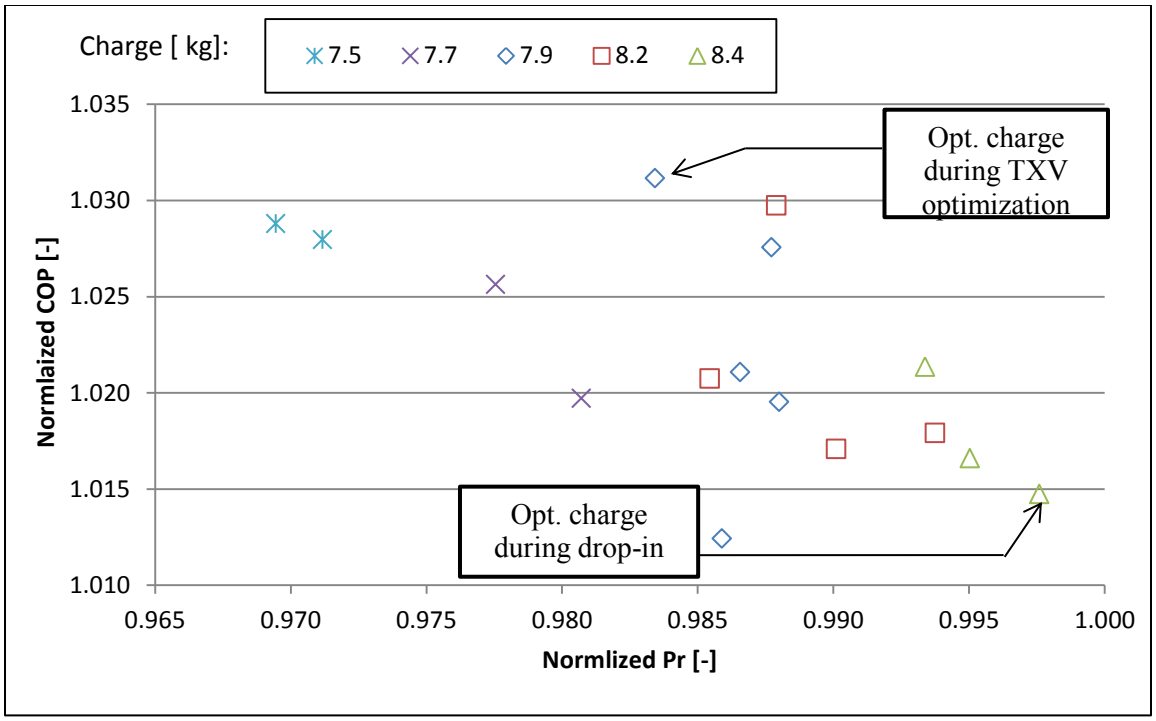

Figure 47: COP vs. Pressure ratio for DR-5 TXV optimization at AHRI A cooling conditions

As shown in Figure 48, during charge optimization at AHRI A-test cooling conditions for DR-5, the normalized capacity was 0.983 with the optimum charge. A higher capacity in comparison to R410A could be attained but only by sacrificing on COP. From the plot it can be seen that at pressure ratio 0.987 and with a refrigerant charge of 8.2 kg, the normalized capacity could be 1.004, but the corresponding normalized COP would be 1.03 only at that point as shown in Figure 47, which is lower than that at the chosen optimum charge.

For DR-5, the degree of superheat was fairly sensitive to the adjustments of the expansion device. As shown in Figure 49, small variations of the needle in the expansion valve yielded to drastic change in the degree of superheat at the compressor suction. The manual valve was turned within 1/8th of a turn to collect all the data points presented in the plot and the superheat would go below 2ºF with the slightest change of the opening of the valve.

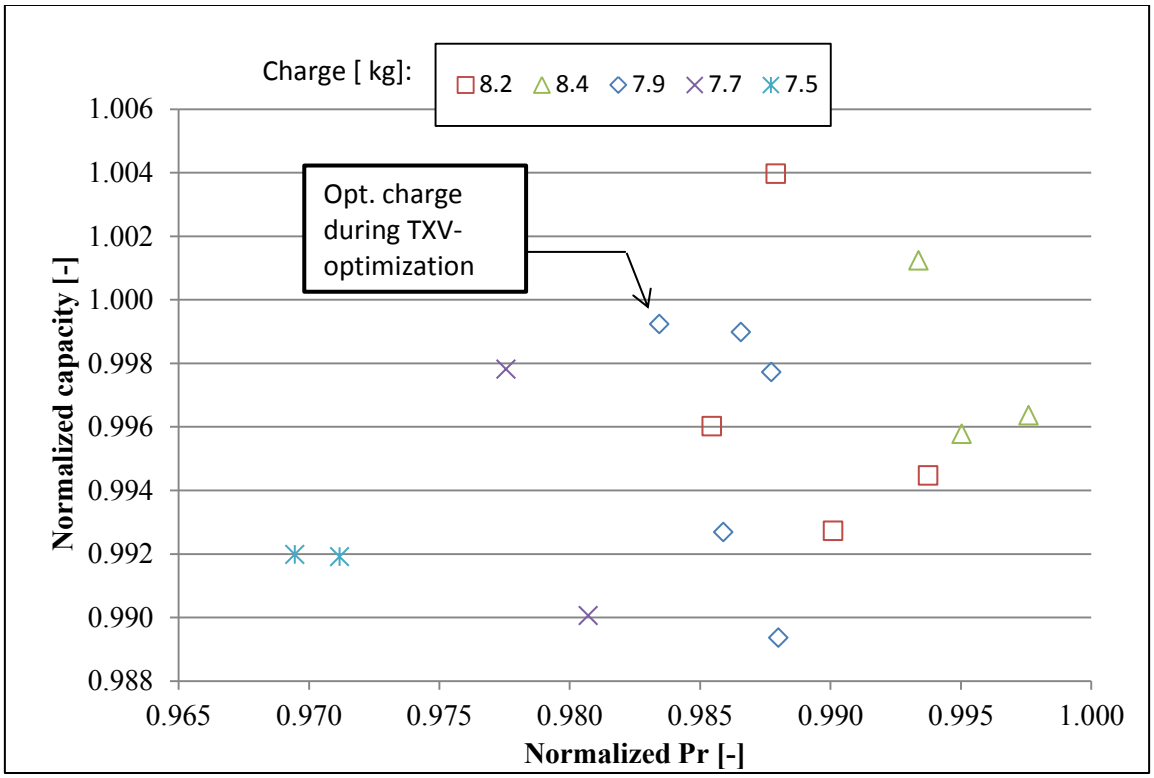

Figure 48: Capacity vs. Pressure ratio for DR-5 TXV optimization at AHRI A cooling conditions

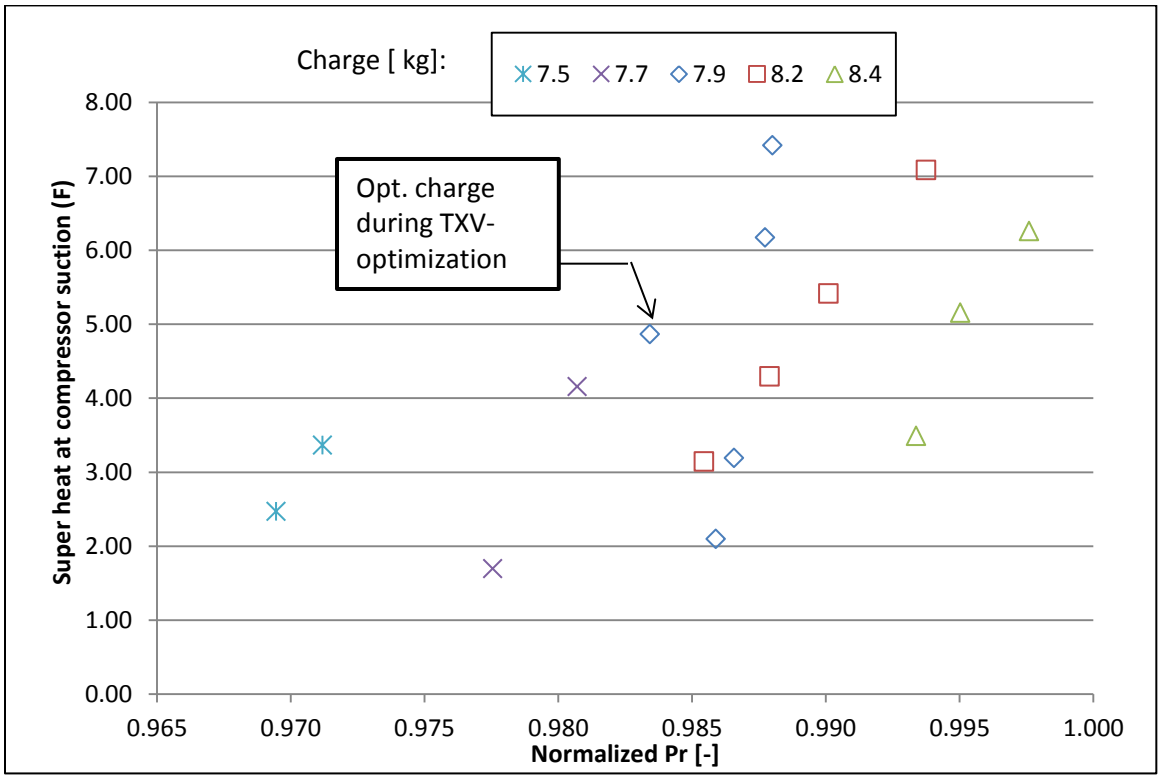

Figure 49: Superheat vs. Pressure ratio for DR-5 TXV optimization at AHRI A cooling conditions

Performance and capacity comparison during TXV optimization tests

With a soft optimization of TXV, the capacity and the COP of DR-4 and DR-5 were further improved with respect to the ones measured during the drop-in tests. These improvements are shown in Figure 50 and Figure 51. The data in solid bars represent the cooling capacities and COPs during drop-in tests.

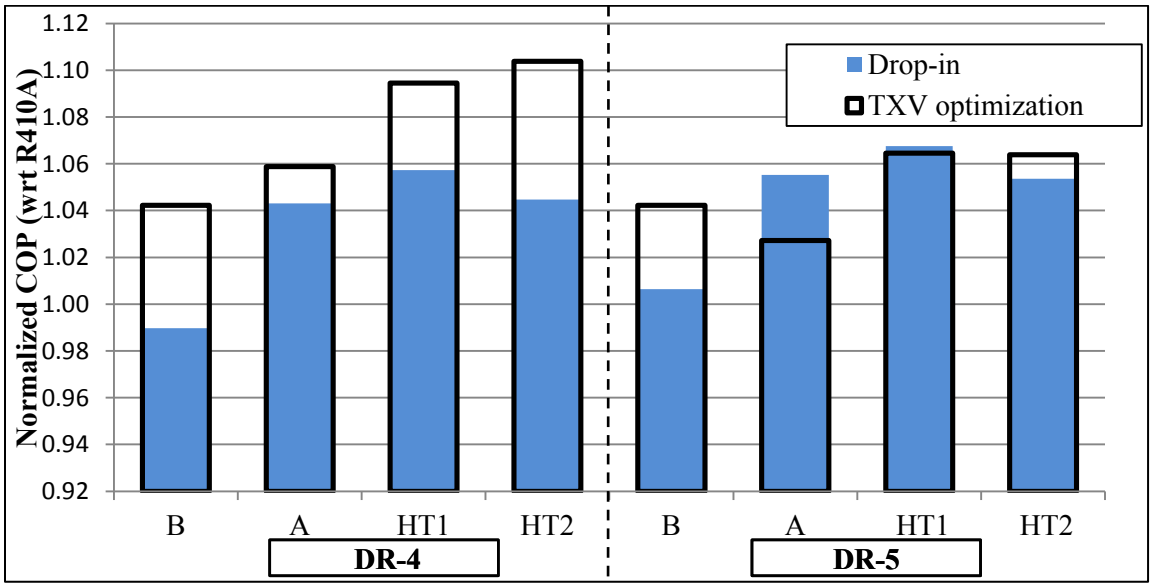

Figure 50: System performance in TXV soft-optimization

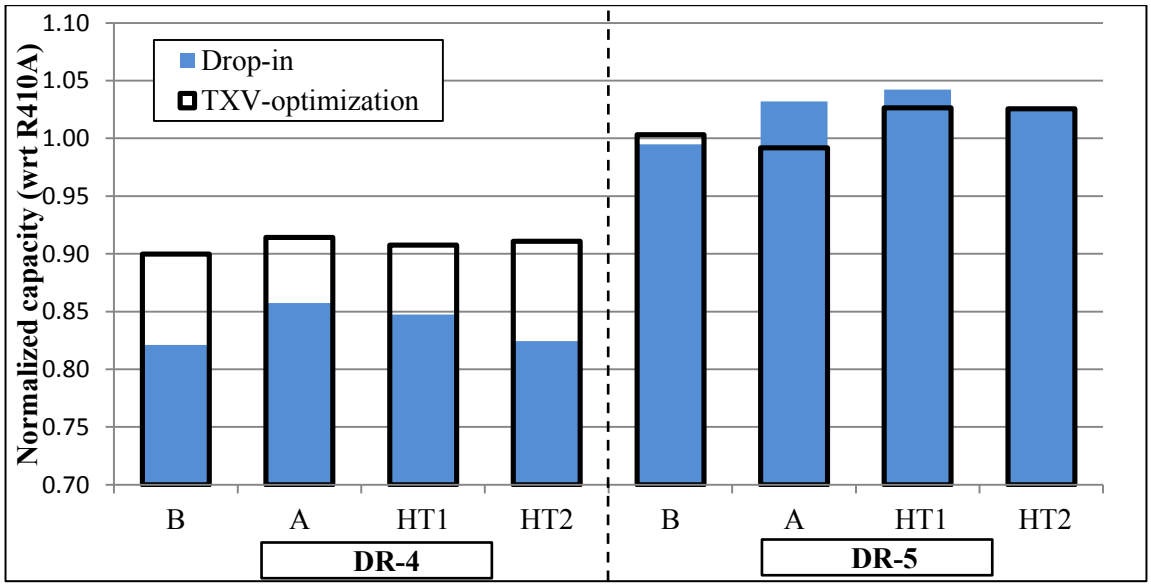

Figure 51: System capacity in TXV soft-optimization

For example, at AHRI A cooling conditions the COP of DR-4 was about 4% higher with respect to R410A and the cooling capacity was about 15% lower. When the TXV and the corresponding refrigerant charge were further optimized, DR-4 COP increased by an additional 2% and DR-4 cooling capacity augmented by an additional 6%. This soft optimization of the unit increased the capacity from 0.85 during the drop-in test to 0.91 for the run with TXV soft optimization test. These results are shown in the bar referred to as "A" for DR-4 in Figure 50 and Figure 51. Figure 50 and Figure 51 showed that optimization of the TXV overall increased the cooling capacity of DR-4 from 5 to 8% and the COP from 2 to 6% with respect to that of drop-in tests considering the range of outdoor temperatures in cooling mode.

For DR-5 it was observed that the manual expansion valve was less efficient than the TXV in the system at design cooling conditions. This could be observed from the values measured for the A-test in Figure 50 and Figure 51 for the case of DR-5. The drop-in values were slightly higher than the values obtained with the TXV optimization leading to the conclusion that the TXV for R410A was already well suited to work with DR-5 at design cooling conditions (A-test). At B-test conditions and at very high extreme outdoor temperature (HT-2) the adjustments of the expansion valve produced additional 1 to 3% higher COPs with respect to those of drop-in tests. The capacity variations between drop-in tests and TXV optimization tests for DR-5 were practically within the experimental uncertainty of the test set up.

Evaporator and condenser coil performance

Temperature distribution

As described earlier in the instrumentation sub-section, right after the indoor coil and before the blower, there was a thermocouple mesh with seven thermocouples, located about 6 inches from

the top of the coil. The thermocouples were numbered from T1 to T7 and located in the mesh as shown in Figure 52.

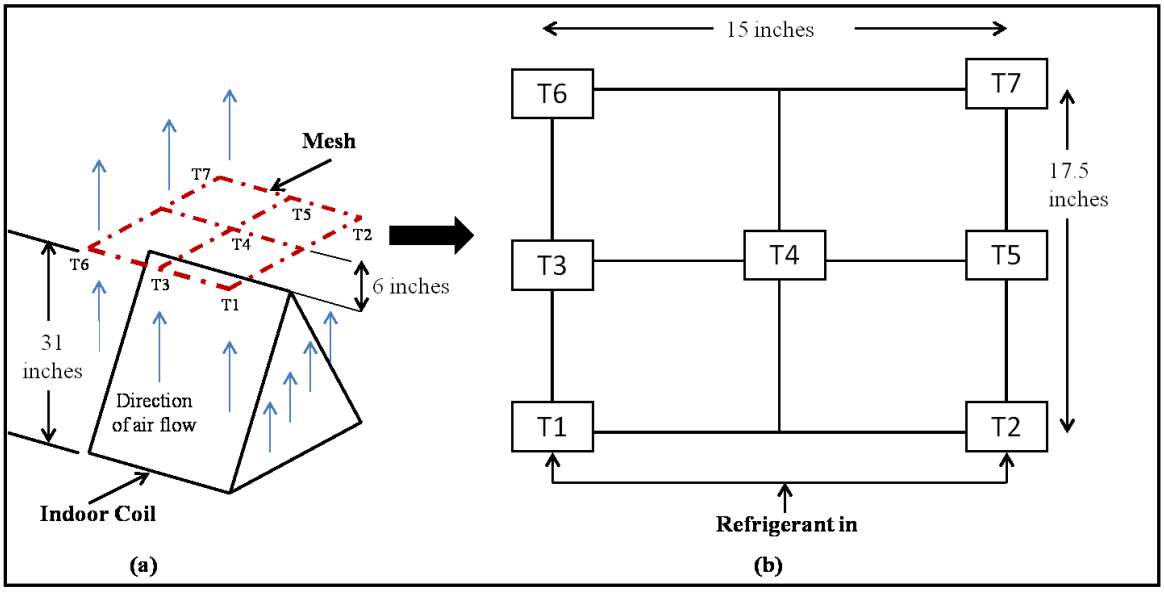

Figure 52: (a) Location of thermocouple mesh after indoor coil and (b) designation of mesh thermocouples [air flow is exiting the paper in (a) and in the upward direction in (b)]

The temperature distribution in the mesh can give an indication on how the refrigerant is distributed along the cross-section of the indoor coil. It should be noted that the refrigerant entered the coil through the distributor from the front-left and front-right with reference to the mesh diagram, as shown in Figure 52(b). Figure 53, Figure 54 and Figure 55 show the temperature distribution in the mesh for the moderate A-test cooling condition and two extreme temperature conditions, high temperature HT2-test cooling condition and low temperature H3-test heating condition. As shown in these figures, T1, T3 and T6 were always higher than T2, T5 and T7. As the differences were consistent for all the testing conditions and for all the refrigerants, it was more likely due to a systematic error rather than the uncertainty of the instrumentation. The convection heat transfer from the refrigerant tube surface to the surrounding air can be expressed with $\dot{Q} = hA(T_{air-}T_w)$, where h is the convection heat transfer coefficient of air, A is the heat

transfer surface area, T_{air} is the bulk air stream temperature and T_w is the wall temperature of the tube. T_w was expected to be almost constant throughout the indoor coil because the refrigerant was mostly in two phase and didn't change temperature until the outlet. As $\dot{Q}$ was constant, the only two parameters that could change were h and T_{air}. Now, h is directly proportional to the Nusselt number (Nu), which is again a function of air Reynolds number (Re). If the local air velocity was higher at any point, the associated Re and Nu would be higher as well. That would result in a higher value of convective heat transfer coefficient and T_{air} would decrease at that point. As the thermocouple mesh was only 6 inches away from the coil and just below the blower, air was not mixed well before the mesh. Air velocity probably was a little higher on the right side of the coil rather than the left side given that the outlet header of the refrigerant was positioned on the left side, creating an additional resistance for the air stream. That could have resulted in comparatively lower air temperatures recorded by the thermocouples T2, T5 and T7 in comparison to T1, T3 and T6.

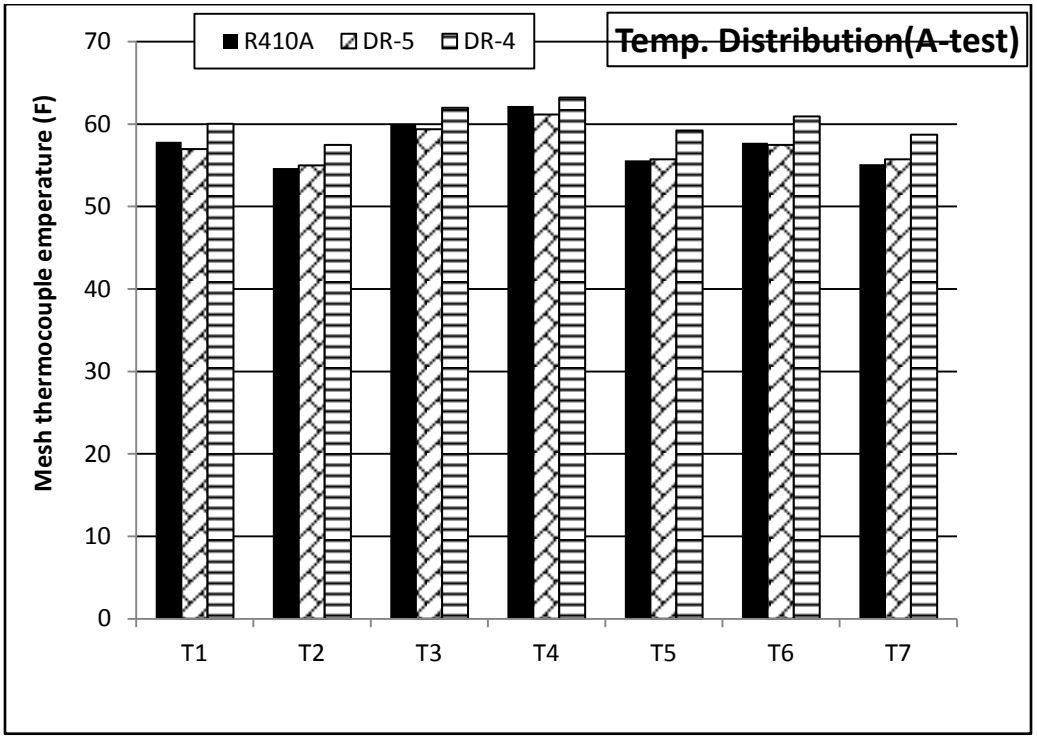

Figure 53: Temperature distribution after evaporator in AHRI A-test condition

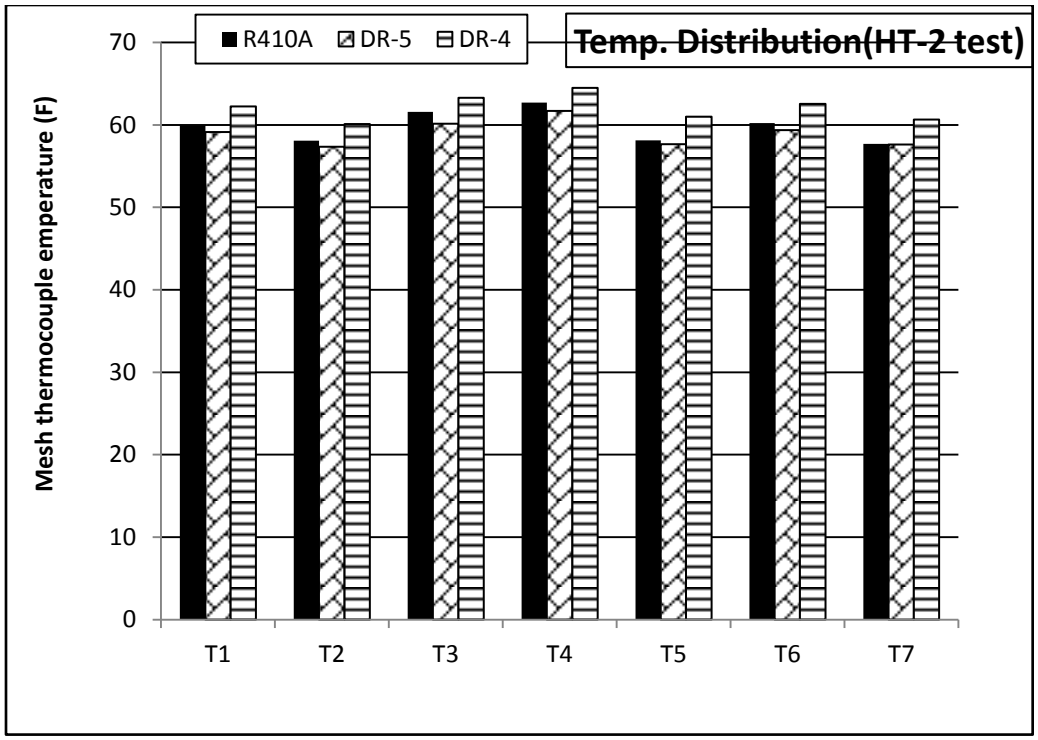

Figure 54: Temperature distribution after evaporator in HT2-test condition

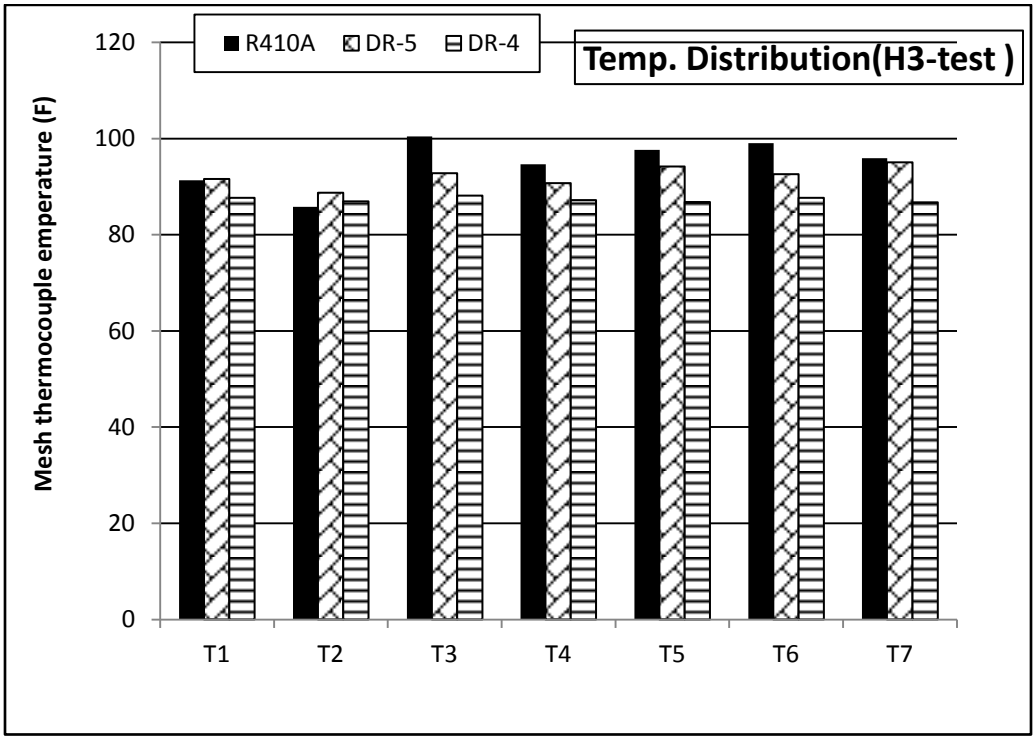

Figure 55: Temperature distribution after condenser in AHRI H3-test condition

For example, for R410A, at A-test condition thermocouples T1 and T6 show a temperature of around 58ºF, T2, T5 and T7 show around 55ºF, and T3 around 60ºF. T4 was located right on top of the middle portion of the A-shaped indoor coil, where the top of A-coil is covered with a thin plate. Thus right at the top of the plate air is warmer because of a local stagnation point. Air does not mix well before T4 which was only 6 inches away from the top plate. As a result T4 exhibits a temperature of around 62ºF, little higher than the others. For DR-5 these temperatures are within ±1ºF, while for DR-4 they are consistently 3 to 4ºF higher than R410A. All these temperatures are represented in Figure 53.

As discussed earlier in the test procedure sub-section, the test data were recorded for at least one hour. It would be interesting to follow the temperature distribution for all the mesh thermocouples along time for this one hour to see how stable the supply temperatures were. Figure 56, Figure 57 and Figure 58 represents the temperature distribution along time for R410A, DR-5 and DR-4 respectively.

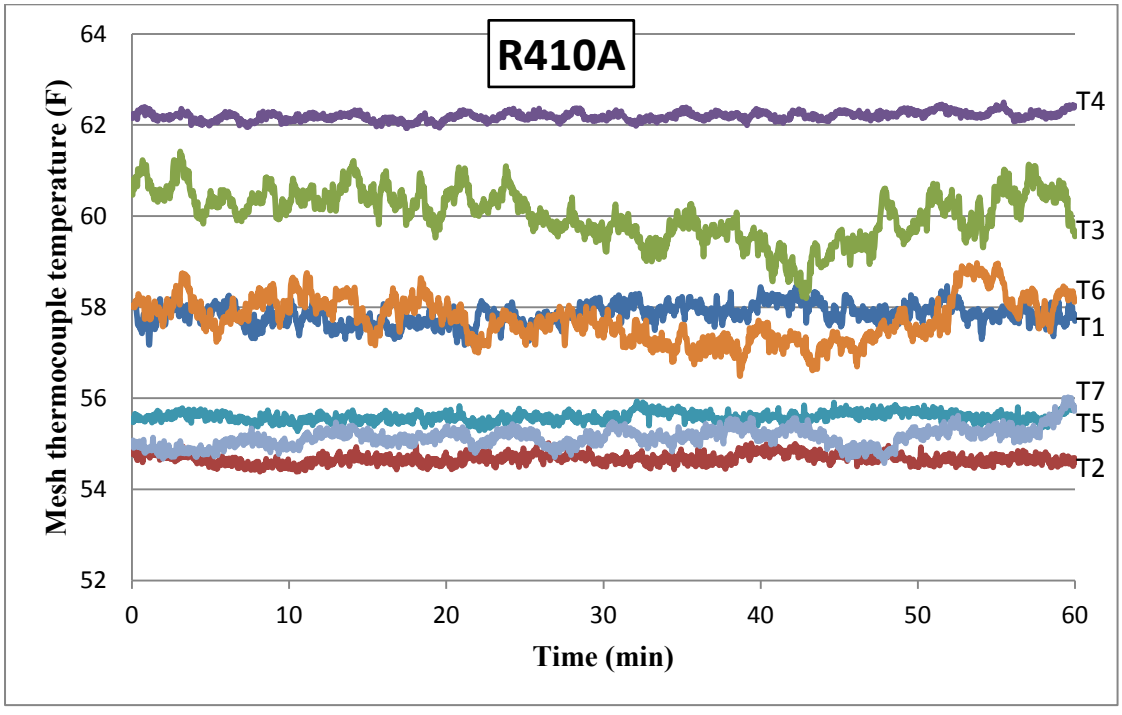

Figure 56: Temperature distribution after evaporator along time for R410A

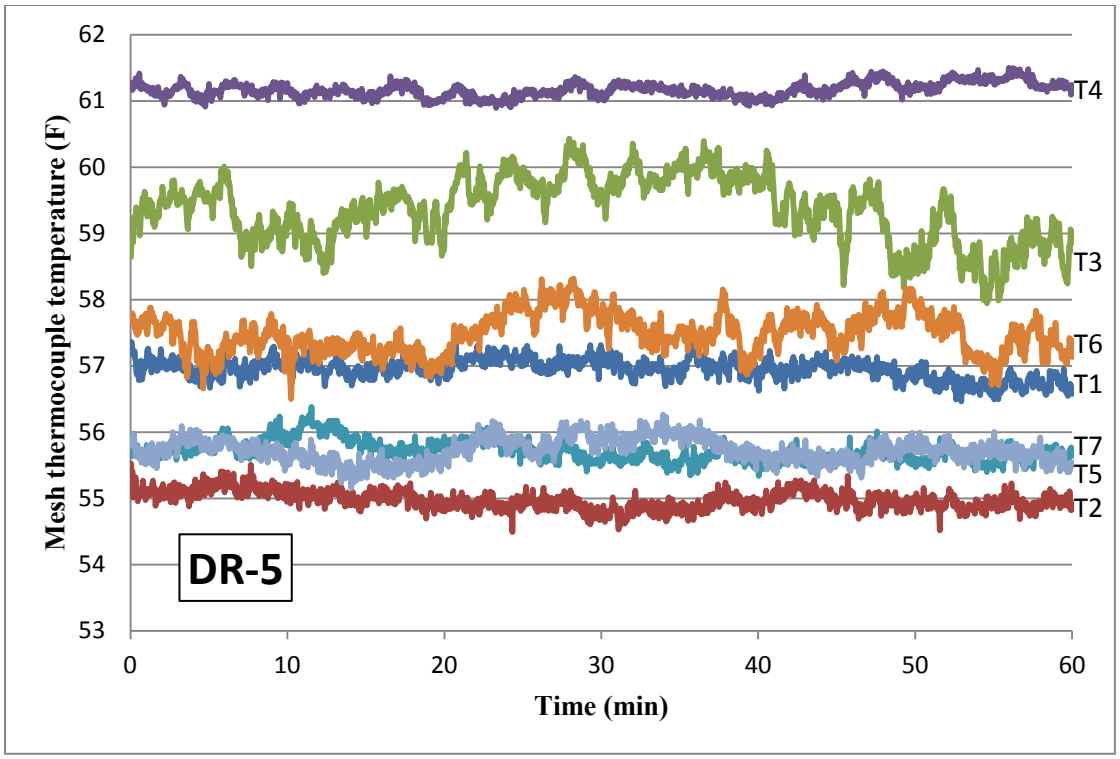

Figure 57: Temperature distribution after evaporator along time for DR-5

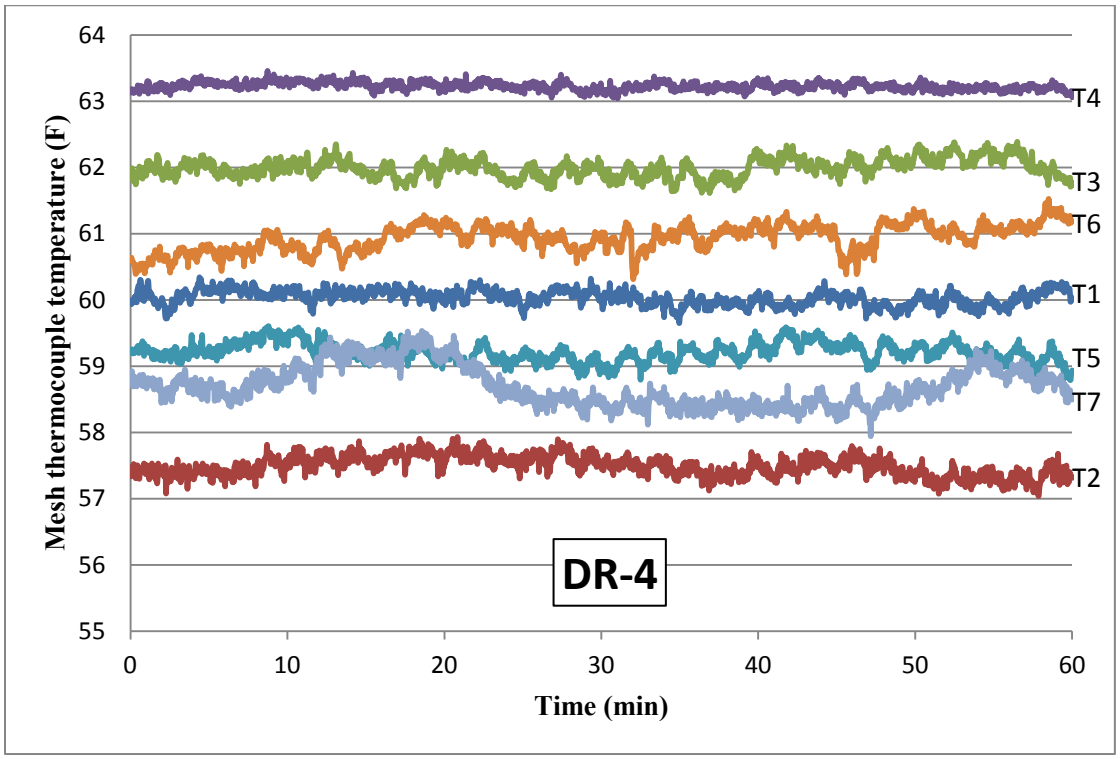

Figure 58: Temperature distribution after evaporator along time for DR-4

As from Figure 56 and Figure 57, both for R410A and DR-5, the thermocouples T3 and T6 exhibited the maximum deviation from stable condition, whereas for DR-4, the maximum deviation was for T6 and T7 as indicated in Figure 58. This instability in temperature means that there was some mal-distribution of refrigerant along the circuitries.

Pressure drop in the evaporator coil

When retrofitting R410A with DR-4 and DR-5 at A-test cooling condition, the flow rates and corresponding pressure drops across the evaporator (including the pressure drop across the inlet distributor) are shown in Figure 59.

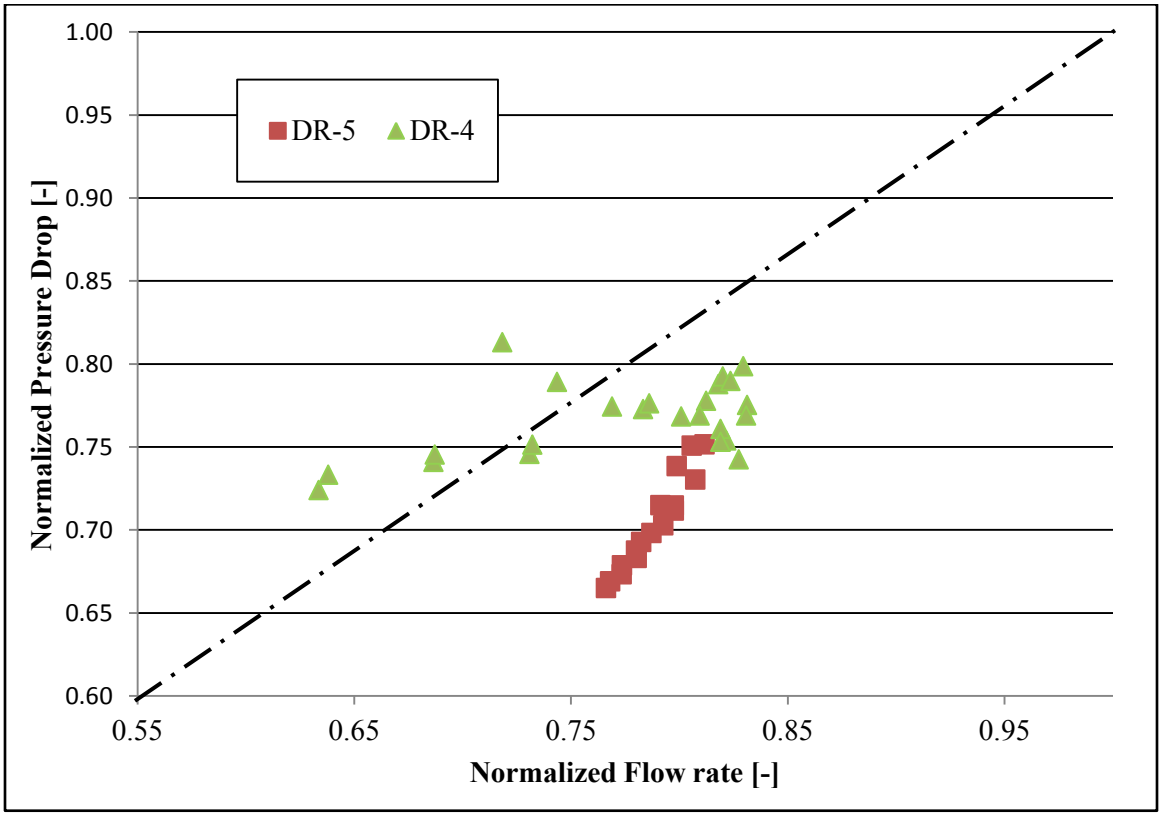

Figure 59: Normalized pressure drop vs. normalized flow rate at A-test condition (during TXV soft-optimization tests)

Data were normalized with respect to flow rates and pressure drops for R410A, that is, the point of coordinates (1, 1) is the operating point of the system at the A-test condition by using optimum charge of R410A. DR-4 flow rates varied from 0.63 to 0.83 and the evaporator pressure drops were from 0.72 to 0.81 times lower than those of R410A. The operating zone of DR-5 was flow rate between 0.77 to 0.81 and evaporator pressure drop in between 0.66 to 0.76. The region above the diagonal line indicates that the flow regimes, refrigerant densities and viscosities of the two phase mixture circulating in the evaporator yielded to higher flow losses with respect to R410A. It should be emphasized that because of physical constraints in the distributor and indoor coil assembly, the refrigerant pressure tap at the inlet of the evaporator was installed at the inlet of the indoor coil refrigerant distributor. Thus, the pressure drops reported in Figure 59 are actually the pressure drops across the coil plus the pressure drop across the refrigerant inlet distributor.

Degree of superheat at evaporator outlet

The original TXV of the R410A unit was designed to adjust the load of the evaporator for a broad range of outdoor temperatures. For all the refrigerants, the superheat at compressor suction was controlled to at least 2.2ºC (4ºF) for the purpose of safe operation of compressor. The superheat at the evaporator outlet is shown in Figure 60 and Figure 61 for the drop-in tests and TXV soft optimization tests respectively. During drop-in tests, R410A had a degree of superheat at the evaporator outlet from 3 to 4ºC (5.6 to 7ºF), which yielded to a degree of superheat at the compressor suction of about 5.5ºC (10ºF). For DR-5, the TXV worked well, that is, it controlled the evaporator loading and provided similar degree of superheat at the outlet of the evaporator. For DR-4 at extreme high temperatures, controlling the superheat to above 0.6ºC to 1ºC (1ºF to 1.7ºF) if the system charge was constant was a major challenge. The charge that yielded to optimum COP at A-test conditions also produced very low degree of superheat at extreme high temperature conditions and very high degree of superheat at B-test conditions.

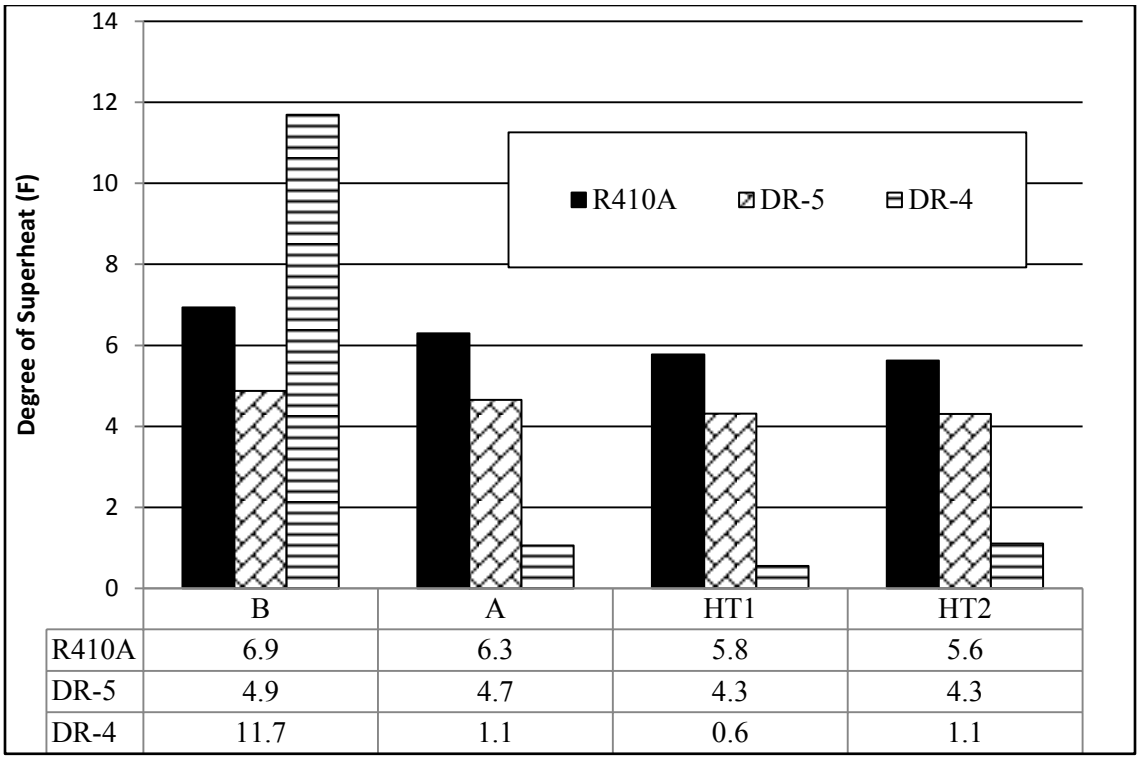

	B	A	HT1	HT2
R410A	6.9	6.3	5.8	5.6
DR-5	4.9	4.7	4.3	4.3
DR-4	11.7	1.1	0.6	1.1

Figure 60: Degree of superheat at evaporator outlet for drop-in tests

Figure 61 shows that it was possible to decrease the degree of superheat by adjusting the TXV, which also resulted in higher capacities and COPs of the system with the LGWP refrigerants. An important observation is that the system charge was not modified for R410A and DR-5 while it was adjusted for DR-4. This means that DR-5 was easier to be used as straight drop-in R410A replacements in the present AC system while DR-4 required charge management strategy and adjustments of the TXV to guarantee enough degree of superheat at the compressor suction, especially for extreme high ambient temperatures in which the unit was operating during the HT1 and HT2 tests. In case of DR-4, there was not any degree of superheat at evaporator outlet (i.e. flooded evaporator) as shown by the negative bars for the A, HT1, and HT2 tests in Figure 61. Due to the heat gained along the suction line and suction accumulator, a minimum acceptable degree of superheat at the compressor suction was achieved but operating conditions with flooded evaporator are not recommended.

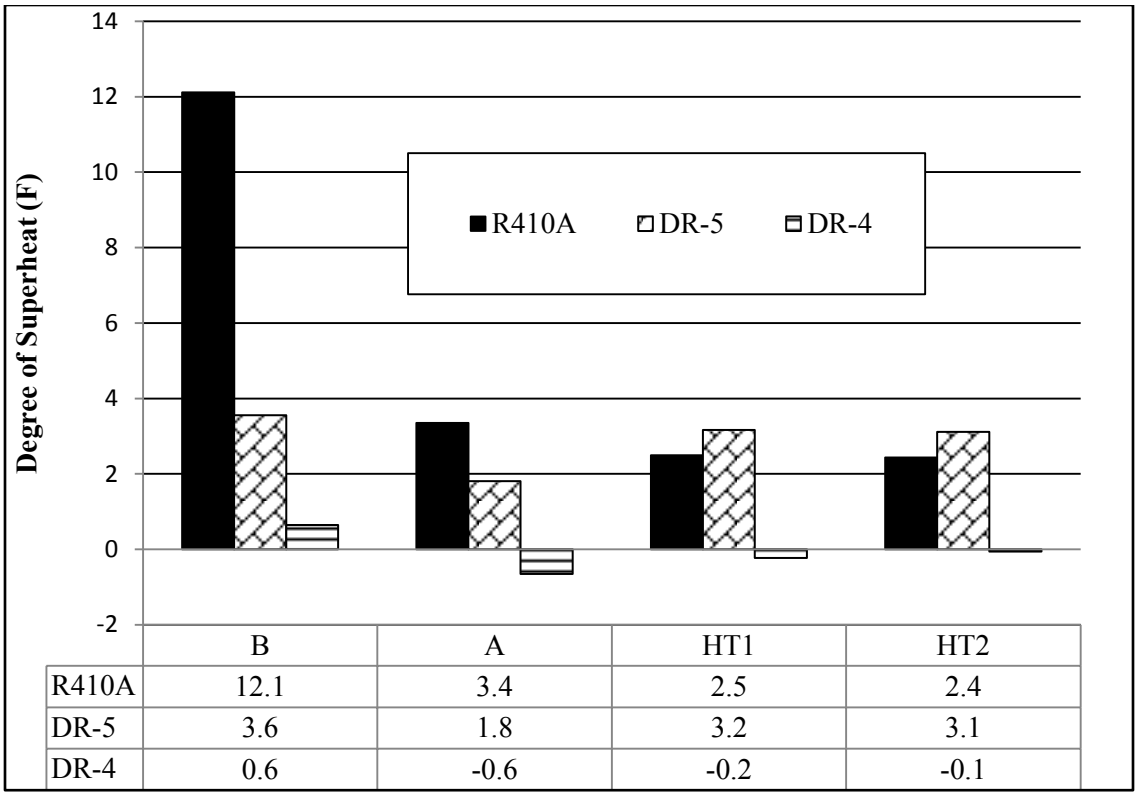

	B	A	HT1	HT2
R410A	12.1	3.4	2.5	2.4
DR-5	3.6	1.8	3.2	3.1
DR-4	0.6	-0.6	-0.2	-0.1

Figure 61: Degree of superheat at evaporator outlet for TXV soft-optimization tests

Degree of sub-cooling at condenser outlet

The degree of sub-cooling at condenser outlet for drop-in tests and TXV-optimization tests are shown in Figure 62 and Figure 63. Figure 62 indicates that R410A had a condenser sub-cooling of about 5.7 to 7.3ºC (10 to 13ºF). The degree of sub-cooling was about 6.6ºC (12ºF) for DR-5 and only about 1ºC (2ºF) for DR-4. For DR-4, the balance between the proper degree of superheat at the evaporator outlet and sufficient degree of the sub-cooling at the condenser outlet needed careful attention if the original TXV was employed (see DR-4 data in Figure 60 and in Figure 62).

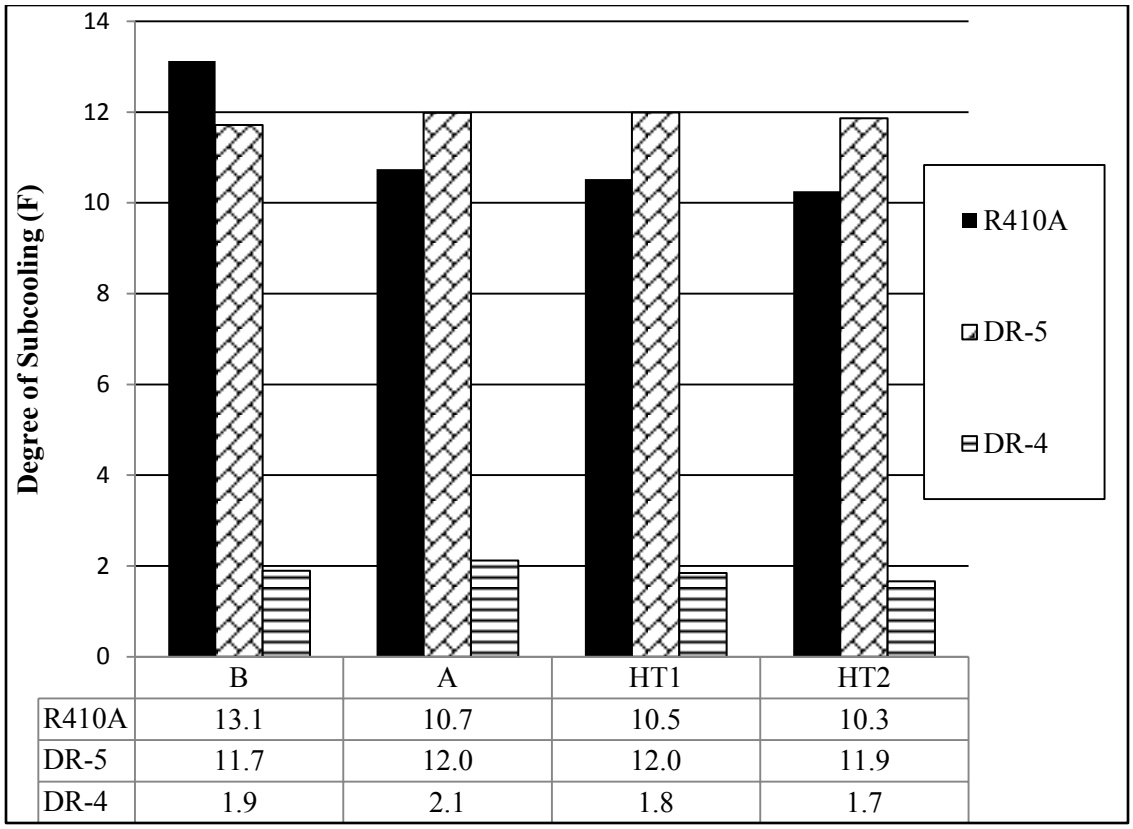

	B	A	HT1	HT2
R410A	13.1	10.7	10.5	10.3
DR-5	11.7	12.0	12.0	11.9
DR-4	1.9	2.1	1.8	1.7

Figure 62: Degree of sub-cooling at condenser outlet for drop-in tests

With the adjustments of the expansion valve and management of the charge 2 to 5ºC (4 to 7ºF) degree of sub-cooling at the condenser outlet were achieved as shown by the DR-4 data of Figure 63 at the expenses of operating with flooded evaporator at high temperature conditions (see DR-4 data in Figure 61). The values of condenser sub-cooling for R410A were similar to those during the drop-in tests, whereas for DR-5 there was a drop of 4 to 5ºF in the degree of sub-cooling between straight drop-in tests and soft optimization tests.

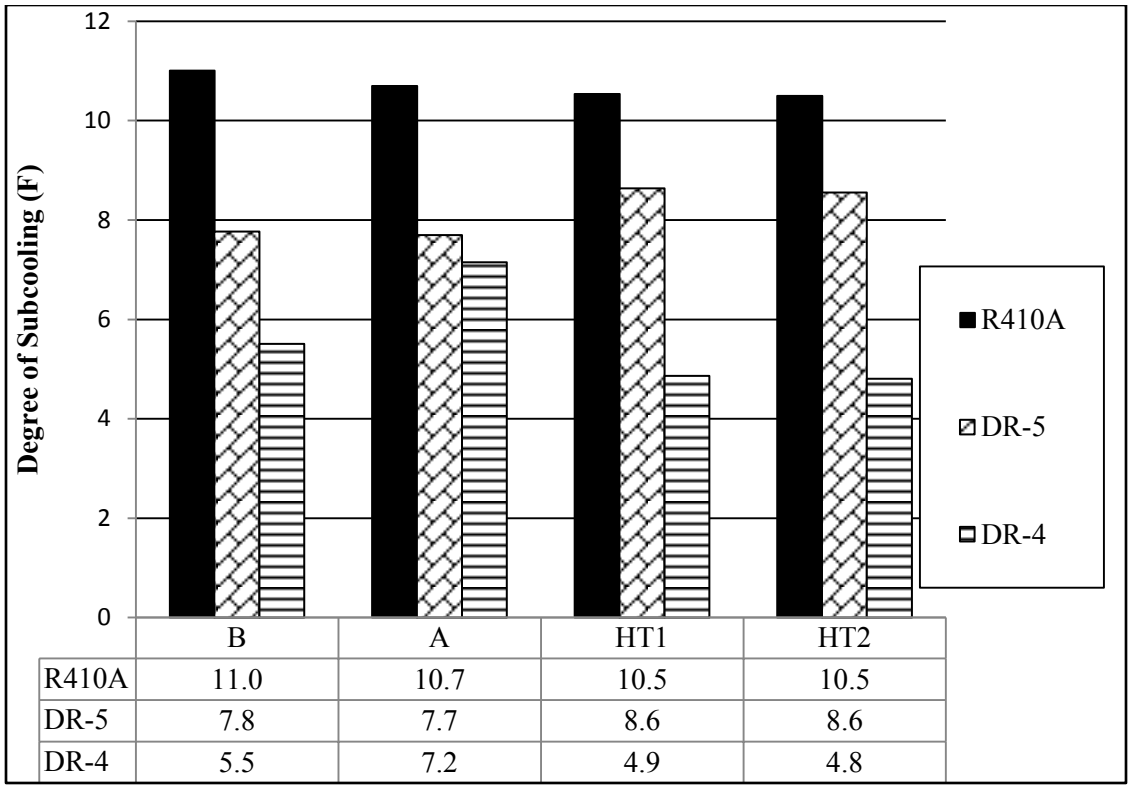

	B	A	HT1	HT2
R410A	11.0	10.7	10.5	10.5
DR-5	7.8	7.7	8.6	8.6
DR-4	5.5	7.2	4.9	4.8

Figure 63: Degree of sub-cooling at condenser outlet for TXV soft-optimization tests

Compressor performance

Compressor reliability might be affected by the compressor discharge temperature and pressure. Excessive discharge temperature might cause metal fatigue of the valves and thermal stress of the lubricant. Figure 64 and Figure 65 show the discharge temperatures for all the refrigerants during straight drop-in and TXV-optimization tests respectively. The temperatures were normalized with respect to the discharge temperatures of R410A at the same system testing condition.

Figure 64 shows that during drop-in tests DR-5 had a slight increase of the discharge temperature of only 3 to 5ºC (5.4 to 9ºF) during cooling and a drop of 1 to 25ºC (2 to 45ºF) during heating. DR-4 had lower discharge temperatures by about 5 to 9ºC (9 to 16.2ºF) during cooling and up to 47ºC (85ºF) during heating in comparison to that of R410A.

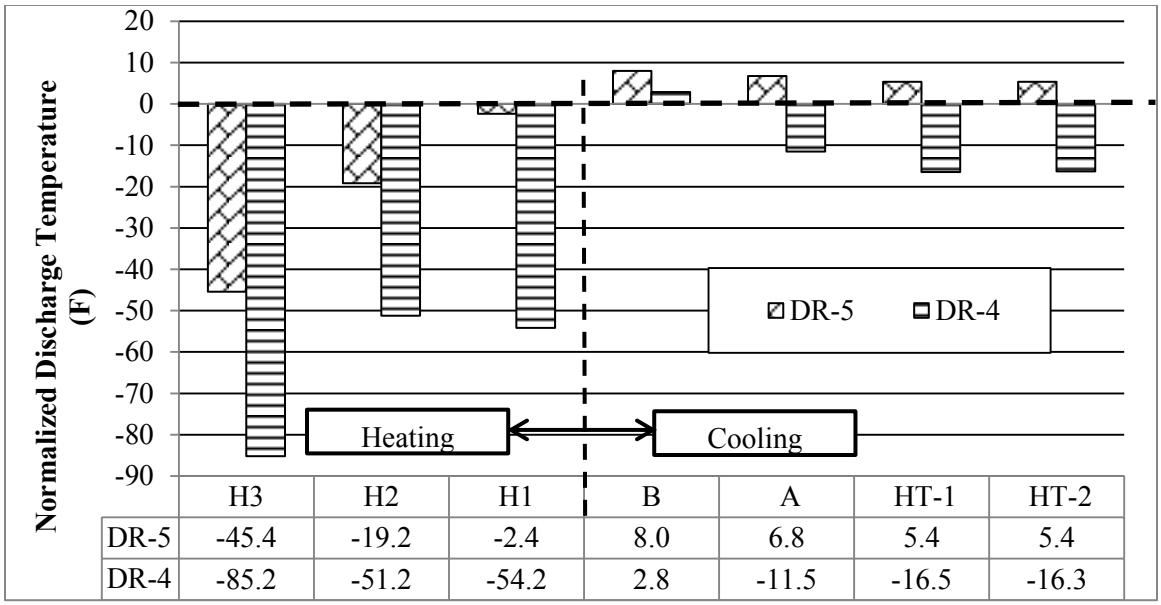

	H3	H2	H1	B	A	HT-1	HT-2
DR-5	-45.4	-19.2	-2.4	8.0	6.8	5.4	5.4
DR-4	-85.2	-51.2	-54.2	2.8	-11.5	-16.5	-16.3

Figure 64: Normalized compressor discharge temperature during drop-in tests

Figure 65 shows that during the TXV soft optimization tests, for DR-5 and DR-4, the increase in capacity was accompanied by an increase of the compressor discharge temperature. DR-5 yielded to an increase of discharge temperature up to 8ºC (14.4ºF) while even if DR-4 discharge temperature increased it was always lower than that of R410A by about 2 to 6ºC (3.6 to 10.8ºF).

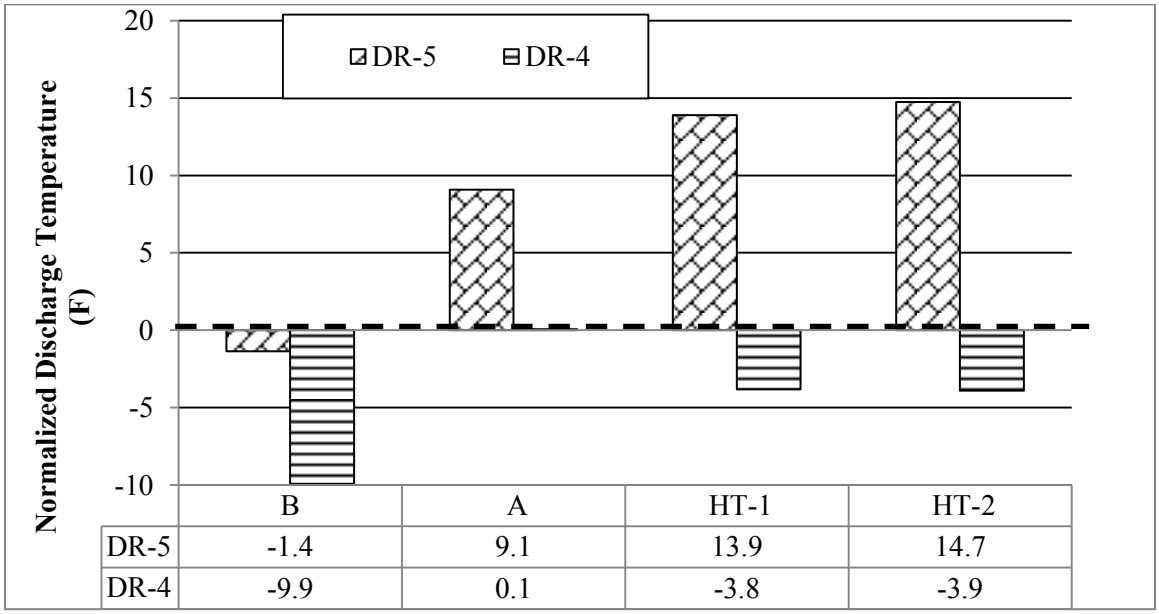

	B	A	HT-1	HT-2
DR-5	-1.4	9.1	13.9	14.7
DR-4	-9.9	0.1	-3.8	-3.9

Figure 65: Normalized compressor discharge temperature during TXV soft-optimization tests

Compressor volumetric efficiency

Volumetric efficiency takes into account the effect due to refrigerant vapor re-expansion in the clearance volume, pressure drop across suction and discharge valves and superheating of the colder vapor being in contact with hot compressor metal surfaces. Figure 66 shows the normalized volumetric efficiency for the DR-4 and DR-5 refrigerants with respect to R410A for the drop-in tests and Figure 67 represents the same quantities for the TXV soft optimization cooling tests for the entire range of outdoor temperatures.

DR-5 yielded to a 2% increase in volumetric efficiency during cooling and up to 8% increase during heating with respect to that of R410A for the drop-in tests and an increase of 1 to 3% for the TXV soft optimization cooling tests. DR-4 volumetric efficiency was 3 to 6% lower for both the drop-in and TXV soft optimization cooling tests. During drop-in heating tests it was up to 37% lower for DR-4. The flow rate data for DR-4 might not be accurate though because of the absence of sub-cooling, and thus one should be careful to generalize conclusions from these data of volumetric efficiencies for DR-4.

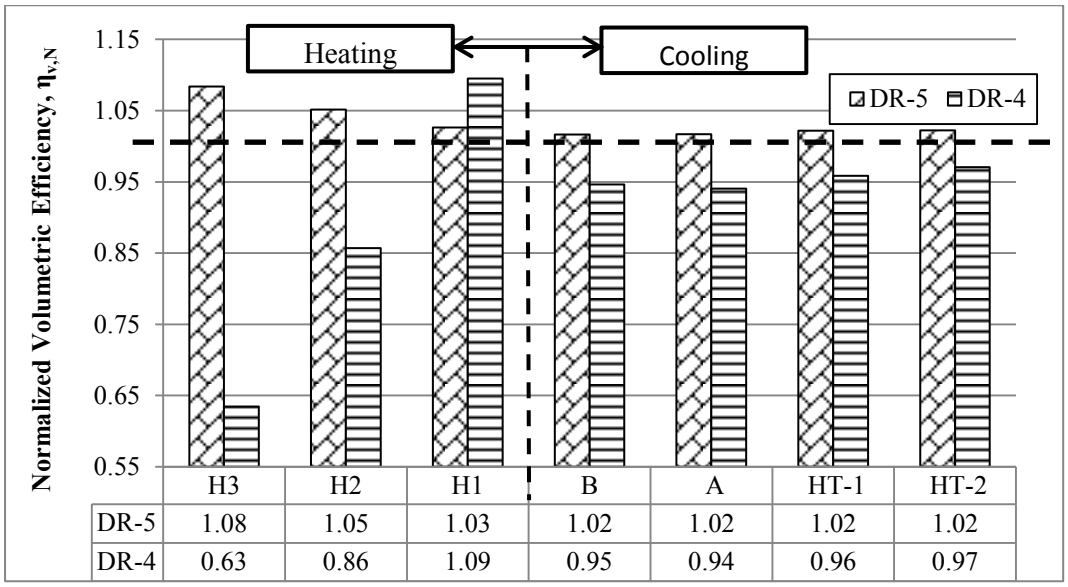

	H3	H2	H1	B	A	HT-1	HT-2
DR-5	1.08	1.05	1.03	1.02	1.02	1.02	1.02
DR-4	0.63	0.86	1.09	0.95	0.94	0.96	0.97

Figure 66: Normalized volumetric efficiency during Drop-in tests

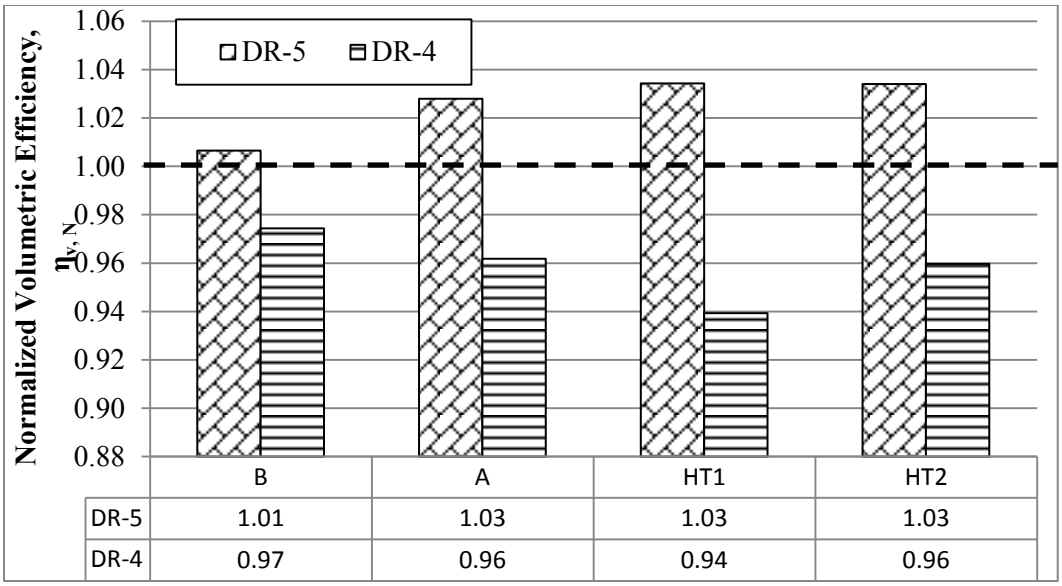

Figure 67: Normalized volumetric efficiency during TXV soft-optimization tests

Compressor thermal efficiency

Figure 68 and Figure 69 represents the thermal efficiency data for DR-4 and DR-5 during drop-in and TXV optimization tests respectively. All the data are normalized with respect to that of R410A at similar testing conditions.

Figure 68 shows that for DR-5 there was a drop of 10 to 15% in thermal efficiency compared to R410A and DR-4 had 13 to 20% lower thermal efficiencies during the drop-in tests. This could be due to the different magnitude of the heat exchanged in the 4-way valve, which could affect the values of the actual discharge temperatures read from the discharge temperature sensor. The actual heat losses from the compressor were not accounted in the estimation of the compressor thermal efficiency. However, the compressor was enclosed in an insulated box inside the unit and the temperature difference between the compressor shell and the surrounding air was expected to be small. Unfortunately the air temperature surrounding the compressor was not measured. So the above assumption cannot be verified.

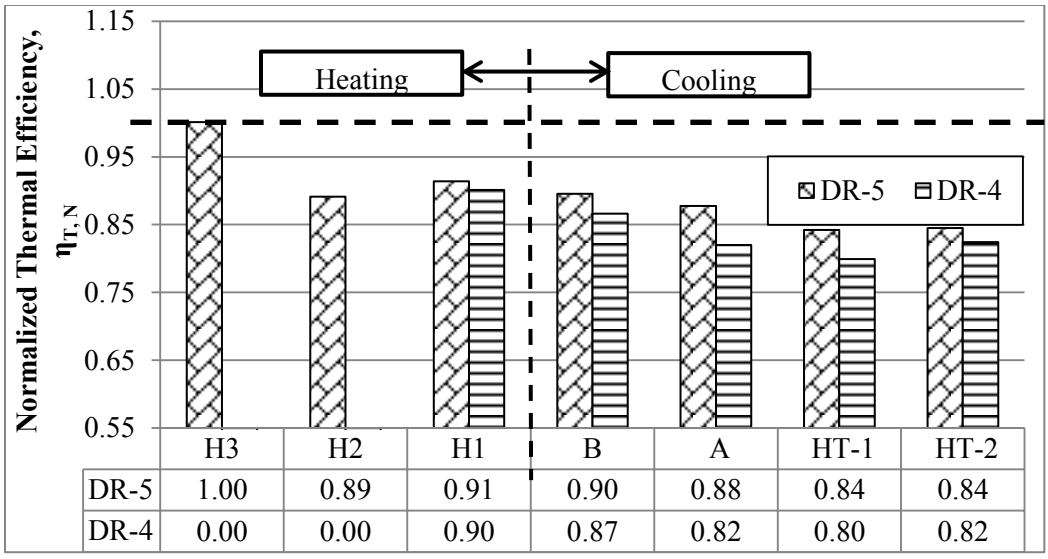

	H3	H2	H1	B	A	HT-1	HT-2
DR-5	1.00	0.89	0.91	0.90	0.88	0.84	0.84
DR-4	0.00	0.00	0.90	0.87	0.82	0.80	0.82

Figure 68: Normalized thermal efficiency during Drop-in tests

Figure 69 shows the normalized thermal efficiencies during the TXV soft optimization tests. The compressor experienced a drop of thermal efficiency from 9 to 12% for DR-5 and from 14 to 23% for DR-4. While these data are still preliminary they indicate that an optimization of the TXV yields to higher thermal efficiencies, higher volumetric efficiency and slightly higher discharge temperatures.

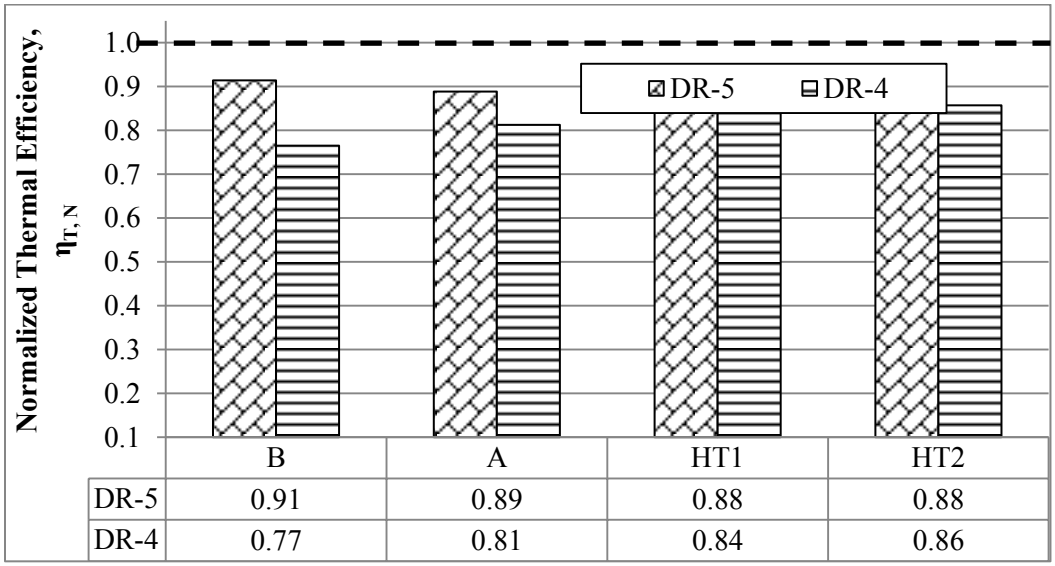

	B	A	HT1	HT2
DR-5	0.91	0.89	0.88	0.88
DR-4	0.77	0.81	0.84	0.86

Figure 69: Normalized thermal efficiency during TXV soft-optimization tests

CHAPTER VII

CONCLUSION

This thesis presents a study and new data on Low Global Warming Potential (LGWP) developmental refrigerants and it focuses on AC and heat pump systems for residential applications. A 17.6 kW (5 ton) AC ducted split unit, originally designed for R410A and commercially available off-the-shelf, was retrofitted with two new developmental refrigerants, DR-4 and DR-5 that have GWP ranging from 300 to 500. The experimental campaign was conducted at the psychrometric chamber of Oklahoma State University.

The following conclusions can be drawn from the work discussed in this thesis:

- The new developmental refrigerants DR-5 and DR-4 had 6% and 4% higher cooling COPs than R410A at A-test conditions, respectively. These two refrigerants had 7% and 10% higher heating COP than R410A at H1-test condition, respectively. The optimization of the expansion valve could improve further the COPs of these two refrigerants when the unit operates at design and extreme high temperature conditions.

- With proper charge management, DR-5 had 3% improvement in cooling capacity than R410A at A-test condition. The heating capacity was about 5% lower in comparison to R410A at H1-test condition. DR-4 had 14% lower cooling capacity at A-test condition and 30% lower heating capacity when compared to R410A. By conducting an optimization of the expansion valves the drop in capacity was partially mitigated.

- The compressor discharge temperatures and pressure of DR-5 were similar to those of R410A while DR-4 had significant lower discharge pressures and lower discharge temperatures than those for R410A. This was due to lower saturation pressures of DR-4 during condensation and evaporation processes in direct-expansion equipment. A soft optimization of the TXV was helpful in increasing the cooling capacity at the expenses of lowering compressor suction degree of vapor superheat and increasing the compressor discharge temperatures.

- The system with DR-5 had an improved compressor volumetric efficiency with an increase of 2% with respect to R410A at A-test condition, while DR-4 had lower volumetric efficiency by about 6%.

- The AC split system with the LGPW refrigerants of the present work had lower flow rates than that of R410A and the pressure drops across the evaporator also decreased.

A summary of the refrigerants characteristics and performance studied in the present thesis and in the literature is given in Table 11. The comparison of cooling COP, cooling capacity, volumetric efficiency, thermal efficiency and pressure drop are given for the A-test cooling condition, and the heating COP and heating capacity are given for the H1-test heating condition, as specified in the table.

Table 11: Summary table of characteristics and performance for refrigerants in the present thesis

	Present thesis			Literature	
	R410A	DR-4	DR-5	DR-4	DR-5
GWP	Not tested			<300	<500
Toxicity	Not tested			Non-toxic	Non-toxic
Flammability	Not tested			Class 2L	Class 2L
Lubricant compatibility	Not tested			POE	POE
Volumetric heat capacity (cooling- A test)	1	0.86	1.03	0.82	1
COP (cooling- A test)	1	1.04	1.06	0.90	1.04
Volumetric heat capacity (heating- H1 test)	1	0.7	0.95	0.81	1
COP (heating- H1 test)	1	1.10	1.07	0.97	1.01
Charge management	excellent	Difficult at extreme high temperatures	excellent	Not reported	
Operation of system with no modification	excellent	Scope of further improvement	excellent		
Normalized discharge temperature	0	-11.5	+6.8		
$\eta_{V,N}$	1	0.94	1.02		
$\eta_{T,N}$	1	0.82	0.88		
ΔP_{evap}	1	0.79	0.71		

The original R410A TXV controlled well the evaporator thermal loads for DR-5 while DR-4 required charge management strategies and adjustments of the TXV. The charge management was critical when the unit was brought to extreme high temperature ambient conditions. From this point of view DR-5 was easier to be used as a replacement for R410A in the present AC system

for residential stationary applications. DR-4 is expected to perform better in the same system with a bigger compressor.

An important lesson I learnt from this research project is the potential energy improvements that new developmental refrigerants might provide when used to retrofit R410A in residential HVAC units. The performance and operation of the system with and without modification of the system expansion valve and the refrigerant charge management for these new refrigerants have never been reported in a comprehensive way in previous published work. This thesis fills these gaps. It also makes the work unique in the sense that it analyzes the performance of the components, such as the compressor and the evaporator at design and off design conditions of extreme high ambient temperatures. This will help the researchers to have a better understating of the challenges when using low GWP refrigerant in current AC systems and how to modify the system components in order to increase the energy efficiency and sustainability of the system.

Although the industry has to heavily focus on the environmental issues at this point, I believe it is important to gauge the energy performance and inspect component compatibility of the system when using new LGWP refrigerants. Using a LGWP refrigerant is beneficial from a GWP perspective but could become detrimental on the system energy performance. A severe reduction of the system performance will result in burning more fossil fuel somewhere else at the power plant stage. If that occurs then the overall effect on the environment of using a LGWP refrigerant in air conditioning and heat pump systems might not be beneficial. While this thesis focuses mainly on measuring the energy performance of the units using LGWP refrigerants as “drop-in” fluids, ongoing and further work is needed to assess potential system modifications and optimizations.

REFERENCES

Abdelaziz, O., Fricke, B., Vineyard, E., 2012, Development of Low Global Warming Potential Refrigerant Solutions for Commercial Refrigeration Systems using a Life Cycle Climate Performance Design Tool, *International Refrigeration and Air Conditioning Conference at Purdue, West Lafayette, Indiana, July 12-15.*

Althof, E. Smithart, and J. Sidebottom, 2001, "The HVAC response to the energy challenge," *ASHRAE Journal, vol. 43, pp. 40-43.*

ANSI/ASHRAE Standard 37, 2009, Methods of Testing for Rating Electrically Driven Unitary Air-Conditioning and Heat Pump Equipment, *Atlanta, GA.*

ANSI/ASHRAE Standard 41.2, 1987, Standard Method for Laboratory Airflow Measurement, *Atlanta, GA.*

ANSI/AHRI Standard 210/240, 2010, Standard for Performance Rating of Unitary Air-Conditioning & Air-Source Heat Pump Equipment, *Arlington, VA.*

ASHRAE/ANSI Standard 34, 2007, Designation and Safety Classification of Refrigerants, *American Society of Heating, Refrigeration, and Air Conditioning Engineers, Atlanta, GA.*

Barve, A., Cremaschi, L., 2012, Drop-in Performance of Low GWP Refrigerants in a Heat Pump System for Residential Applications, *International Refrigeration and Air Conditioning Conference at Purdue, West Lafayette, Indiana, July 16-19*

Barve, A., 2012, Study of Low Global Warming Potential Refrigerants in Heat Pump Systems for Stationary Applications, *MS thesis, Oklahoma State University.*

Berntsen, T.K., *et al.*, 2005, Climate response to regional emissions of ozone precursors; sensitivities and warming potentials. *Tellus, 4B, 283–304.*

Collins, W.J., R.G. Derwent, C.E. Johnson, and D.S. Stevenson, 2002, The oxidation of organic compounds in the troposphere and their global warming potentials. *Clim. Change, 52, 453–479.*

Chen, W., 2008, A comparative study on the performance and environmental characteristics of R410A and R22 residential air conditioner, *Applied Thermal Engineering 28, pp. 1–7*

Cremaschi, L. and E. Lee., 2008, Design and heat transfer analysis of a new psychrometric environmental chamber for heat pump and refrigeration systems testing. *ASHRAE Transactions 114(2):619-631.*

Domanski, P.A., Yashar, D., Kim, M., 2005, Performance of a finned-tube evaporator optimized for different refrigerants and its effect on system efficiency, *International Journal of Refrigeration 28, pp. 820–827.*

EIA, 2011, Annual Energy Outlook 2011: Statistics on Potential efficiency improvements in alternative cases for appliance standards and building codes, *Energy Information Administration, DOE/EIA report 0383(2011), available on line at http://www.eia.gov/forecasts/aeo/pdf/0383(2011).pdf*

EPA, 2011, Energy Conservation Program. Environmental Protection Agency. Available on line: http://www.epa.gov/greeningepa/energy/

Forster, P., V. Ramaswamy, P. Artaxo, T. Berntsen, R. Betts, D.W. Fahey, J. Haywood, J. Lean, D.C. Lowe, G. Myhre, J. Nganga, R. Prinn, G. Raga, M. Schulz and R. Van Dorland, 2007, Changes in Atmospheric Constituents and in Radiative Forcing. In: Climate Change 2007: The Physical Science Basis. Contribution of Working Group I to the Fourth Assessment Report of the Intergovernmental Panel on Climate Change [Solomon, S., D. Qin, M. Manning, Z. Chen, M. Marquis, K.B. Averyt, M.Tignor and H.L. Miller (eds.)], report, *Cambridge University Press, Cambridge, United Kingdom and New York, NY, USA.*

Fuglestvedt, J.S., *et al.*, 2003, Metrics of climate change: assessing radiative forcing and emission indices. *Clim. Change, 58, 267–331.*

Horie, H., Kamiaka, T., Dang, C., Hihara, E., 2010, Study On Cycle Property And Lccp Evaluation of Heat Pump Using HFO-1234yf, HFC-32, And HFC-410a as Refrigerant, *2010 International Symposium on Next-generation Air Conditioning and Refrigeration Technology,17 – 19 February 2010, Tokyo, Japan.*

IEA, 2010, Energy Technology Perspective: Scenarios and Strategies to 2050, report, *Paris, France.* Available on line at http://www.iea.org/techno/etp/etp10/English.pdf: International Energy Agency.

IPCC, 1994, Climate Change 1994: Radiative Forcing of Climate Change and an Evaluation of the IPCC IS92 Emission Scenarios [Houghton, J.T., L.G. Meira Filho, J. Bruce, H. Lee, B.A. Callander, E.F. Haites, N. Harris, and K. Maskell (eds.)]. *Cambridge University Press, Cambridge, United Kingdom and New York, NY, USA.*

Kontomaris, K., T. J. Leck, 2009, Low GWP Refrigerants for Centrifugal Chillers, *ASHRAE Annual Conference, June 20-24, Louisville, Kentucky.*

Kontomaris, K., Leck, T.J., Hughes, J., 2010, A Non-Flammable, Reduced GWP, HFC-134a Replacement in Centrifugal Chillers: DR-11, *International Refrigeration and Air Conditioning Conference at Purdue, West Lafayette, IN , July 12-15.*

Kontomaris, K., Kauffman, J.K., Kulankara, S., 2012, A Reduced GWP Replacement for HFC-134a in Centrifugal Chillers: XP10 Measured Performance and Projected Climate Impact,

International Refrigeration and Air Conditioning Conference at Purdue, West lafayette, Indiana, July 16-19.

Kim, M., Pettersen, J., Bullard C.W., 2004, Fundamental process and system design issues in CO_2 vapor compression system, *Progress in Energy and Combustion Science 30 (2004) 119–174*

Kim, S.G., Kim, M.S., Ro, S.T., 2002, Experimental investigation of the performance of R22, R407C and R410A in several capillary tubes for air-conditioners, *International Journal of Refrigeration 25 , pp. 521–531*

Kim, W., Braun, J.E., 2010, Impacts of Refrigerant Charge on Air Conditioner and Heat Pump Performance, *International Refrigeration and Air Conditioning Conference at Purdue, West Lafayette, IN, July 12-15*

Kruse, H. (1998). Is the TEWI Number Suitable for Evaluating the Combined Global Warming Effect of Refrigeration and Heat Pump Systems? *HVAC&R Research, 4:3, 203-204. http://dx.doi.org/ 10.1080/10789669.1998.10391400*

Leck, T.J., 2009, Evaluation of HFO-1234yf as a Potential Replacement for R-134a in Refrigeration Applications, *The Third Conference on Thermophysical Properties and Transfer Processes of Refrigerants, by The National Institute of Standards and Technology and the International Institute of Refrigeration, Boulder, Colorado, USA, June 23-26.*

Leck, T.J., 2010, New High Performance, Low GWP Refrigerants for Stationary AC and Refrigeration, *International Refrigeration and Air Conditioning Conference at Purdue, West Lafayette, IN , July 12-15*

Leck, T.J. and Yamaguchi, Y. 2010, Development and Evaluation of Reduced GWP AC and Heating Fluids *Proc. JRAIA Int'l Symposium, Kobe, Japan, Dec 2-3*

Lifferth, S.O., 2009, Design and Construction of A New Psychrometric Chamber, *M.S. Thesis, Oklahoma State University.*

McLinden, M.O., 2011, Property Data for Low-GWP Refrigerants, *ASHRAE Winter Meeting, Las Vegas, NV, Seminar 6—Removing Barriers for Low-GWP Refrigerants, January 30, 2011*

Minor, B., Spatz, M., 2008, HFO-1234yf Low GWP Refrigerant Update, *International Refrigeration and Air Conditioning Conference at Purdue, West Lafayette, IN, July 14-17, 2008*

Moezzi, M., 2000, Decoupling energy efficiency from energy consumption, *Energy and Environment, vol. 11, pp. 521-537.*

Papasavva, S., Hill, W.R., and Andersen, S.O., 2010, GREEN-MAC-LCCP: A Tool for assessing the Life Cycle Climate Performance of MAC Systems, *Env. Sc. Tech., vol. 44, no. 19, p. 7666-7672.*

Pande M., Hwang Y.H., Judge J., Radermacher R., 1996, An Experimental Evaluation of Flammable and Non-Flammable High Pressure HFC Replacements for R-22, *International Refrigeration and Air Conditioning Conference, West Lafayette, IN.*

Payne, W.V., Domasnki, P.A., 2002, A Comparison Of An R22 And An R410A Air Conditioner Operating At High Ambient Temperatures, *International Refrigeration and Air Conditioning Conference at Purdue, West Lafayette, IN.*

Pham, H., 2010, Next Generation Refrigerants: Standards and Climate Policy Implications of Engineering Constraints, *2010 ACEEE Summer Study on Energy Efficiency in Buildings*.

Pham, H., Rajendran, R., 2012, R32 and HFOs as Low-GWP Refrigerants For Air Conditioning, *International Refrigeration and Air Conditioning Conference at Purdue, West lafayette, Indiana, July 16-19.*

Prather, M.J., *et al.*, 2001, Atmospheric chemistry and greenhouse gases. In: Climate Change 2001: The Scientific Basis. Contribution of Working Group I to the Third Assessment Report of the Intergovernmental Panel on Climate Change [Houghton, J.T., *et al.* (eds.)], report, *Cambridge University Press, Cambridge, United Kingdom and New York, NY, USA, pp. 239–287.*

Ramaswamy, V., O. Boucher, J. Haigh, D. Hauglustaine, J. Haywood, G. Myhre, T. Nakajima, G.Y. Shi and S. Solomon, 2001: Radiative Forcing of Climate Change. In: Climate Change 2001: The Scientific Basis. Contribution of Working Group I to the Third Assessment Report of the Intergovernmental Panel on Climate Change [Houghton, J.T., Ding, Y., Griggs, D.J., Noguer, M., van der Linden, P.J., Dai, X., Maskell, K., and Johnson, C.A. (eds.)], report, *Cambridge University Press, Cambridge, United Kingdom and New York, NY, USA.*

Rasmussen, B., A. Musser, A. Alleyne, C. Bullard, P. Hrnjak, and N. Miller, 2003, "A Control-Oriented Model of Transcritical Air-Conditioning System Dynamics," *SAE 2002 Transactions Journal of Passenger Cars--Mechanical Systems, pp. 374-381.*

Reasor, P., Radermacher, R., Aute, V., 2010, Refrigerant R1234yf Performance Comparison Investigation, *International Refrigeration and Air Conditioning Conference at Purdue, West Lafayette, IN, July 12-15.*

Richter, M. R., S. M. Song, J. M. Yin, M. H. Kim, C. W. Bullard, and P. S. Hrnjak, 2003, "Experimental Results of Transcritical CO2 Heat Pump for Residential Application," *Energy, 28:10, pp. 1005-1019.*

Rigola, J., Morales, S., Raush, G., Segarra, C.C.P., Ablanque, N., 2004, Numerical Study and Experimental Validation of aTranscritical Carbon Dioxide Refrigerating Cycle, *International refrigeration and Air Conditioning Conference at Purdue, West lafayette, IN.*

Sand, J.R., Fischer, S.K., Baxter, V.D., 1999, TEWI Analysis: Its Utility, Its Shortcomings, and Its Results, *International Conference on Atmospheric Protection, Taipei, Taiwan, September 13-14.*

Shine, K.P., T.K. Berntsen, J.S. Fuglestvedt, and R. Sausen, 2005a: Scientific issues in the design of metrics for inclusion of oxides of nitrogen in global climate agreements. *Proc. Natl. Acad. Sci. U.S.A., 102, 15768–15773.*

Shine, K.P., J.S. Fuglestvedt, K. Hailemariam, and N. Stuber, 2005b: Alternatives to the global warming potential for comparing climate impacts of emissions of greenhouse gases. *Clim. Change, 68, pp. 281–302.*

Smith, S.J., and T.M.L. Wigley, 2000: Global warming potentials: 2. *Accuracy. Clim. Change, 44, 459–469.*

Solomon, S., Qin, D., Manning, M., Chen, Z., Marquis, M., Averyt, K.,B., Tignor, M., and Miller, H.L. (eds.), 2007, Contribution of Working Group I to the Fourth Assessment Report of the Intergovernmental Panel on Climate Change, report, *Cambridge University Press, Cambridge, United Kingdom and New York, NY, USA.*

Spatz, M.W., 2012, Latest Developments of Low Global Warming Refrigerants for Chillers, *International Refrigeration and Air Conditioning Conference at Purdue, West lafayette, Indiana, July 16-19.*

Taira, S., Yamakawa, T., Nakai, A., Yajima, R., 2011, Analysis of LGWP Alternatives for Small Refrigeration (Plugin) Applications, IEH Heat Pump Conference, Tokyo, Japan, vol. 29, P. 22-29.

UNEP, 1987, Montreal Protocol on Substances That Deplete The Ozone Layer, report, *Montreal, Canada.*

Wang, X., Amrane, K., Johnson, P., 2012, Low Global Warming Potential (GWP) Alternative Refrigerants Evaluation Program (Low-GWP AREP, *International Refrigeration and Air Conditioning Conference at Purdue, West lafayette, Indiana, July 16-19.*

WMO, 2003: Scientific Assessment of Ozone Depletion: 2002. *Global Ozone Research and Monitoring Project Report No. 47, World Meteorological Organization, Geneva, 498 pp.*

Worthington, K., 2011, Calibration of The Osu Psychrometric Chamber and First Experiments, *M.S. Thesis, Oklahoma State University.*

Worthington, K., Cremaschi., L., and Aslan, O., 2011, A new experimental low temperature facility to measure comprehensive performance rating of unitary equipment and systems operating at design and off-design conditions, *Proceedings of the International Conference on Air-Conditioning and Refrigeration ICACR 2011, July 6-8, 2011, Yongpyong Resort, Gangwon-Do, KOREA, paper no 147, Page81.*

Yana Motta, S., F., Vera Becerra, E., D., Spatz, M., W., 2010, Low Global Warming Alternative Refrigerants For Stationary AC&R Applications, *International Refrigeration and Air Conditioning Conference at Purdue, West Lafayette, IN, July 12-15.*

Yana Motta, S., F., Spatz, M., W.,Vera Becerra, E., D., 2012, Low Global Warming Refrigerants for Commercial Refrigeration Systems, *International Refrigeration and Air Conditioning Conference at Purdue, West lafayette, Indiana, July 16-19.*

Yin, J. M., Park, Y., C. , McEnaney, R., P. , Boewe, D., E., Beaver, A., Bullard, C., W., and Hrnjak, P., S. , 1998, Experimental and model comparison of transcritical CO2 versus R134a and R410A system performance, *IIR conference Gustav Lorentzen, Oslo, Norway, pp. 331-340.*

APPENDICES

Appendix A: EES code for uncertainty analysis

```
"Procedure for finding CFM (AHRI/ASHRAE statndard 37)"

Procedure CFM_calc(T_db_nozzle,omega_supply,P_nozzle_inlet,delta_P_nozzle, N_1, N_2,
N_3, N_4, N_5, N_6, N_7, N_8, N_9, N_10:CFM)

    T_abs= T_db_nozzle+459.67
    v=0.370486*T_abs*((1+1.607858*omega_supply)/P_nozzle_inlet)
    rho=1/v*(1+omega_supply)

    D[1]=N_1*0.5/12
    D[2]=N_2*3/12
    D[3]=N_3*4/12
    D[4]=N_4*4/12
    D[5]=N_5*5.5/12
    D[6]=N_6*5.5/12
    D[7]=N_7*5.5/12
    D[8]=N_8*5.5/12
    D[9]=N_9*5.5/12
    D[10]=N_10*5.5/12

    CA=0
    i=0

    Repeat
        i= i+1
        Re=1.363E6*D[i]*(delta_P_nozzle*rho)^0.5
        C=2.2E-31*Re^5-6.09E-25*Re^4+6.77E-19*Re^2+1.28E-7*Re+0.969
        A=3.1416*D[i]^2/4
        CA=CA+C*A
    Until (i=10)

    alpha=1-(5.187*delta_P_nozzle)/(rho*53.35*T_abs)
    Y=1- 0.548*(1-alpha)
    CFM=1096*CA*Y*(delta_P_nozzle/rho)^0.5

End CFM_calc


"Converting pressure units"

delta_P_unit_psi=delta_P_unit*0.0361
```

```
delta_P_nozzle_psi=delta_P_nozzle*0.0361
P_room_psi=P_room*0.0361
Barometer_psi=Barometer*0.0361
P_before_nozzle_psi=P_before_nozzle*0.0361


"Defining Pressures"

P_return=P_room_psi+ Barometer_psi
P_supply=P_return+delta_P_unit_psi
P_nozzle_inlet=P_before_nozzle_psi+Barometer_psi

"Return air properties"
h_return=Enthalpy(AirH2O,T=T_db_return,B=T_wb_return,P=P_return)
omega_return=HumRat(AirH2O,T=T_db_return,B=T_wb_return,P=P_return)

"Supply air peroperties"
omega_supply=HumRat(AirH2O,T=T_db_supply,B=T_wb_supply,P=P_supply)
h_supply=Enthalpy(AirH2O,T=T_db_mesh,w=omega_supply,P=P_supply)

C_p_supply=Cp(AirH2O,T=T_db_nozzle,w=omega_supply,P=P_supply)
rho_supply=density(AirH2O,T=T_db_nozzle,w=omega_supply,P=P_supply)

"Calculate CFM"
Call CFM_calc(T_db_nozzle,omega_supply,P_nozzle_inlet,delta_P_nozzle, 0,1,1,0,1,0,0,0,0,0
:CFM)


"Capacity calculations"
delta_h=abs(h_return-h_supply)
Capacity=CFM*rho_supply*(h_return-h_supply)*60
Capacity_sen=CFM*rho_supply*C_p_supply*(T_db_return-T_db_mesh)*60
Capacity_lat=CFM*rho_supply*(omega_return-omega_supply)*60

"COP calculation"
COP=Capacity/(Power*3.413)
```

Appendix B: DAQ Channels for the Project

Table 12: DAQ channels for the project

Index no.	Label	Function	DAQ module no.	Ch. no.	Type of data	Signal type	Type/model of sensor	Connection location
Inline Thermocouples								
196	T4_11	T_1	SCXI 1-MODULE7	Ch_4	Temperature	-	T-type TC	DAQBOX_4
197	T4_12	T_2	SCXI 1-MODULE7	Ch_5	Temperature	-	T-type TC	DAQBOX_4
198	T4_13	T_6	SCXI 1-MODULE7	Ch_6	Temperature	-	T-type TC	DAQBOX_4
153	T7_35	T_4	SCXI 1-MODULE5	Ch_25	Temperature	-	T-type TC	DAQBOX_7
396	T7_41	T_3	SCXI 2-MODULE6	Ch_12	Temperature	-	T-type TC	DAQBOX_7
397	T7_42	T_5	SCXI 2-MODULE6	Ch_13	Temperature	-	T-type TC	DAQBOX_7
Surface Thermocouples								
199	T4_14	T_{s6}	SCXI 1-MODULE7	Ch_7	Temperature	-	T-type TC	DAQBOX_4
200	T4_15	T_{s1}	SCXI 1-MODULE7	Ch_8	Temperature	-	T-type TC	DAQBOX_4
202	T4_17	T_{s7}	SCXI 1-MODULE7	Ch_10	Temperature	-	T-type TC	DAQBOX_4
203	T4_18	T_{s0}	SCXI 1-MODULE7	Ch_11	Temperature	-	T-type TC	DAQBOX_4
204	T4_19	T_{s8}	SCXI 1-MODULE7	Ch_12	Temperature	-	T-type TC	DAQBOX_4
205	T4_20	T_{s9}	SCXI 1-MODULE7	Ch_13	Temperature	-	T-type TC	DAQBOX_4
398	T7_43	T_{s4}	SCXI 2-MODULE6	Ch_14	Temperature	-	T-type TC	DAQBOX_7
399	T7_44	T_{s5}	SCXI 2-MODULE6	Ch_15	Temperature	-	T-type TC	DAQBOX_7
Air-side Thermocouples								
410	T7_55	Supply TC	SCXI 2-MODULE6	Ch_26	Temperature	-	T-type TC	DAQBOX_7
411	T7_56	Supply TC	SCXI 2-MODULE6	Ch_27	Temperature	-	T-type TC	DAQBOX_7
412	T7_57	Supply TC	SCXI 2-MODULE6	Ch_28	Temperature	-	T-type TC	DAQBOX_7
413	T7_58	Supply TC	SCXI 2-MODULE6	Ch_29	Temperature	-	T-type TC	DAQBOX_7
415	T7_60	Supply TC	SCXI 2-MODULE6	Ch_31	Temperature	-	T-type TC	DAQBOX_7
400	T7_45	After coil TC	SCXI 2-MODULE6	Ch_16	Temperature	-	T-type TC	DAQBOX_7
402	T7_47	After coil TC	SCXI 2-MODULE6	Ch_18	Temperature	-	T-type TC	DAQBOX_7

404	T7_49	After coil TC	SCXI 2-MODULE6	Ch_20	Temperature	-	T-type TC	DAQBOX_7
405	T7_50	After coil TC	SCXI 2-MODULE6	Ch_21	Temperature	-	T-type TC	DAQBOX_7
406	T7_51	After coil TC	SCXI 2-MODULE6	Ch_22	Temperature	-	T-type TC	DAQBOX_7
407	T7_52	After coil TC	SCXI 2-MODULE6	Ch_23	Temperature	-	T-type TC	DAQBOX_7
408	T7_53	After coil TC	SCXI 2-MODULE6	Ch_24	Temperature	-	T-type TC	DAQBOX_7
In/Out signals								
302	In/Out4_5	P_1	SCXI 1-MODULE11	Ch_14	Pressure	4-20 mA	1000 psi PG	DAQBOX_4
339	In/Out7_6	P_3	SCXI 1-MODULE12	Ch_19	Pressure	4-20 mA	500 psi PG	DAQBOX_7
340	In/Out7_7	P_5	SCXI 1-MODULE12	Ch_20	Pressure	4-20 mA	500 psi PG	DAQBOX_7
341	In/Out7_8	P_4	SCXI 1-MODULE12	Ch_21	Pressure	4-20 mA	500 psi PG	DAQBOX_7
326	In/Out6_5	P_6	SCXI 1-MODULE12	Ch_6	Pressure	4-20 mA	500 psi PG	DAQBOX_6
327	In/Out6_6	P_2	SCXI 1-MODULE12	Ch_7	Pressure	4-20 mA	500 psi PG	DAQBOX_6
337	In/Out7_4	MFM	SCXI 1-MODULE12	Ch_17	Flow Rate	4-20 mA	MFM	DAQBOX_7
RTDs								
270	RTD4_9	Outdoor DB	SCXI 1-MODULE9	Ch_14	Temperature	-	RTD	DAQBOX_1
271	RTD4_10	Outdoor WB	SCXI 1-MODULE9	Ch_15	Temperature	-	RTD	DAQBOX_1
259	RTD2_1	Nozzle DB	SCXI 1-MODULE9	Ch_3	Temperature	-	RTD	DAQBOX_2
260	RTD2_2	Supply DB	SCXI 1-MODULE9	Ch_4	Temperature	-	RTD	DAQBOX_2
261	RTD2_3	Supply WB	SCXI 1-MODULE9	Ch_5	Temperature	-	RTD	DAQBOX_2
280	RTD5_9	Return DB	SCXI 1-MODULE9	Ch_24	Temperature	-	RTD	DAQBOX_5
281	RTD5_10	Return WB	SCXI 1-MODULE9	Ch_25	Temperature	-	RTD	DAQBOX_5

Appendix C: Miscellaneous Lab View Screenshots

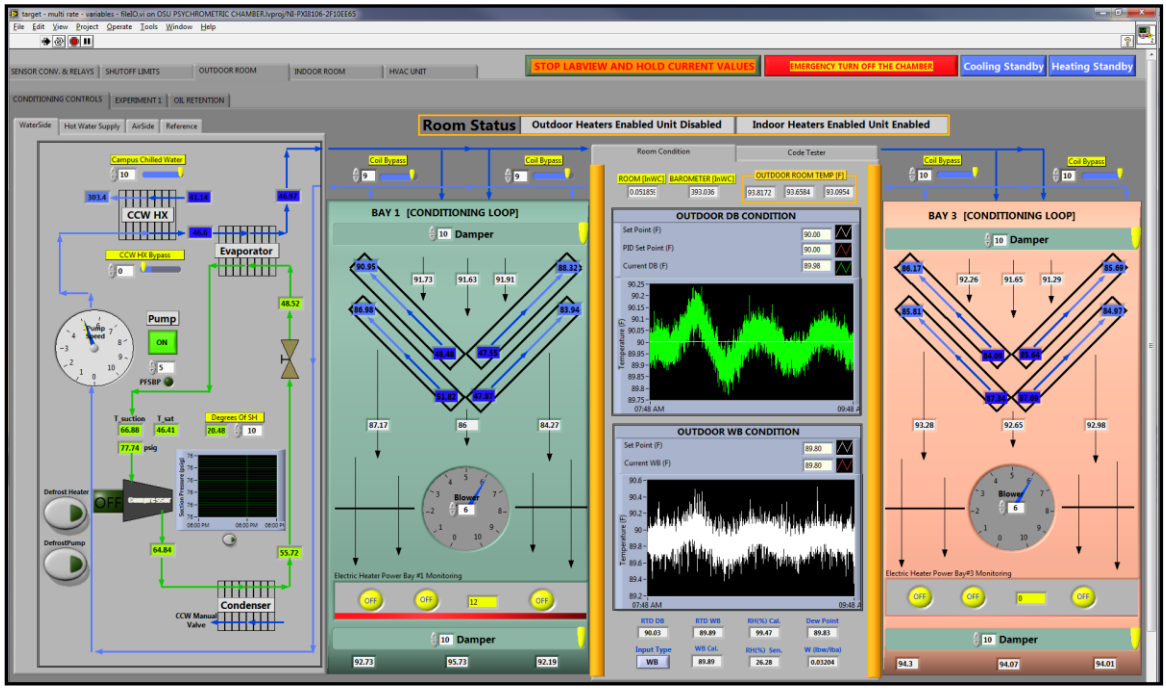

Figure 70: Outdoor conditioning loop

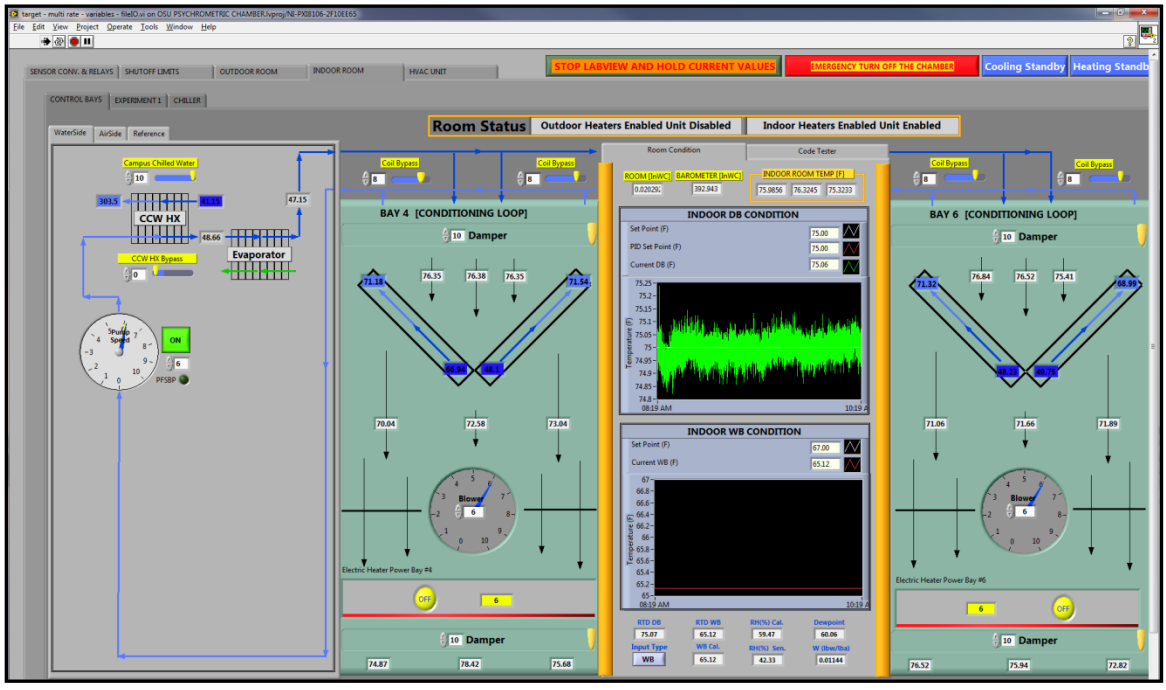

Figure 71: Indoor conditioning loop

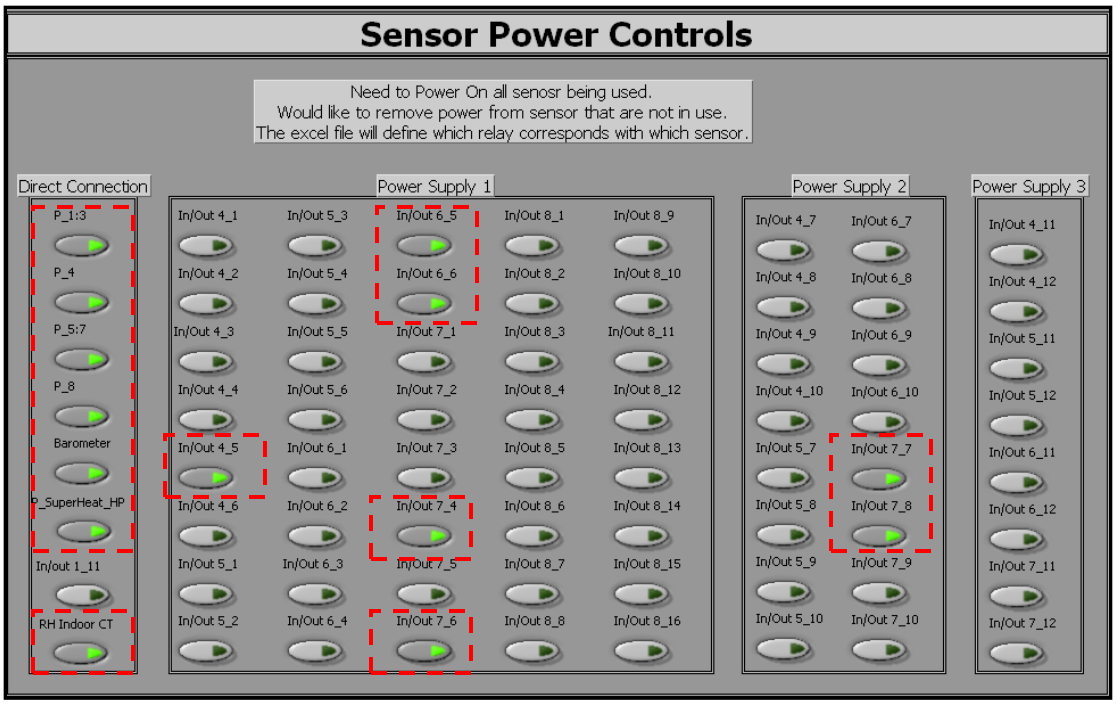

Figure 72: Sensor relay tab

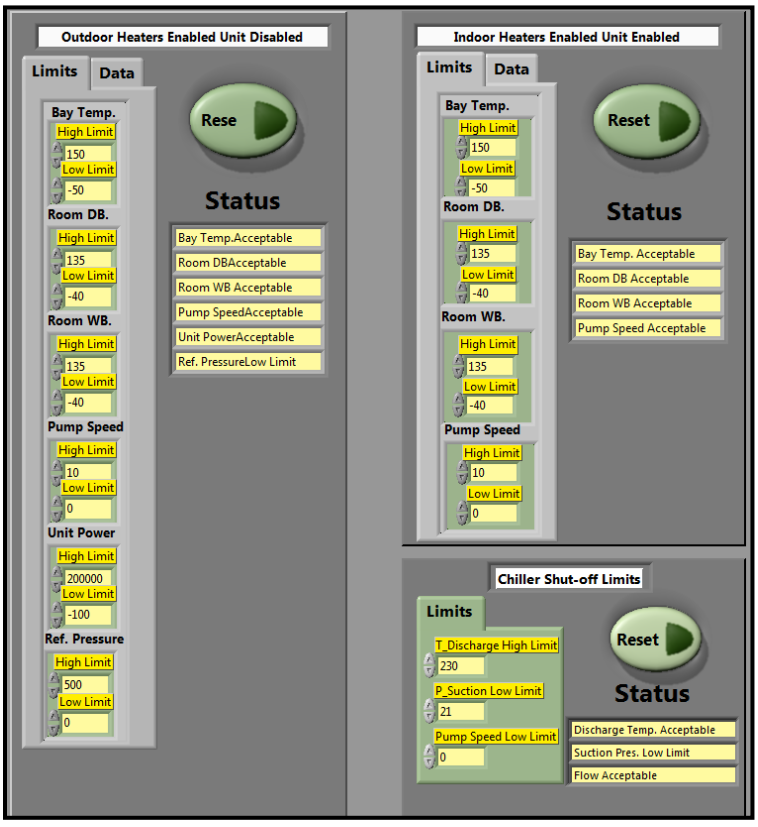

Figure 73: Shut-off limits for chamber and unit

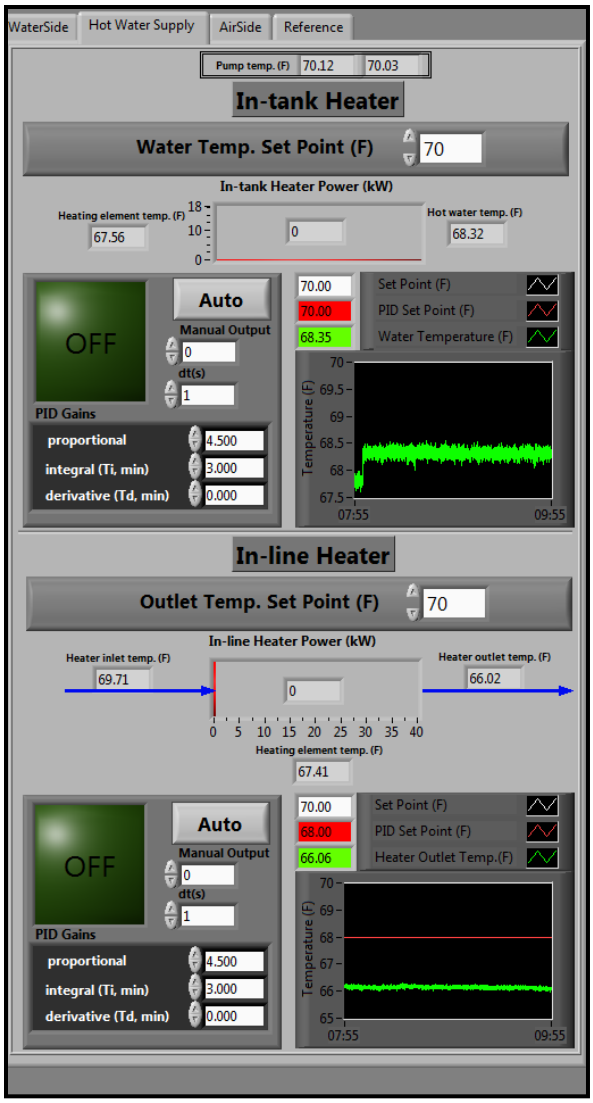

Figure 74: PID controls for the heaters supplying hot water

VITA

Auvi Biswas

Candidate for the Degree of

Master of Science

Thesis: PERFORMANCE AND CAPACITY COMPARISON OF TWO NEW LGWP REFRIGERANTS ALTERNATIVE TO R410A IN RESIDENTIAL AIR CONDITIONING APPLICATIONS

Major Field: Mechanical and Aerospace Engineering

Biographical: From the town of Pabna, Bangladesh; son of Aminul Haque Biswas and Rowshan Ara Biswas; younger brother to Eva Biswas; married to Tasnia Reza.

Education:

Completed the requirements for the Bachelor of Science in Mechanical Engineering at Bangladesh University of Engineering and Technology, Dhaka, Bangladesh in October, 2009.

Experience:

-Worked in the psychrometric chamber at Oklahoma State University as a graduate research assistant
-Graduate teaching assistant at Oklahoma State University

Professional Memberships:

-American Society of Heating, Refrigeration and Air-conditioning (ASHRAE) student member

Name: AUVI BISWAS

Date of Degree: DECEMBER, 2012

Title of Study: PERFORMANCE AND CAPACITY COMPARISON OF TWO NEW LGWP REFRIGERANTS ALTERNATIVE TO R410A IN RESIDENTIAL AIR CONDITIONING APPLICATIONS

Major Field: Mechanical and Aerospace Engineering

Abstract:

Scope and Method of Study:

This thesis presents a ground breaking study on Low Global Warming Potential (LGWP) developmental refrigerants. An R410A 17.6 kW (5 ton) heat pump split unit commercially available off-the-shelf for US ducted HVAC applications, was retrofitted with two new developmental refrigerants, DR-4 and DR-5 that have GWP ranging from 300 to 500, which is significantly lower than that of R410A. The experiments were conducted at design and off-design conditions with outdoor temperature ranging from -8°C (17°F) to 46°C (115°F).

Findings and Conclusions:

The findings for this work showed that DR-5 had up to 3% higher capacity and up to 6% higher COP, while DR-4 showed up to 4% higher COP but 14% lower capacity in comparison with R410A. The experimental results showed that the thermal expansion valve could be further optimized for the new refrigerants to maximize the COP of the unit while preserving the cooling capacity and data showed that the COP of DR-4 could be augmented by an additional 6% with respect to drop-in tests. The experimental data discussed in this thesis are part of a broader campaign on LGWP refrigerants performance in heat pump systems. The analysis in thesis could inform the HVAC&R industry and regulatory agencies about characteristics and system level behavior of two new developmental LGWP refrigerants.

ADVISER'S APPROVAL: Dr. Lorenzo Cremaschi